TEMPLATE SYNTHESIZED MEMBRANES FOR ION TRANSPORT MODULATION AND SILICA-BASED DELIVERY SYSTEMS

By

FATIH BUYUKSERIN

A DISSERTATION PRESENTED TO THE GRADUATE SCHOOL
OF THE UNIVERSITY OF FLORIDA IN PARTIAL FULFILLMENT
OF THE REQUIREMENTS FOR THE DEGREE OF
DOCTOR OF PHILOSOPHY

UNIVERSITY OF FLORIDA

2007

To my parents, my wife Miyase, and my son Faruk Eren Buyukserin.

ACKNOWLEDGMENTS

Many individuals have been there to help me during my graduate studies. I would like to thank Dr. Charles R. Martin for his patience, guidance and support throughout my career at the University of Florida. He has been an excellent mentor by providing scientific discussions about my research and at the same time a great teacher in paper writing and presentation skills.

The Martin group members have been very supportive. I am very grateful to Myungchan Kang, Punit Kohli, Mark Wirtz, Shufang Yu and Dave Mitchell for providing insightful discussions about my experiments and training me in surface modification, analytical detection techniques and instrumentation. Mario Caicedo, Lane Baker, John Wharton, Lacramioara Trofin, Damian Odom, JaiHai Wang and Fan Xu shared their experiences and provided helpful suggestions. Miguel Mota spent many hours growing aluminum oxide for my experiments. Heather Hillebrenner was a perfect collaborator and a great friend.

I want to thank Drs. Weihong Tan and Rick Rogers for their valued advice on my research and career. I am also grateful to Karen Kelly and Lynda Schneider from the ICBR for their help with SEM and TEM, to Eric Lambers from the MAIC for his help with XPS, and to Colin Medley from the Tan research group for his help with confocal microscopy.

Finally, my family and friends provided enormous help and moral support during my graduate career. My wife Miyase Buyukserin has always been there with her patience and unconditional love. My parents Husniye and Hasan Fehmi Buyukserin, my brothers Mehmet and Mustafa Buyukserin deserve most of the credit for my success as they were constant sources of encouragement and support before and during my graduate career. I want to also thank members of the Gainesville Turkish community, especially Fatih Gordu, Erkan Kose, Ahmet Basagalar, Onur Kahya, Zafer Demir, Cem Demiroglu, Kaan Kececi, Nezih Turkcu and Ugur Baslanti, for providing a very friendly, calming, home-like atmosphere.

TABLE OF CONTENTS

page

LIST OF TABLES

LIST OF FIGURES

Abstract of Dissertation Presented to the Graduate School
of the University of Florida in Partial Fulfillment of the
Requirements for the Degree of Doctor of Philosophy

TEMPLATE SYNTHESIZED MEMBRANES FOR ION TRANSPORT MODULATION AND SILICA-BASED DELIVERY SYSTEMS

By

Fatih Buyukserin

May 2007

Chair: Charles R. Martin
Major Department: Chemistry

The objective of this research is to prepare membrane platforms for potential applications in ion transport modulation and biomolecule delivery-device fabrication. Template synthesis approach is used to obtain gold nanotube membranes and silica nano test tubes that are the two main tools used in this dissertation. Chapter 1 provides an overview of the template synthesis method and its applications. The preparation of the track-etched polycarbonate and anodized aluminum oxide template membranes is provided. Reviews of deposition-modification techniques and plasma etching that are used in later chapters are then given.

Chapter 2 describes an alternative method for electromodulating ion transport through template synthesized Au nanotube membranes. This method entails attaching to the nanotubes a molecule that contains a redox-active ferrocene (Fc) substituent. Using these redox-active nanotubes, excess cationic charge can be placed on the membrane by oxidizing Fc to ferricinium (Fc^+) by external voltage. It has been found that when the nanotube-bound Fc is oxidized to Fc^+, the flux of a cationic permeate species is suppressed relative to when the Fc is in its reduced state. Hence, with these redox-active tubes, the membrane can be gated between high and low cation-transporting states.

In Chapter 3, the effect of constrained geometry on the decay properties of Fc^+ is examined. The Fc^+ decay properties of four membranes with different pore sizes were investigated in an aqueous electrolyte and compared to the decay for commercial gold button electrode. After the membrane samples were modified with Fc-thiol monolayer, they were exposed to argon plasma that removes Fc-thiol on Au surface films leaving only the Fc-thiol lining the Au nanotube walls. The results suggest that the decay rate increases with increasing pore size and in all cases it is found to obey first order decay kinetics.

Chapter 4 describes the fabrication of a unique nanopore polymer template and its use for silica nano test tube production by sol-gel chemistry. Our objective with these test tubes was to impart multifunctionality through differential modification for developing a technology for cell specific biomolecule delivery. A plasma etch method, using a nanopore alumina film as the mask, was used to etch a replica of the alumina pore structure into the surface of a polymer film. The distance that the pores propagate into the photoresist film is determined by the duration of the etching process. The pores in such plasma-etched nanopore photoresists films were used as templates to prepare silica nano test tubes with lengths as small as 380 nm.

In Chapter 5, we have compared the preparation techniques for silica nano test tube fabrication from alumina templates and then illustrated the response of breast carcinoma cells to test tubes that have been biochemically modified. Defect-free uniform silica nano test tubes were obtained by the surface sol-gel method. These test tubes were differentially modified with a fluorophore on the inner surface and with an antibody (target or control) on the outer surface for the cell incubation studies. The fluorescence data suggest that the tubes modified with the target antibody attaches much more readily to the cell membrane surfaces than the tubes modified with the control antibody. Chapter 6 summarizes the results and conclusions of this research.

CHAPTER 1
INTRODUCTION AND BACKGROUND

Introduction

Nanoscience, the science of small particles of materials, is one of the most important research and development frontiers of modern science.[1,2] The systems being studied in nanoscience are measured by nanometer length scale and a nanometer is one billionth of a meter. Materials of nanoscopic dimensions are of fundamental interest since the properties of a material, such as optical, electronic and magnetic etc, can change in this regime of transition between the bulk and molecular scale.[3] These new material properties have led to potential technological applications in areas as diverse as microelectronics, coatings and biotechnology.[2] For instance, one such application that is now in use involves using gold nanoparticles as visual indicators in over-the-counter medical diagnostic kits.[4]

Nanomaterials can be fabricated through various methods, ranging from chemical methods to lithographic techniques.[5,6] The template method, pioneered by the Martin group, is a general approach for preparing nanomaterials that involves the synthesis or deposition of the desired material within the cylindrical and monodisperse pores of a nanopore membrane or other solid surface.[3,6] The applications of template synthesized nanomaterials composed of polymers, metals, semiconductors, and carbons have been applied in chemical separation, sensing, catalysis, electrochemistry, biomolecule extraction and delivery.[3,4,6-8]

Template synthesized gold nanotube membranes and silica nano test tubes are the main scientific tools used in this research. This chapter provides background information on the preparation and application of these tools. An overview of template synthesis is given which is followed by past and recent important applications related to the presented research. The preparation of the track-etched polycarbonate and anodized aluminum oxide template

membranes is examined. Reviews of electroless gold deposition, sol-gel technology, silane chemistry and plasma etching that are used in later chapters are then given. Finally, a brief overview of the delivery vehicles used in biomolecule transport is provided.

Background

Template Synthesis

Many methods for the fabrication of nanoparticles have been developed, ranging from lithographic techniques to chemical methods.[5,6] Our research group has pioneered a general method called template synthesis for the preparation of nanoparticles.[3,6] This method entails synthesis or deposition of the desired material within the cylindrical and monodisperse pores of a nanopore membrane or other solid. We have used nanopore polycarbonate filters, prepared via the track-etch method,[9] and nanopore alumina, prepared electrochemically from Al foil,[10] as our template materials. A variety of other porous materials such as glass nanochannel arrays, zeolites, and polypeptide tubes can also be used as templates.[11-13] Depending on the properties of the synthesized material and the chemistry of the pore wall, hollow nanotubes or solid nanowires can be obtained.[6]

Probably the most useful feature of the template synthesis is that it is extremely general with regard to the materials that can be prepared. For example, we have used this technique to prepare nanotubes and nanowires composed of conductive polymers, metals, semiconductors, carbon, Li^+-intercalation materials, and biomolecules such as DNA and protein.[6,14,15] Methods used to synthesize such materials within the pores of the template membranes include electroless and electrochemical metal deposition, chemical and electrochemical polymerization, sol-gel deposition, chemical vapor deposition[3,6] and layer- by-layer deposition.[14,15] In addition, template membranes contain cylindrical pores of uniform diameter which yields monodisperse nanocylinders of the desired material with controllable dimensions. Finally, the resultant

nanotubes or nanowires can be assembled into a variety of architectures. The nanostructure can remain inside the pores of the template membrane or they can be freed from the template membrane and collected as an ensemble of free nanoparticles.[6]

Applications in electrochemistry and sensing

One very exciting application of the template synthesis is in the area of electrochemistry.[16] The electroless deposition of chemistry allows us to routinely prepare ensembles of gold nanodisk electrodes with diameters as small as 10 nm.[17] Long plating times (24 h) results in the deposition of Au nanowires into the pores. These nanoelectrode ensembles (NEE) can be used in ultra trace detection of electroactive species. The signal-to-background (S/B) ratio at the NEE is orders of magnitude larger than at a macroelectrode because the double-layer charging currents at the NEE are orders of magnitude lower than those at a macroelectrode of equivalent geometric area. This great increase in the S/B ratio allows detecting ultra trace amounts of electroactive analytes.[17]

Nanostructured Li^+ -intercalation materials that are synthesized by the template method have been used to design novel Li-ion battery electrodes.[18] These nanostructured electrodes have improved rate capabilities compared to the thin film electrodes composed of the same material.[19-21] In addition, Sides and Martin demonstrated that V_2O_5 nanofibers prepared by sol-gel synthesis in polymer templates show increased low-temperature performances compared to the micrometer-sized V_2O_5 fibers.[22]

There has been a significant amount of research in the area of template synthesis of conductive polymers.[6] Such nanofibers of conducting polymers have been shown to be more conductive than the bulk material.[23,24] A detailed review of this topic can be found elsewhere in the literature.[25] Cho et al. recently fabricated well defined nanotube arrays of poly(3,4-ethylenedioxythiophene) (PEDOT) that can be used as an extremely fast electrochromic display

(switching time less than 10 ms).[26] The thin nature of the template synthesized nanotube walls offers a short diffusion distance and results in ultrafast switching rates.

Finally, there is a great current interest in nanopores that have a conical pore shape and the correspondingly conical nanostructures synthesized via the template method within these pores.[27] A number of applications utilizing the conical pore geometry have been reported. For example, such conically shaped nanopores can be used as the sensing element for new types of small molecule,[28] DNA,[29,30] protein,[31] and particle[32] sensors. Conically shaped gold nanotubes deposited within such pores can also mimic the function of voltage gated ion channels.[33] The details of the fabrication of the pore geometry and the sensing mechanism for such platforms has been recently reviewed by Choi and Martin.[8]

Applications in control of ion transport and electromodulation

Ensembles of Au nanotubes are obtained in the multipore track-etched polycarbonate (PC) templates when the electroless plating is done for shorter times. We discovered that by controlling the Au deposition time, we could prepare Au nanotubes with inside diameters that can be of molecular dimensions.[34] We have demonstrated four transport-selectivity paradigms with these Au nanotube membranes (Au-NTM). First, because the nanotubes can have inside diameters of molecular dimensions (<1 nm), these membranes can be used to cleanly separate small molecules on the basis of molecular size.[34] The ability to control the tube diameter has also been used in the separation of a mixture of protein molecules with different sizes.[35] Second, chemical transport selectivity can be introduced by chemisorbing thiols to the Au nanotube walls.[36-38] Third, by using a thiol with both acidic and basic functional groups, ion transport across the Au-NTM can be modulated by controlling the pH of the contacting solution phases.[38] Finally, because the Au nanotubes are electronically conductive, excess charge can be placed on the nanotube walls by electrostatic charging in an electrolyte solution.[39,40] This introduces ion-

transport selectivity as well, and the Au-NTM can be electromodulated between cation and anion transporting states.

Lee and Martin described a unique way for the electromodulation of neutral molecules across Au-NTMs.[41] This approach makes use of an anionic surfactant which, when a positive potential is applied to the Au-NTM, partitions into the nanotubes. Because of hydrophobic tail of the surfactant, this renders the nanotubes interior hydrophobic, and the membrane preferentially extracts and transports hydrophobic molecules.[36] The anionic surfactant can then be expelled from the nanotubes by applying a negative potential. This provides a route for reversibly electromodulating neutral molecule transport.

We have recently been investigating an alternative method for electromodulating transport in nanotube membranes.[42] This method entails attaching to the nanotubes a molecule that contains a redox active ferrocene (Fc) substituent. With these redox-active nanotubes, excess cationic charge can be placed on the membrane by oxidizing Fc to ferricinium (Fc^+) by external voltage. Buyukserin et al. has shown that cation transport through Au-NTMs can be electromodulated by controlling the extent of oxidation of Fc- thiol monolayer attached to the Au surface.[43] Miller and Martin demonstrated the control of surface charge, and thus electroosmotic flow (EOF) in poly (vinylferrocene) coated carbon nanotube membranes.[42] Reversible switching between the neutral and polycationic forms of the redox-active polymer results in changes in the rate and direction of EOF.

Applications with silica and biomolecule nanotubes

The use of silica nanotubes, whether still embedded within the template or freed from the template, has been shown in a variety of applications.[44-46] The preparation method is generally sol-gel chemistry and the template material is commercial or home-made porous alumina membranes. We have shown that silica nanotubes synthesized within the pores of a home-made

alumina template can be used to separate two enantiomers of a chiral drug.[44] An antibody that selectively binds one of the enantiomers of the drug was attached to the inner walls of the silica nanotubes. Such membranes selectively transport the enantiomer that specifically binds to the antibody, relative to the enantiomer that has lower affinity for the antibody.[44]

Ensembles of silica nanotubes are obtained when such a membrane is dissolved. The nature of template synthesis allows independent modification of the inner and outer surfaces of silica nanotubes.[45,46] For example, silica nanotubes, that have been modified with a fluorophore on the inside and a hydrophobic silane group on the outside, have been shown to selectively partition into the organic phase in a mixture of aqueous/organic solvents.[45] Furthermore, silica nanotubes that have been modified with a certain antibody on both inner and outer tube surfaces can be used to selectively extract the enantiomer that specifically binds to the antibody from a racemic mixture of enantiomers.[45]

Novel nanostructures called nano test tubes have been recently introduced by the Martin group.[47-49] Silica nano test tubes are prepared by sol-gel synthesis of silica in the pores of an alumina template that remains attached to underlying aluminum metal. Unlike the previously mentioned nanotubes that are open on both ends, nano test tubes are closed on one end and open on the other. The use of test tubes as potential universal drug delivery vehicles was exploited where these nano test tubes could be filled with payload and then the open end corked with a chemically labile cap.[48] For such studies, the tube dimensions can have an important effect. Buyukserin et al. very recently fabricated a nanopore polymer template that can be used to prepare silica nano test tubes with lengths as small as 380 nm.[49]

Nanotubes composed of biomolecules such as DNA or protein have been fabricated by Hou et al.[14,15] Layer-by-layer deposition has been applied in both cases using a commercial

alumina membrane as the template. Protein nanotubes are obtained by alternately exposing the template to a solution of the desired protein and then to a solution of glutaraldehyde, which acts as crosslinking agent to hold the protein layers together. Biologically active tubes are collected by removing the template and their activity depends on the number of layers deposited.[15] The DNA nanotubes, however, have an outer skin of one or more α,ω-diorganophosphonate/Zr(IV) layers, to provide structural integrity, surrounding an inner core of multiple double-stranded DNA layers held together by hybridization between the layers. The DNA components can be released from the nanotube by melting of the DNA duplexes comprising the nanotubes.[14]

Track-Etched Polycarbonate Membranes

The use of nuclear tracks for the production of porous membranes was proposed almost immediately after the discovery of particle track etching in thin sheets of materials.[50] Progress in this field was further accomplished through new particle sources, studies of new polymeric materials, search for new applications and development of numerous methods of modification.[51]

There are two basic methods of producing latent tracks in the foils to be transformed into porous membranes.[51] The first method is based on the irradiation with fragments from the fission of heavy nuclei such as californium or uranium.[9,50] The main advantages of this technique are the relatively low cost, good stability of a particle flux in time, and non-parallel particle flux that enables the production of membranes with high porosity and low percent of overlapping pore channels. The contamination of the tracked foil with the radioactive product is a major limitation of the method which requires cooling of the material for few months. In addition, angle distributions of pore channels and the range of fission fragments (membrane thickness) are limited.[51] The second method involves the use of ion beams from accelerators.[9,52-54] Thicker foils with higher pore densities and controllable pore distributions can be obtained with higher energy

non-radioactive ions. Although the cost of irradiation is higher, the popularity of the ion-accelerator facilities has been increased in the past decade.[51]

After irradiation, the material is subjected to chemical etching that preferentially removes the latent ion tracks.[51] As a result the latent ion track is transformed into a hollow channel. Pore size and pore shape is determined during this chemical etching stage. The simplest description of pore geometry is based on two parameters: bulk etch rate and track etch rate. The bulk etch rate depends on the material, on the etchant and on the temperature. The sensitivity of the material, irradiation conditions, post-irradiation conditions and etching conditions determines the track etch rate. Cylindrical, conical, funnel-like, and cigar-like pore shapes can be made by controlling the bulk and the track etching rates.[51] Track etched membranes can be prepared from various polymeric materials such as polycarbonate (PC),[9] poly (ethylene terephthalate) (PET),[51] polypropelene[55] and polyimide.[53,56] Track membranes are known as precise porous films with a very narrow pore size distribution. The pore diameter can be from 10 nm to tens of micrometers. The pore density can vary from 1 to 10^{10} cm^{-2}.[51]

PC has been used for track membrane production for over thirty years.[9] The chemical etching of PC involves the rupture of chemical bonds on both sides of the carbonate group, leading to the formation of carbonate ions (Figure 1-1A). PC has a high sensitivity for irradiation which allows producing membranes with a pore diameter as small as ~ 10 nm without UV sensitization stage. When compared to PET, PC has a lower resistance to organic solvents and lower wettability.[51] Poly (vinylpyrrolidone) (PVP) coating can be used to render the PC membranes hydrophilic.[17] Track-etched PC filtration membranes are commercially available from a number of companies (e.g. Whatman, Osmonics). Cylindrical pores are randomly distributed on the membrane surface in these commercial membranes and pore diameters ranging

from 10 nm up to 20 μm and pore densities between 10^4 and 10^9 pores.cm^{-2} are available (Figure 1-1B).

Electroless plating of polymeric templates

The Martin group has developed a new class of synthetic membranes that consist of a porous polymeric support that contains an ensemble of gold nanotubes.[34,36-41] Monodisperse Au nanotubes that span the complete thickness of the polymeric support can be prepared. The support used in this work is the track-etched polycarbonate filter described above. The gold nanotubes are prepared via electroless deposition of Au onto the pore walls; that is the pores act as templates for the nanotubes (Figure 1-2). Electroless metal deposition, in general, involves the use of a chemical reducing agent to plate a metal from solution onto a surface.[57] The key requirement of an electroless deposition bath is to arrange the chemistry such that the kinetics of homogeneous electron transfer from the reducing agent to the metal ion is slow. Otherwise, the metal ion would simply be reduced in the bulk solution. A catalyst that accelerates the rate of metal ion reduction is then applied to the surface to be coated.[17]

The electroless deposition method for the preparation of gold nanotube membranes can be summarized as follows; the template membrane is first "sensitized" by immersion into a $SnCl_2$ solution which results in deposition of Sn(II) onto all the membrane surfaces (pore walls and membrane faces). Sn^{2+} adheres to the membrane because it is precoated with PVP during production to render the membranes hydrophilic. Amine and carboxyl groups of PVP are thought to act as "molecular anchors"[58] that bond the Sn^{2+} to the membranes surfaces.[59]

The sensitized membrane is then immersed into an aqueous basic $AgNO_3$ solution. This causes a surface redox reaction in which the surface-bound Sn(II) is oxidized to Sn(IV) and the Ag^+ is reduced to nanoscopic metallic Ag particles on the membrane surface (Equation 1-1); some silver oxide is also obtained.[60]

$$Sn(II)_{surf} + 2Ag(I)_{aq} \rightarrow Sn(IV)_{surf} + 2Ag(0)_{surf} \quad (1\text{-}1)$$

The subscripts "surf and "aq" denote species adsorbed to the membranes surfaces and species dissolved in solution, respectively. The membrane is then immersed into a commercial gold plating solution and a second surface redox reaction occurs, to yield nanoscopic Au nanoparticles on the surfaces.

$$Au(I)_{aq} + Ag(0)_{surf} \rightarrow Au(0)_{surf} + Ag(I)_{aq} \quad (1\text{-}2)$$

These Au nanoparticles are excellent catalytic sites for the oxidation of formaldehyde and the concurrent reduction of Au. As a result, Au deposition will begin at the pore walls, and Au tubes will be obtained within the pores. In addition, the faces of the membrane become coated with thin gold films without blocking the mouths of the nanotubes.[59] The Au nanotubes can have inside diameters of molecular dimensions (<1 nm),[34] and inside diameter can be controlled at will.[36] Various applications of these membranes are presented in the template synthesis section.

Estimation of nanotube inside diameter

We use a gas-transport method to determine the effective inside diameter of the template-synthesized Au nanotubes.[36] Briefly, the tube containing membrane was placed in a gas-permeation cell, and the upper and lower half-cells are evacuated. The upper half-cell will then be pressurized, typically to 20 psi, with He, and the pressure-time transient associated with the leakage of He through the tubes is measured using a pressure transducer in the lower half-cell. The pressure-time transient was converted to gas flux (Q, mol.s^{-1}) which is related to the radius of the nanotubes (r, cm) via[61,62]

$$Q = (4/3)\,(2\pi/MRT)^{1/2}\,(nr^3\Delta P/l) \quad (1\text{-}3)$$

where ΔP is the pressure difference across the membrane (dynes.cm^{-2}), M is the molecular weight of the gas, R is the gas constant (erg K^{-1} mol^{-1}), n is the number of nanotubes in the membrane sample, l is the membrane thickness (cm) and T is the temperature (K). This equation

is based on the following assumptions: 1) that we know the number of tubes in the sample, 2) that the tubes have a constant diameter down their entire length, 3) that the mechanism of gas-transport through the membrane is Knudsen diffusion in the nanotubes.[59] The presence of cigar-shaped pores and bottlenecked tubes causes slight deviations in the first two assumptions. For this reason, the calculated diameters are sometimes referred to as "effective inside diameters." The current plating conditions have shown to decrease the formation of these bottlenecked tubes and provide more uniform Au depositions.[36]

Gas transport through the membranes occurs via three different mechanisms; ordinary (viscous), Knudsen or surface diffusion.[63] In addition, a solution-diffusion model is adopted for describing the transport through the non-porous solid-phase**.** Knudsen diffusion occurs when the mean-free path of the gas is much larger than the average pore radius in the membrane. In our case, equation 1-3 is predicated on Knudsen diffusion in the nanotubes. The validity of this assumption is explored by comparing the diffusion of He/H_2 and O_2/N_2 gas pairs through the Au nanotubes membranes.[36] The ratios of the fluxes of the two gases in each pair across membranes of different pore sizes are compared. If the gas transport occurs via Knudsen diffusion, this ratio is the inverse square root of the molecular weights for the two gases in each pair, and it does not change with changing pore sizes (i.e. plating times). It has been shown that the He/H_2 pair perfectly applies the Knudsen type gas diffusion[36] and He gas was used in this work to determine the approximate inside diameter of Au nanotubes.

Anodic Alumina Templates

Anodic aluminum oxide (AAO) films formed by the electrochemical oxidation of aluminum have been investigated and used in numerous products for more than 100 years.[64-66] In recent years, nanoporous AAO with a hexagonal arrangement of monodisperse nanopores has become a popular template system for the synthesis of various functional nanostructures.[44,45,67-69]

In addition, the use of these well-ordered structures as evaporation or etching masks yields novel nanometric materials such as nanodots, nanotubes, nanowires, nanowells and nanopores made of metals, metaloxides and semiconductors.[70-72] Nanopore arrays with interpore spacing ranging from 50 to 400 nm, pore diameter from 10 to 200 nm, membrane thickness from 0.1 to 200 μm, and pore density as high as 10^{12} pore.cm^{-2} can be prepared.[72-74] Alumina membranes are commercially available as 60 μm-thick filtration membranes with pores of nominally 20, 100 and 200 nm diameters from Whatman International, Maidstone, England. Generally the pores of commercial membranes are not uniform in size or shape (Figure 1-3A). Due to these limited and non-uniform membrane parameters, we prepare the alumina membranes in-house (Figure 1-3B).

High purity aluminum metal (99.999%) is used in order to prepare alumina films with highly monodisperse cylindrical pores. This metal is first mechanically polished with sand paper (600 grit) and then electropolished at 15 V in a solution that is 95 wt% H_3PO_4 and 5 wt % H_2SO_4 with 20 g/L in CrO_3 which prevents pitting. Using smooth electropolished aluminum surfaces is necessary for obtaining ordered hexagonal structures.[72] The aluminum is the anode, a Pb plate is the cathode and the voltage is supplied by a variable power supply. The temperature of the electrolyte is kept around 70 °C and the polishing is done for periods of 5 minutes for at least 2 times on both surfaces for a mirror-like finish. Concentrated acid solution at high temperature is used for immediate dissolution of alumina.[75] Following the electropolishing, the Al foil is subjected to a two step anodization process developed by Masuda and Fukuda.[76]

Two-step anodization method

Traditionally, the ordered pore arrangements are formed under some specific anodizing conditions after a long anodization time, and as a result, they can only be observed on the bottom part of the films.[77] Masuda and Fukuda first showed that straight ordered nanoholes could be formed in a thin membrane of porous alumina by striping away the thick oxides obtained from

the first long anodization and subsequently anodizing it for a short time.[76] The first long anodization allows sufficient time for self-organization and homogenization of pore size.[75] Once it is removed, an indention or pit is left in the underlying Al substrate corresponding to each pore. The second anodization at the same voltage and in the same electrolyte results in pore nucleation in these pits that are already highly ordered and monodisperse; thus the alumina film grows as patterned.[76] Mechanical imprinting,[78] electron-beam[79] and focused-ion-beam lithographic methods[80] have also been used to create nanosized indentations on the Al surface to precisely control the pore growth process.[81]

Densely packed ordered hexagonal pore structure, has been reported in oxalic, sulfuric and phosphoric acid solutions.[76,82-84] We have used 5 wt % aqueous oxalic acid at ~ 1 °C under 50 V in both the first and the second anodization steps. The cathode is a cylindrical stainless steel tube that supports homogenous ion flow to both surfaces of the aluminum and the solution is vigorously stirred. The solution temperature is kept between 0 and 4 °C for low reaction rates to prevent a runaway reaction and to keep Al in contact.

The freshly electropolished Al foil is rinsed with purified water and then anodized for ~ 12 h. This first step produces a precursor film which is then dissolved in an aqueous solution that was 0.2 M in CrO_3 and 0.4 M in H_3PO_4 at 80 °C. The same conditions were applied to this textured Al substrate for different anodization times for the second step, and the growth rate we obtained was ~ 12 min anodization per 1 μm alumina film thickness. The size of the pores to be grown is dependent on the applied potential and on the type of acid electrolyte used. In general, smaller pores require lower voltages and highly conductive electrolytes (e.g., sulfuric acid) where as lower conductivity electrolytes (e.g., oxalic acid) are used for larger pores.[85] In

addition, immersing the resultant alumina film in dilute H_3PO_4 solutions can also be used to tailor the pore dimension as it slowly reacts with alumina film and opens the pore diameter.

Membrane detachment

After the second-step anodization, the nanopore alumina can be used as a template film while it is still attached to the underlying Al metal that gives mechanical support to the film. (See Chapter 5.) Generally the alumina is separated from the Al base, however, and further processed into a freestanding membrane of nanopores that is open on the top and bottom and may be used as a base template stencil or mask for fabricating a variety of highly ordered nanostructures.[72] There are three reported ways to separate the alumina film.[71,73] Dissolving Al in $HgCl_2$ solution, alumina film separation by voltage reduction and coating an organic compound layer on the surface of alumina to protect the original morphology from erosive $CuCl_2$-based aluminum removal.[86] The first two methods will be discussed here.

The simplest way of separating alumina is to dissolve Al in $HgCl_2$. Generally, thin Al foils are most appropriate for dissolving, and the solvent does not damage alumina. Since there is a nonporous barrier alumina layer closest to the metal surface, dissolving aluminum results in films that are closed on one end and open on the other. The resultant film can be further chemically etched to obtain films with pores that are open on both sides. Hazardous Hg is produced during Al dissolution, and one foil is consumed to prepare one alumina film. The use of progressive reduction in the anodizing voltage to create a perforation of the barrier layer and to achieve separation of alumina film from Al is described by Furneaux et al.[73] When the film reaches the desired thickness, the voltage is reduced to about 70 % of its original value. Since the pore size and the film thickness are dependent on the applied voltage, the pores at the barrier layer branch to smaller sizes and the barrier layer becomes thinner. After many voltage

reduction cycles, the film/metal composite is immersed into an etchant solution. This quickly dissolves the thin barrier layer and the alumina is detached.

In our case, total reduction process takes about 1 h, the final voltage is 15 V and the etchant is 10 wt % H_3PO_4. The resultant alumina film has two distinct faces; the barrier side and the solution side. The barrier side has small branched pores that can be widened by an acid or base etchant to have uniform pores. In the Martin group, both commercial and home-grown alumina membranes are extensively used as templates and etching masks for the preparation of various functional nanostructured materials. A detailed discussion is presented under the template synthesis section.

Sol-Gel Technology

Interest in the sol-gel processing of inorganic ceramic and glass materials began as early as the mid-1800s with Ebelmanl's[87] and Graham's[88] studies on silica gels. The motivation for sol-gel processing is primarily the potentially higher purity and homogeneity and the lower processing temperatures associated with sol-gels compared with traditional glass melting or ceramic powder methods.[89] In addition, the technique can be used to obtain homogeneous multicomponent systems by mixing precursor solutions; this allows for easy chemical doping of the materials prepared. Finally, the rheological properties of the sol and the gel can be utilized in processing the material, for example, by dip coating of thin films, spinning of fibers, etc.[90,91]

In sol-gel synthesis a soluble precursor molecule is hydrolyzed to form a dispersion of colloidal particles (the sol). Further reaction causes bonds to form between the sol particles resulting in an infinite network of particles (the gel).[91] The gel is then typically heated to yield the desired material.[92] Organometallic compounds are used as precursor to form the colloids, and in the case of glass, alkoxysilane precursors such as tetramethoxysilane (TMOS) and tetraethoxysilane (TEOS) are most widely used.[93,94] These alkoxysilanes readily hydrolyze in the

presence of water to form silanols (Equation 1-4). Further polycondensation reactions occur between these silanols with other silanols (Equation 1-5, water condensation) and alkoxysilanes (Equation 1-6, alcohol condensation).[95,96]

$$R'_3\,Si\text{-}O\text{-}R + H_2O \rightarrow R'_3\,Si\text{-}OH + R\text{-}OH \quad (1\text{-}4)$$

$$R'_3\,Si\text{-}OH + HO\text{-}SiR'_3 \rightarrow R'_3\,Si\text{-}O\text{-}SiR'_3 + H_2O \quad (1\text{-}5)$$

$$R'_3\,Si\text{-}OH + RO\text{-}SiR'_3 \rightarrow R'_3\,Si\text{-}O\text{-}SiR'_3 + R\text{-}OH \quad (1\text{-}6)$$

Simultaneous hydrolysis and polycondensation of alkoxysilane precursors with two or more functional groups form an interconnected 3-D silica gel network. Many factors influence the kinetics of hydrolysis and condensation, and the systems are considerably complex as different species are present in the solution.[89] In addition, hydrolysis and condensation occur simultaneously. Some important variables are temperature, nature and concentration of electrolyte (acid, base), nature of the solvent and type of alkoxide precursor. Increasing temperature and water amount increases the rate of gelation. Acid and base catalysts can be used for rapid and complete hydrolysis so either high or low pH extremes will speed the reaction. The nature of solvent influences the reaction rates; for example, 20 times faster rate constants were found in acetonitrile as opposed to formamide.[97] Finally, the reaction rate decreases as the alkoxide group gets longer and bulkier.[98]

Hypercriticial or ambient conditions are used to convert gel into silica. When the liquid (resultant alcohols or water) is removed as a gas phase from the interconnected solid gel network under hypercritical conditions (critical-point drying), the network does not collapse and a low density aerogel is produced. If the liquid is removed at or near ambient pressure by thermal evaporation, shrinkage occurs and the monolith is called a xerogel.[89] Materials with various shapes and sizes can be obtained through molding or dip-coating of the sol since it is a liquid

form. When a template is immersed in the sol through dip-coating; a gel layer forms at the interface of the template. This layer can be dried and converted silica that replicates the surface topology of the template.[95] Template synthesized TiO_2, ZnO, WO_3, MnO_2, Co_3O_4,V_2O_5 and SiO_2 nanotubes[21,91,99,100] can be prepared with the sol-gel method.

Surface Sol-Gel Method

Precise control over the thickness and morphology of nanotubes synthesized with the conventional sol-gel technique can be challenging.[101] More reliable control over the quality of planar thin films can be achieved by layer-by-layer deposition techniques, where colloidal particles[102,103] or molecular precursors[104-106] are successively adsorbed as a layer at a time onto the growing surface. The latter is called surface sol-gel (SSG) method and it involves repeats of two-step deposition cycles. In this case, the adsorption of a molecular precursor and the hydrolysis steps (for oxide film growth) are separated by a post-adsorption wash. The washing step desorbs weakly bound molecules that form additional layers.[104] The SSG technique ideally can limit each deposition cycle to a single monolayer; however, in practice, thicker layers have been found for planar oxide SSG films.[104,106] Nevertheless, SSG allows very fine control over film thickness because a nanometer or sub-nanometer thick layer is grown in each two-step adsorption/hydrolysis cycle.[101]

Mallouk and coworkers recently reported the synthesis of silica nanotubes in anodic aluminum oxide membranes using the SSG technique where they have achieved a sub-nanometer control over the tube thickness.[101] Furthermore, when coated on metal nanowires, this silica layer can be a high-quality dielectric oxide coating. For this thin silica layer, they have used $SiCl_4$ as the precursor and CCl_4 as the solvent/washing solution. See Chapter 5 for more details on SSG based silica nanotubes synthesis. The same group has also demonstrated applicability of the first

layer-by layer technique to membrane substrates by preparing uniform and smooth free-standing semiconductor/polymer nanotubes.[107]

Silane Chemistry

The organofunctional silanes were first introduced over 50 years ago as coupling agents for fiberglass and have subsequently proved to be useful in various fields such as chromatography, catalysis and polymers applications.[108-110] Organosilanes form stable covalent bonds with siliceous materials (e.g., silicates, aluminates, borates) and various metal oxides. Thus, silanization provides a simple method for tailoring the surface chemistries of such materials. The general formula for an organosilane ($R_nSiX_{(4-n)}$) indicates two classes of functionality.[108] X is a hydrolyzable group typically halogen, alkoxy, acyloxy, or amine. After hydrolysis, a reactive silanol group is formed, which can condense with other silanol groups, for example, those on the surface of siliceous materials. The R group is a nonhydrolyzable organic radical that may possess a functionally that imparts desired characteristics.[108] Attachment of proteins, fluorophores, genetic material etc. can be done using this R group as reactive handles.[44,45]

When a monolayer of surface modification is desired, silanes with one hydrolyzable group are used. With a single reactive group, these molecules can either bind to the surface or dimerize and the dimers are removed by successive washing steps. Most of the widely used organosilanes have one organic substituent.[108,109] There are four steps in the reaction of these silanes and they are analogous to the steps in sol-gel chemistry. First, hydrolysis of the three labile groups occurs. Condensation of oligomers follows. The OH groups of the substrate then hydrogen bond with the oligomers. Finally, a covalent linkage is formed with the substrate by the loss of water through drying or curing. Water for hydrolysis may come from several sources. Aqueous alcoholic silane solutions that are made acidic with acetic acid are commonly used to initiate the

formation of silanols.[110] Water can also be present on the substrate surface or it may come from atmosphere.

The degree of polymerization of the silanes is determined by the amount of water available and the organic substituent. The concentration of the siloxane solution correlates with the thickness of the polysiloxane layer. It has been calculated that deposition from a 0.2% silane solution onto glass could result in eight molecular layers. These multi-layers could be either interconnected through a loose network structure, or intermixed, or both, and are in fact formed by most deposition techniques.[108] There is a certain amount of reversibility during the formation of covalent bonds to the surface. As water is removed by evacuation for 2 to 6 hours or by heating to 120° for 30 to 90 minutes, bonds may form, break and reform to relieve the internal stress.[108]

Silanes with four hydrolyzable groups provide a model for substrate reactivity and can be utilized in surface modifications. $SiCl_4$, for example, is commercially important since it can be hydrolyzed in the vapor phase to form amorphous fused silica.[108] Organic aprotic solvents can be used for surface treatment of chlorosilanes. Treatment from dry solvent tends to deposit a more nearly monomolecular layer of silane than can be obtained from water.[110] Chlorosilanes react with alcohols to form alkoxysilanes which undergo most of the reactions of chlorosilanes. Alkoxysilanes are more convenient reagents than tetrahalosilanes since they do not generate acid on hydrolysis and are generally less reactive.[108] TEOS and TMOS are common reagents used in sol-gel based material synthesis that have four alkoxy substituents.[93,94]

Plasma-Assisted Dry Etching

The most important subtractive processes encountered in miniaturization science are wet and dry etching, focused ion-beam milling, laser machining, ultrasonic drilling, electrical discharge machining, and traditional precision machining.[111] Dry etching involves a family of

methods by which a solid surface is etched in the gas phase, physically by ion bombardment, chemically by a chemical reaction through a reactive species at the surface, or by combined physical and chemical mechanisms. Plasma-assisted dry etching is categorized according to specific setup as either glow discharge (substrate and plasma are located in the same vacuum chamber) or ion beam (substrate and plasma are in separate chambers).[111]

In physical etching, momentum transfer occurs between energetic ions (e.g., Ar^+) and the substrate surface. Although the selectivity is poor, directional etching patterns (anisotropic) are obtained with this method. Some type of chemical reaction takes place in the chemical etching method through which faster and selective etching is achieved, but the etched features are isotropic. The most important dry etching technique is the reactive ion etching (RIE).[111] It combines physical and chemical etching mechanisms and enables profile control due to synergistic combination of physical sputtering with the chemical activity of reactive species with a high etch rate and high selectivity.

A plasma is an area of high energy electric or magnetic field that rapidly dissociates a suitable feed gas to form neutrals, energetic ions, photons, electrons, and highly reactive radicals.[111] The simplest plasma reactor consists of opposed parallel-plate electrodes in a chamber maintainable at low pressures. In argon plasma, electrical breakdown of argon gas in this reactor will occur when electrons, accelerated in the existing electrical field, transfer an amount of kinetic energy greater than the argon ionization potential to the argon neutrals. These energetic collisions generate a positive ion and a second free electron for each successful strike. Both free electrons reenergize, creating an avalanche of electrons and ions that results in a gas breakdown emitting a characteristic glow (blue, in the case of argon). In an RF-generated plasma, a radio-frequency voltage applied between two electrodes causes free electrons to

oscillate and collide with gas molecules, leading to a sustainable plasma. Unlike the dc plasma, RF plasma allows etching of dielectrics as well as metals and it sustains the plasma at lower potentials.[111]

There is a wide range of applications for plasma-assisted dry etching from integrated circuit design and micro/nano machining[111] to nanobatteries,[18] chemical sensors[70] and optical lenses.[112] In this dissertation we have used physical etching to remove Ferrocene-thiol monolayers from the gold membrane surfaces in Chapter 3, and chemical/physical etching to selectively remove a polymer film to fabricate silica nanostructures in Chapter 4.

Biomolecule Delivery with Nanoparticles and Viruses

The use of nanomaterials in biomolecule delivery has been shown to present various advantages such as increased efficacy,[113] protection of drugs[114] or genetic material[115,116] from potential environmental damage and reduced drug toxicity.[117] Spherical nanoparticles are almost always used because these shapes are easier to make and can be synthesized from a diverse range of materials, such as liposomes,[118,119] polymers,[120,121] dendrimers[122] and various inorganic compounds.[46,115,123]

Liposomes are spherical colloidal particles in which the internal aqueous cavity is surrounded by a self-assembled lipid membrane. Due to their size, biocompatibility and biodegradability, liposome are very promising systems for biodelivery applications.[118] The nature of the liposomes and their features are directly related to the preparation method, the phospholipid composition and the capability of binding other chemical species. Mixtures of egg phosphatydilcholine (PC) are primarily used because of their low cost and neutral charge although other neutral phospholipids are also used, such as sphingomyelin and phosphatidylethanolamine. Although liposomes could be formed spontaneously upon hydration of lipids, they do not generally have a thermodynamically stable structure; so that external

energy, such as sonication, extrusion or homogenization, is usually required to produce liposomes.[124] They have been widely used for both drug delivery[120,121,125] and gene transfection[118,120,126] after their surface is altered by adding hydrophilic substituents, such as poly(ethylene glycol) (PEG).[120] This reduces the liposome uptake by reticuloendothelial system (RES), thereby prolonging their circulation time.[127] The main drawback for the liposome based delivery applications is the stability (either releasing the biomaterial too quickly or entrapping too strongly).[121]

Polymeric micelles are self-assembling colloidal aggregates of block copolymers which occur when the concentration reaches the crucial micelle concentration.[121] The copolymer involves a hydrophilic and a hydrophobic component where in most cases the hydrophilic component is poly(ethylene oxide).[128] There are two principal methods for the preparation of block copolymer micelles, the direct dissolution method and the dialysis method. The direct dissolution method simply involves adding the copolymer to water or buffer solution where as dialysis is used for copolymers with limited water solubility.[128,129] In an aqueous environment, the hydrophobic blocks of the copolymer forms the core and the hydrophilic blocks form the corona. These micelles are the most common vehicles for drug delivery[130-132] where the lipophilic drug is incorporated in the microenvironment of a hydrophobic micelle core. Another polymer type used for such studies is dendrimers. Dendrimers are self-assembling synthetic branched polymers with exquisitely tunable nanoscale dimensions[133] and their application in drug delivery[134] and targeting[135] has been recently investigated. Their potential for gene delivery has also been examined where increased DNA payloads and decreased cell toxicity were observed with these dendrimer based delivery systems.[136,137] Despite various advantages,

polymeric delivery systems can present challenges for characterization and relatively low payload capacities.[121]

Viral systems with highly evolved and specialized components are by far the most effective means of DNA delivery, achieving high efficiencies (usually > 90%) for both delivery and expression.[126] Most of the recent clinical protocols involving gene therapy use recombinant virus-based vectors for DNA delivery. However no definitive evidence has been presented for the clinical effectiveness of any gene therapy protocol except for a few anecdotal reports of success in individual patients.[138] The impotence of current methodology is attributable to the limitations of viral mediated delivery, including toxicity, restricted targeting of specific cell types, limited DNA carrying capacity, production and packaging problems, recombination, and high cost.[139,140] These systems are also likely to cause unexpected cytotoxicity and immunogenicity which hamper their routine use in basic research laboratories.[116] For these reasons, nonviral synthetic DNA delivery systems have become increasingly desirable in both basic research laboratories and clinical settings.[126]

The application of some inorganic nanoparticles for biomolecule delivery has been recently shown; gold and silica nanoparticles, for example have been employed in DNA delivery.[115,141] Unlike nanoparticles or nanorods, nanotubes have a unique hollow structure which allows the modification of their inner surface and filling with specific biomolecules. However, the applications of nanotubes as biomolecule carriers are still very rare.[116,142] The template method developed in Martin group allows independent modification of inner and outer surfaces of the nanotubes through which multifunctional tubes with controllable dimensions can be obtained.[46] Multifunctionality is highly required for modern biomedical applications[125] and

these differentially modified tubes are potential novel tools for such studies. See Chapter 5 for more details on differentially modified nanotubes and nano test tubes.

Chapter Summaries

Chapter 2 describes an alternative method for electromodulating ion transport through template synthesized Au nanotube membranes. This method entails attaching to the nanotubes a molecule that contains a redox-active ferrocene (Fc) substituent. Electrochemical characterization of the Fc-thiol modified Au nanotube membranes is first examined. Surface confined cyclic voltammograms were obtained and the stability of these voltammograms was found to depend on the redox state of Fc and the electrolyte type. Using these redox-active nanotubes, excess cationic charge can be placed on the membrane by oxidizing Fc to ferricinium (Fc^+) by external voltage. It has been found that when the nanotube-bound Fc is oxidized to Fc^+, the flux of a cationic permeate species is suppressed relative to when the Fc is in its reduced state. Hence, with these redox-active tubes, the membrane can be gated between high and low cation-transporting states.

Chapter 3 examines the effect of constrained geometry on the decay properties of Fc^+. Previous studies have shown that the Fc^+ decomposition is a first order decay in bulk aqueous solutions. The Fc^+ decay properties of four membranes with different pore sizes were investigated in an aqueous electrolyte and compared to the decay for commercial gold button electrode. After the membrane samples were modified with Fc-thiol monolayer, they were exposed to argon plasma that removes Fc-thiol on Au surface films leaving only the Fc-thiol lining the Au nanotube walls. The results suggest that the decay rate increases with increasing pore size and in all cases it is found to obey first order decay kinetics. Furthermore, the decay pattern resembles a surface-like decay as the pore size of the membrane increases. These results

were attributed to the varying hydrophobic character of Fc-thiol monolayer and availability of counterions inside the pores as the pore dimensions change.

In Chapter 4, the fabrication of a unique nanopore polymer template and its use for silica nano test tube production is described. Our objective with these test tubes is to develop a technology for cell specific biomolecule delivery. A plasma etch method, using a nanopore alumina film as the mask, was used to etch a replica of the alumina pore structure into the surface of a polymer film. The distance that the pores propagate into the photoresist film is determined by the duration of the etching process. Hence, by controlling the etch time, we effectively control the thickness of the nanopore layer etched into the surface of the photoresist. The pores in such plasma-etched nanopore photoresists films were used as templates to prepare silica nano test tubes via sol-gel chemistry. As expected the length of the test tubes is determined by the thickness of the porous part of the photoresist film. Test tubes with lengths of 380 nm were obtained, shorter than any of the nano test tubes previously reported where the alumina film was used as the template.

Chapter 5 compares the preparation techniques for uniform silica nano test tube fabrication and then illustrates the response of breast carcinoma cells to test tubes that have been biochemically modified. Defective test tubes were obtained with the conventional sol-gel method and it was attributed to the small changes in the viscosity of the gel. Layer-by-layer addition of silica with the surface sol-gel method allowed preparation of defect-free uniform silica nano test tubes. We have differentially modified these test tubes for the cell studies. Before the template was removed, the inner tube surfaces were labeled with a fluorophore. The liberated fluorescent tubes were then modified with a target or a control antibody and then incubated with breast carcinoma cells. The preliminary results suggest that the tubes modified with target antibody

attaches much more readily to the cell membrane surfaces than the tubes modified with control antibody. The results and conclusions of this dissertation are summarized in Chapter 6.

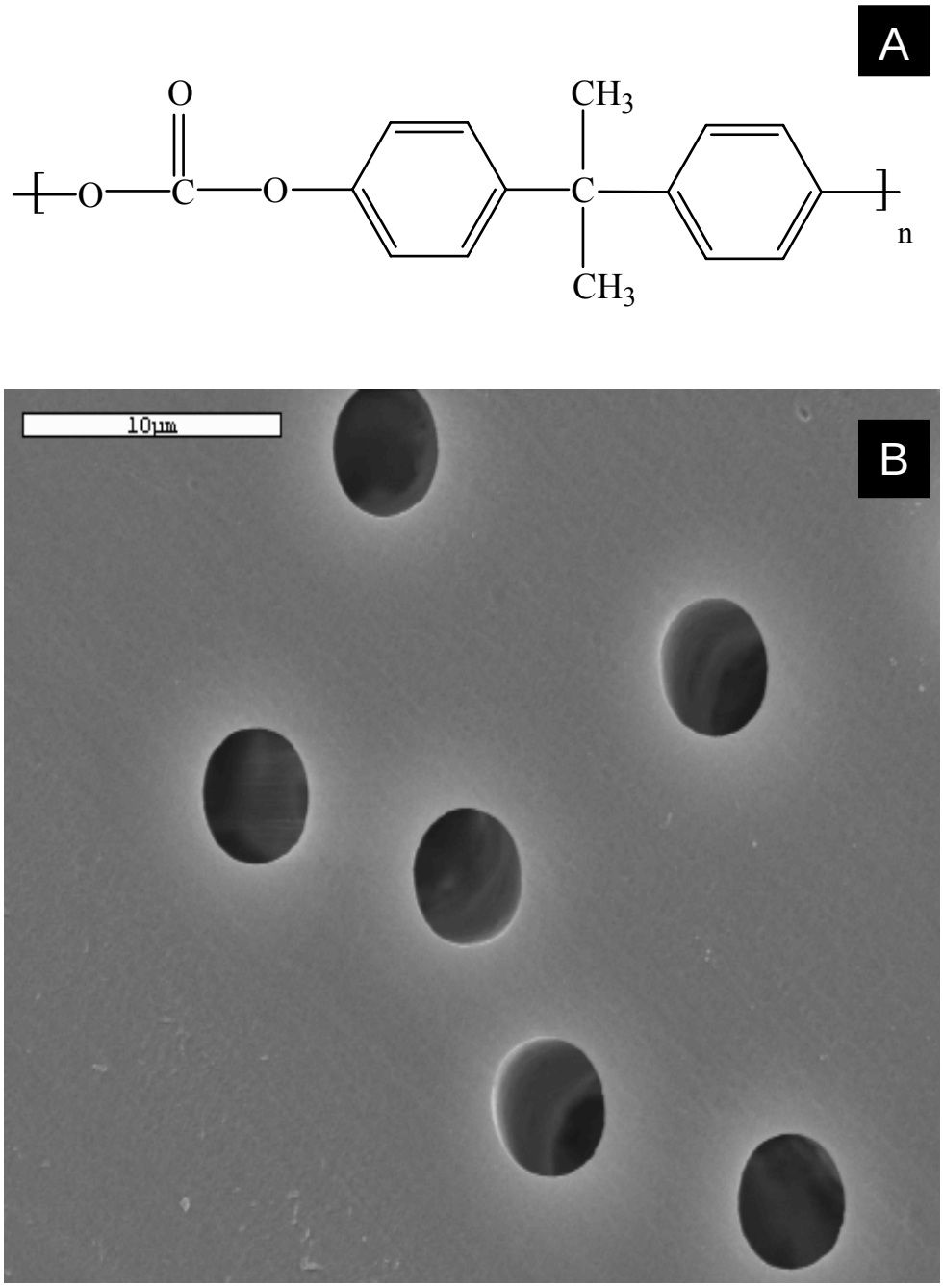

Figure 1-1. A) The chemical structure of polycarbonate. B) Scanning Electron Micrograph (SEM) of the surface of a commercial track-etched polycarbonate membrane.

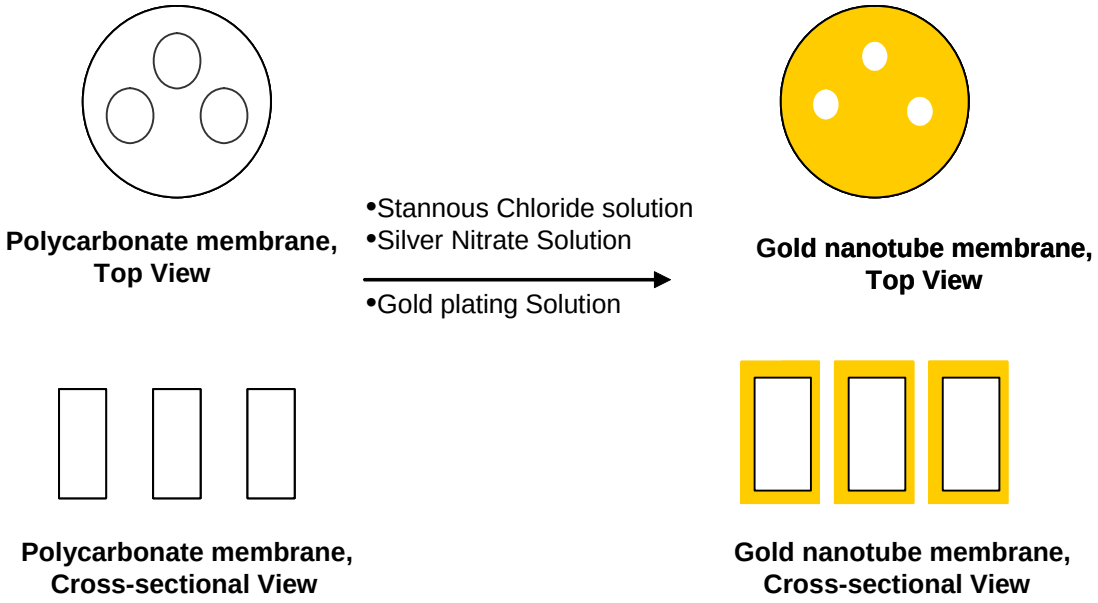

Figure 1-2. Top and cross-sectional view of PC membrane before & after the gold plating.

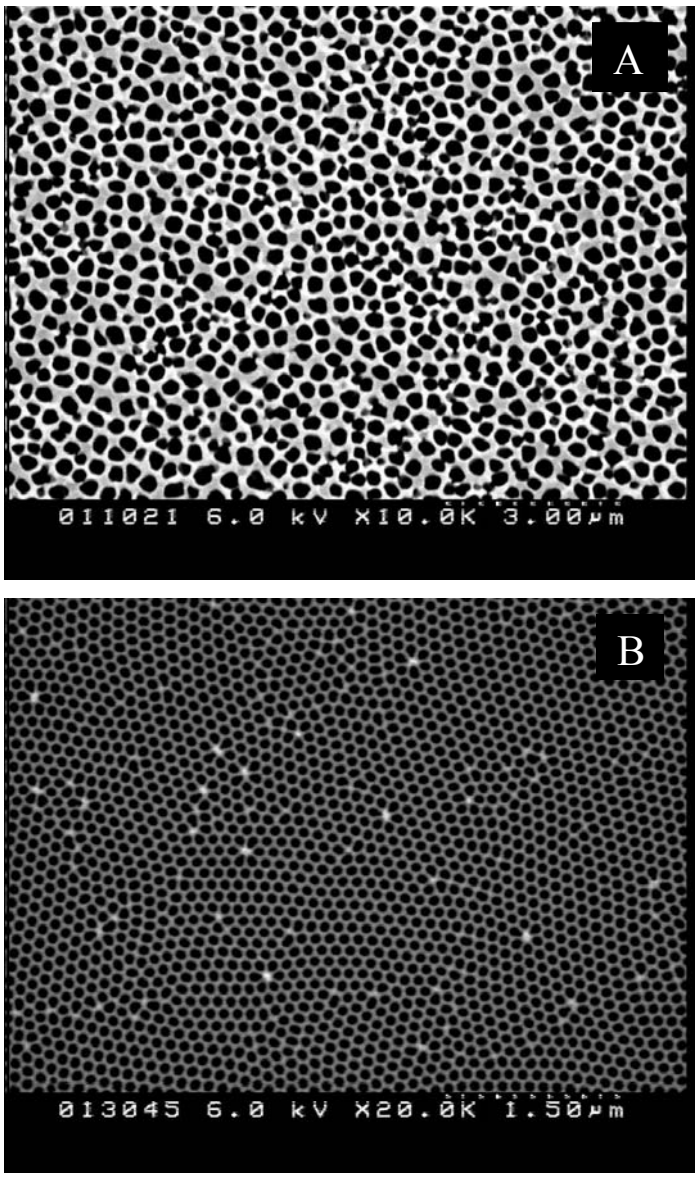

Figure 1-3. SEM images of the surface of anodized aluminum oxide (alumina) membranes. A) Commercially available alumina membrane. B) Home-grown alumina membrane.

CHAPTER 2
ELECTROACTIVE NANOTUBES MEMBRANES AND REDOX-GATING

Introduction

We have developed a new class of synthetic membranes that contains monodisperse Au nanotubes with inside diameters that can be of molecular dimensions (<1 nm).[34,36-41] The Au nanotubes span the complete thickness of the membrane and can act as conduits for molecule and ion transport between solutions placed on either side of the membrane. We have demonstrated four transport-selectivity paradigms with these Au nanotube membranes. First, because the nanotubes can have inside diameters of molecular dimensions (<1 nm), these membranes can be used to cleanly separate small molecules on the basis of molecular size.[34] Second, chemical transport selectivity can be introduced by chemisorbing thiols to the Au nanotube walls.[36-38] Third, by using a thiol with both acidic and basic functional groups, ion transport across the Au nanotube membrane can be modulated by controlling the pH of the contacting solution phases.[38] Finally, because the Au nanotubes are electronically conductive, excess charge can be placed on the nanotube walls by electrostatic charging in an electrolyte solution.[39-41] This introduces ion-transport selectivity as well, and the Au nanotube membranes can be electromodulated between cation and anion transporting states.

We have recently been investigating an alternative method for electromodulating transport in nanotube membranes.[42] This method entails attaching to the nanotubes a molecule that contains a redox-active ferrocene (Fc) substituent. With these redox-active nanotubes, excess cationic charge can be placed on the membrane by using the potential applied to the membrane to driving the following redox reaction:[42,143-145]

$$Fc \rightarrow Fc^{+} + e^{-} \qquad (2\text{-}1)$$

We have found that when the nanotube-bound Fc is oxidized to Fc^+, the flux of a cationic permeate species is suppressed relative to when the Fc is in its reduced state. While similar results have been achieved using membranes composed of redox-active conductive polymers,[146-148] this paradigm for gating ion transport has not been demonstrated for redox-active nanotube membranes. We describe the results of such redox-modulated transport experiments here.

Experimental

Materials

Polycarbonate filtration membranes (6 μm-thick, 30 nm- and 50 nm-diameter pores, $6x10^8$ pores cm^{-2}) were obtained from Osmonics Inc. Commercial gold-plating solution (Oromerse SO Part B) was obtained from Technic Inc. Na_2SO_3, $NaHCO_3$, NH_4OH, HNO_3, KCl, methanol and formaldehyde were obtained from Fisher and used as received. $SnCl_2$, methyl viologen dichloride hydrate, and 1,5-naphthalene disulfonic acid disodium salt hydrate were used as received from Aldrich, as were $KClO_4$, $AgNO_3$ and triflouoroacetic acid from Acros Organics, ethanol (absolute) from Aaper, and 11-ferrocenyl-1-undecanethiol from Dojindo Chemicals. Purified water was obtained by passing house-distilled water through a Millipore, Milli-Q system.

Electroless Gold Deposition

The electroless deposition or plating method described previously was used to deposit gold nanotubes within the pores of the nanopore polycarbonate membranes.[59] In general terms, this entails depositing gold along the pore walls so that each pore becomes lined with a gold nanotube. Briefly, the template membrane was first immersed into methanol for five minutes and then immersed for 45 min into a solution that was 0.025 M in $SnCl_2$ and 0.07 M in trifluoroacetic acid. This yields the Sn-sensitized form of the membrane.[17] The membrane was

then immersed into an aqueous ammoniacal $AgNO_3$ solution (0.029 M Ag^+) for 7.5 minutes and then immersed in methanol for 5 minutes. The gold plating bath was prepared by mixing 0.5 ml of the commercial gold-plating solution with 20 mL of an aqueous solution that was 0.127 M in Na_2SO_3, 0.625 M in formaldehyde, and 0.025 M in $NaHCO_3$. The bath pH was lowered to 10 by drop wise addition of 1 M H_2SO_4 prior to immersion of the membrane. During electroless deposition, the temperature of the bath was maintained at 4 ^oC. Membranes were placed in the gold-plating bath for different periods of time to obtain nanotubes of different inside diameters.[36,149] The inside diameter of the nanotube was determined using the gas-flux measurement described previously.[36]

Membrane Sample Preparation and Thiol Modification

The electroless-plating method yields the Au nanotubes lining the pore walls as well as thin Au films covering both faces of the membrane.[17] The Au films do not block the mouths of the nanotubes at the membrane faces and can be used to make electrical contact to all of the nanotubes in parallel.[39] This was accomplished by applying a copper tape with a conductive adhesive (3M, #1181) to the outer edge of one Au surface film.[17]

The membrane sample was prepared by sandwiching the nanotube membrane between two pieces of electrically insulating plastic tape (3M Scotch brand no. 375). Each piece of tape had a 0.2 cm^2-area hole punched through it, and the holes were aligned on either side of the membrane. This insulating tape also covered the conductive tape used to make electrical contact to the membrane. The end of the copper tape protruding from the membrane sample was used as the electrode lead for electrochemical experiments in which the membrane sample was the working electrode. Details of this electrode fabrication method can be found elsewhere in the literature.[17] The Au surface films and Au nanotube walls were modified with the thiol 11-ferrocenyl-1-undecanethiol, here after called Fc-thiol. This was accomplished by mounting the assembled

membrane sample between the two halves of a U-tube permeation cell[34,36,39] and filling both half-cells with a 2 mM solution of Fc-thiol dissolved in ethanol. The membrane sample was exposed to this solution for 20 h, followed by thorough washing with ethanol.

For some membranes, the Fc-thiol on the Au surface films was removed by brief (30 sec) exposure to a mild Ar plasma. A Samco model RIE-1C reactive-ion etch system was used. The plasma conditions were as follows: 13.56 MHz, 50 W, 10 Pa Ar pressure, Ar flow rate =12 sccm.

Electrochemical Experiments

Electrochemical experiments were done with the membrane sample mounted in the U-tube cell. Electrolyte solution was added to both half-cells, and the Au nanotube membrane was made the working electrode in a conventional three-electrode experiment. The counter electrode was a Pt wire and the reference was an Ag/AgCl electrode with 3 M NaCl. In the transport experiments one half-cell solution, the feed half-cell, contained the permeating species and the other half-cell received the permeating species. The reference and counter electrodes were placed in the feed half-cell. A Solartron SI 1287 electrochemical interface module (Solartron Analytical, Hampshire, England) connected to a PC running CorrView and CorrWare software (Scribner Asc. Inc., NC) was used.

Transport Experiments

The same U-tube cell was used for the transport experiments. The permeating specie investigated was the dication methylviologen (MV^{2+}). The feed half-cell was charged with 20 mL of a 20 mM aqueous MV^{2+} solution, and the receiver half-cell was charged with 20 mL of purified water. The flux of MV^{2+} from the feed half-cell, through the membrane and into the receiver half-cell was obtained by continuously measuring the UV absorbance (at 260 nm) of the receiver half-cell solution. A flow-through Agilent 8458 spectrophotometer was used.[34,39,150]

The data were processed as plots of moles MV^{2+} transported vs. time. Straight line plots were obtained, and the flux of the permeating ion was calculated from the slope.

Results and Discussion

Electrochemistry of the Fc-Thiol

Figure 2-1A shows a cyclic voltammogram for a Fc-thiol-modified Au nanotube membrane (nanotube inside diameter = 8 nm). The redox waves associated with the oxidation of the Fc to Fc^+ and the re-reduction back to Fc are clearly seen.[145,151-153] Figure 2-1B shows that the anodic peak current is linearly related to scan rate as would be expected for a surface-confined voltammogram.[154]

It is of interest to note, however, that there are in essence two different Au surfaces in these membranes - The Au on the inside walls of the nanotubes running through the membrane and the Au surface films on both faces of the membrane. If the number of moles of Fc obtained from the area under the anodic wave is divided by the total Au area (tube walls plus surface films), a coverage by Fc of 1.0×10^{-9} moles.cm^{-2} is obtained. This is about a factor of two larger than the value calculated from the footprint of the Fc molecule on an atomically flat Au surface.[145,153] The higher value obtained experimentally here simply reflects the surface roughness of our electrolessly deposited gold.

Figure 2-2 shows the effect of electrolyte on the stability of the Fc/Fc^+ redox couple. When KCl was used, the voltammogram current decayed continuously with scan number (Figure 2-2A). As has been discussed previously[153], this is due to nucleophilic attack of Cl^- on the Fe(III) center of Fc^+. As shown by the analogous set of 30 cyclic voltammograms in Figure 2-2B, the redox chemistry is much more stable in 0.1 M $KClO_4$.[153] This is because ClO_4^- is a poorer nucleophile than Cl^-. For long-term use, however, it is best to store the Fc-thiol-modified

membrane in its reduced (Fc) state. If this is done in the $KClO_4$ solution, Fc-thiol electrochemistry can be observed, unchanged, for periods of at least one week (Figure 2-3).

Figure 2-2 also shows that the oxidation of Fc-thiol proceeds at more negative potentials in $KClO_4$ than in KCl. Such effects have been observed previously for ferrocene-modified electrodes and have been attributed to the different extents to which the anions of the electrolyte form ion-pairs with Fc^+.[151,152] Fc^+ is a lipophilic cation, present in a lipophilic monolayer film, and therefore ion pairs preferentially with the more lipophilic ClO_4^-. This ion-pair interaction makes the oxidation thermodynamically easier in ClO_4^- vs. Cl^-. The shift in the position of the Fc-thiol voltammetric wave with time in KCl (Figure 2-2A) has also been observed previously, although no explanation was offered.[153] We suggest that as decomposition of the lipophilic cyclopentadienly ring occurs (with increasing scan number in KCl, Figure 2-2A) the monolayer film becomes less lipophilic, and this allows Cl^- to have greater ion-pairing access to the remaining intact Fc^+ groups.

Electromodulated Transport Experiments

A solution of the cationic permeating species MV^{2+} was placed on one side of the Fc-thiol-modified membrane, and the quantity of this species transported through the nanotubes and into the receiver solution on the opposite side was measured as a function of time (Figure 2-4). During the time interval from 0 to ~1700 sec, a potential of 0.7 V was applied to the membrane. At this potential the ferrocene is present as oxidized Fc^+, yielding excess positive charge on the nanotube walls and membrane faces. This charge causes MV^{2+} to be electrostatically repelled from the membrane, yielding the low-flux state for MV^{2+} transport. Complete exclusion of MV^{2+} is not observed because at the 20 mM salt ($MVCl_2$) concentration used in this experiment, the electrical double layer on the walls of the 10 nm-diameter nanotube does not completely fill the total nanotube volume. As we have discussed in detail previously,[39,40] this means that there

is a region in the center of the nanotube where MV^{2+} is not excluded, and transport occurs in the region.

At 1800 sec a potential of 0 V was applied to the membrane. At this potential the ferrocene on the nanotube walls, and membrane faces, is present as neutral Fc. Because there is now no excess positive charge on the membrane, MV^{2+} is not repelled, and a higher MV^{2+} flux (relative to the short time data) is obtained (data points for line 2, Figure 2-4). The slopes of the straight-line segments in Figure 2-4 provide the fluxes for MV^{2+} across the nanotube membrane. We define an "electromodulation-transport cycle" as a period when 0.7 V was applied (low flux state) followed by a period when 0 V was applied (high flux state). This allows us to define an electromodulated-transport selectivity coefficient (α) as the flux during the high-flux state (0 V) divided by the flux during the low-flux state (0.7 V). The larger the value of α, the greater is the electromodulated cation-gating effect.

Table 2-1 shows flux and α values for various cycle numbers for membranes with 10 and 16 nm-diameter Au nanotubes. Considering the flux data first, we see as would be expected, that the fluxes in the membrane with the larger-diameter nanotubes is higher. However, the selectivity for the membrane containing these larger diameter nanotubes is lower. Again, this is due to the fact that the electrical double layer that is responsible for repelling MV^{2+} fills a smaller fraction of the total nanotube volume for the larger diameter nanotube.[39,40]

The electromodulated selectivity coefficient, α , decreases with increasing cycle number (Table 2-1). Part of this decay in selectivity is due to the fact that the magnitude of the flux in the low-flux (Fc^{+}) state increases with each successive cycle. To understand the origins of this effect we obtained a cyclic voltammogram after each cycle, and from the area under the anodic wave obtained the moles of electroactive Fc remaining in the membrane (Figure 2-5). We see

that there is a steady drop in amount of electroactive Fc with cycle number. While this may at first seem to contradict the data in Figure 2-3, the key difference is that in Figure 2-3 the ferrocene was left in the neutral Fc state between cycles, and in Figure 2-5 the Fc was held in the charged Fc^+ for long periods (Figure 2-4) during each cycle. Because it is the Fc^+ state that is susceptible to nucleophilic attack,[155,156] electroactivity decays much more quickly in Figure 2-5 than in Figure 2-3.

This steady drop in electroactive Fc in the membrane with cycle number (Figure 2-5) explains why the selectivity decays with cycle number (Table 2-1). This is because it is the positively charged Fc^+ groups that repel MV^{2+}, and since the quantity of Fc^+ decreases with cycle number, the selectivity decreases with cycle number. The other factor causing the selectivity to decay with cycle number is that the magnitude of the flux in the high flux state decreases with cycle number (Table 2-1). This suggests that membrane fouling occurs. One possible source of membrane fouling is that the decomposition products that result from nucleophilic attack on the Fc^+ causes partial occlusion of the nanotubes.

Conclusions

We have shown that cation transport through Au nanotube membranes can be electromodulated by controlling the extent of oxidation of a Fc-thiol attached to the Au surfaces. We have defined an electromodulation selectivity coefficient for cation transport, α. As would be expected, higher α values are obtained for membranes containing smaller inside-diameter nanotubes. For the 10 nm-diameter nanotubes a maximum value of $\alpha = 9.4$ was obtained. It is possible to make smaller diameter nanotubes,[34] and it would be of interest to see if correspondingly higher selectivity coefficients could be obtained. Unfortunately, the electromodulated selectivity decreases with membrane use because when the Fc is present in the Fc^+ state it is susceptible to nucleophilic attack and decomposition. It is well-known that

decamethyl-ferrocence is less susceptible to this degradation pathway,[157,158] and for this reason would be a better choice for the nanotube-bound electromodulating agent.

Table 2-1. Flux and electromodulated selectivity coefficients (α) for membranes containing 10-nm and 16-nm diameter nanotubes.

Nanotube Diamater (nm)	Cycle Number	Low Flux nmole $min^{-1}cm^{2-}$	High Flux nmole $min^{-1}cm^{2-}$	α
10	1	1.2	11	9.4
10	2	1.5	11	7.3
10	3	2.0	10	5.1
16	1	6.4	38	5.9
16	2	7.3	38	5.2
16	3	7.8	34	4.3
16	4	8.3	32	3.8
16	5	9.5	28	2.9

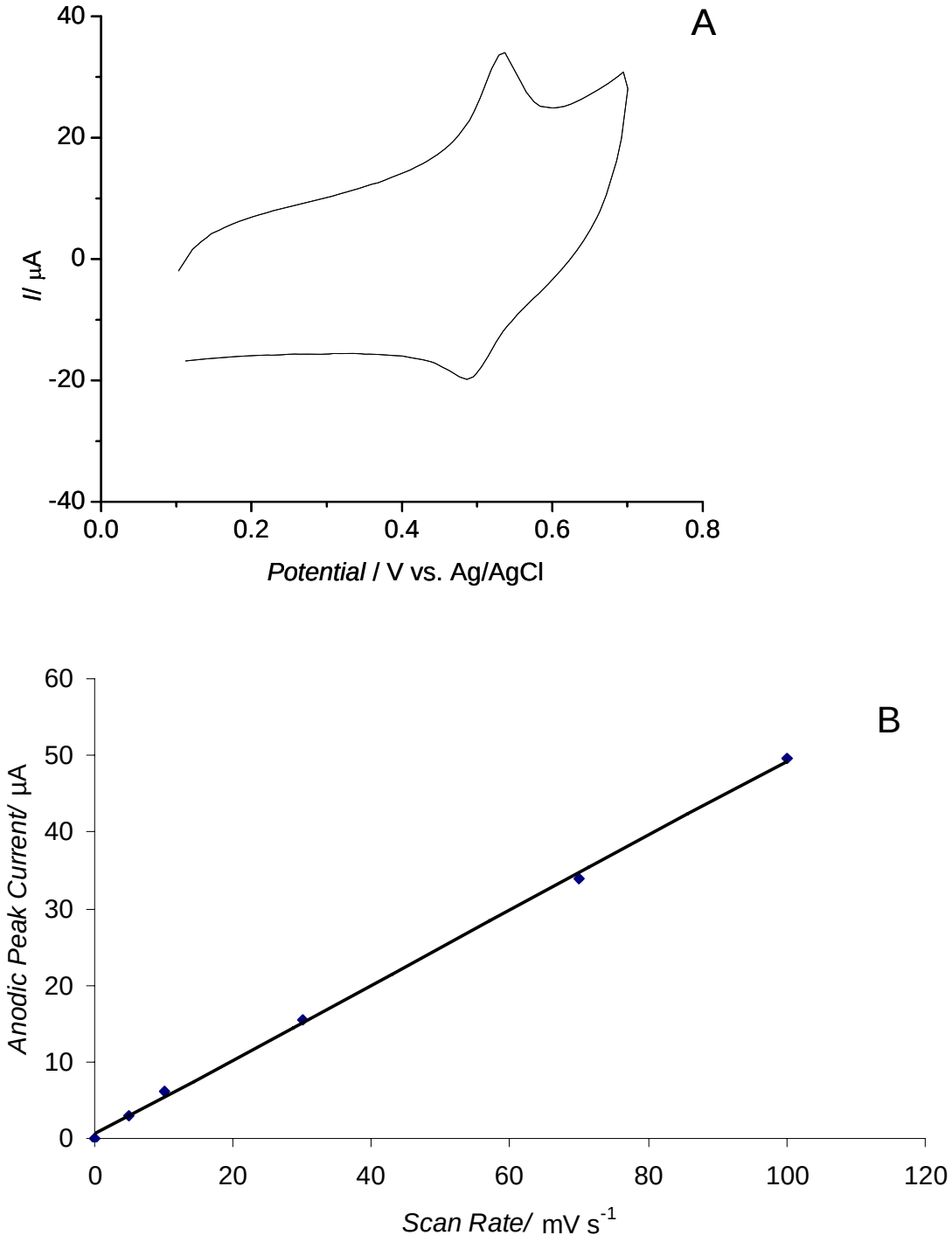

Figure 2-1. A) Cyclic voltammogram for a Fc-thiol-modified Au nanotube membrane with nanotube inside diameter = 8 nm. Scan rate = 70 mV s^{-1}. B) Anodic peak current from such voltammograms vs. scan rate. The electrolyte in both half-cells was 0.1 M KCl.

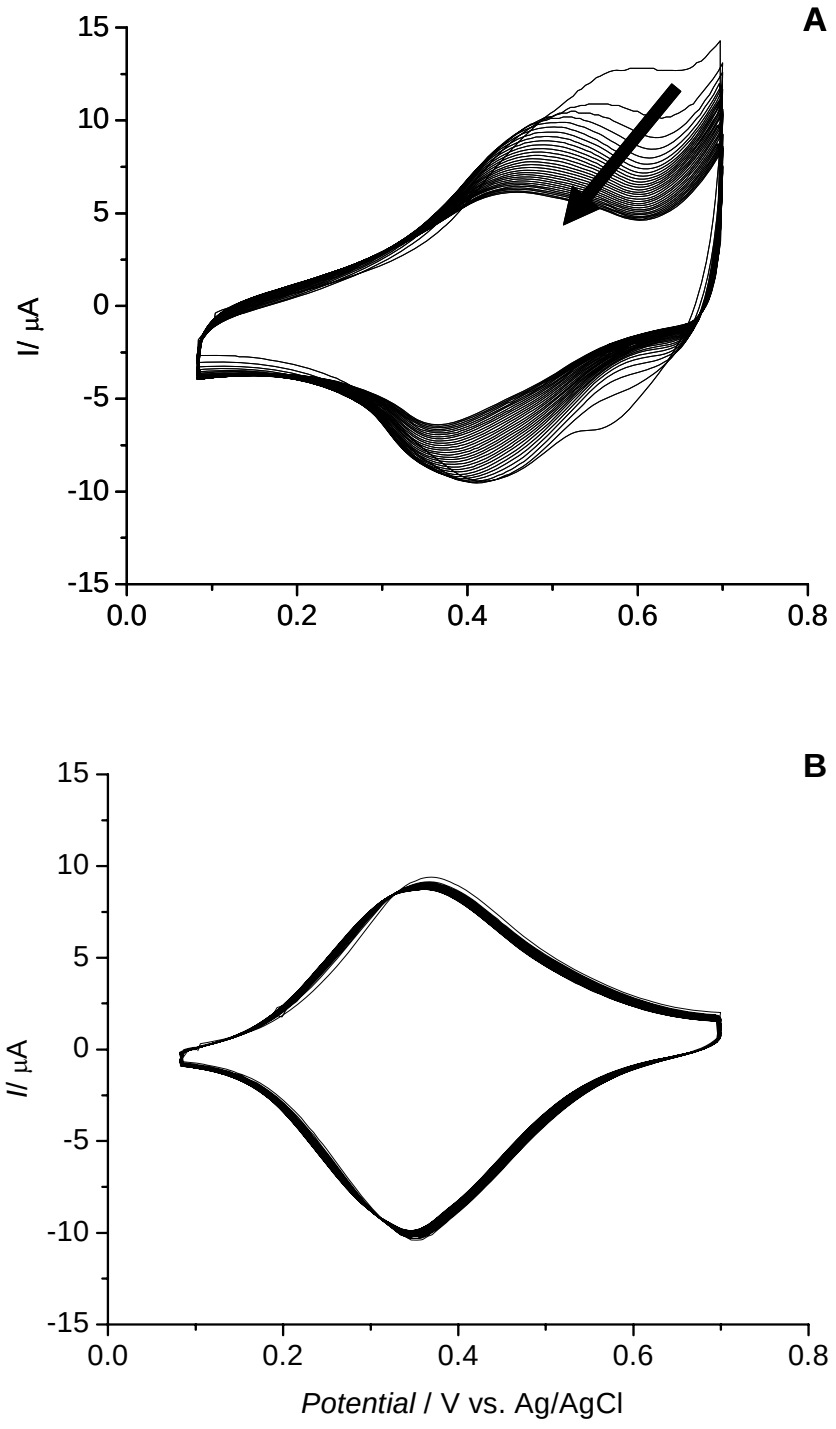

Figure 2-2. Effect of electrolyte on the stability of the Fc^{+}/Fc voltammogram. The potential was swept continuously through the voltammetric waves for 30 scans at 20 mV s^{-1}. The membrane contained nanotubes with inside diameter of 26 nm. A) Electrolyte was 0.1 M KCl. The arrow points in the direction of increasing scan number (scan 1 to scan 30). B) Electrolyte was 0.1 M $KClO_4$.

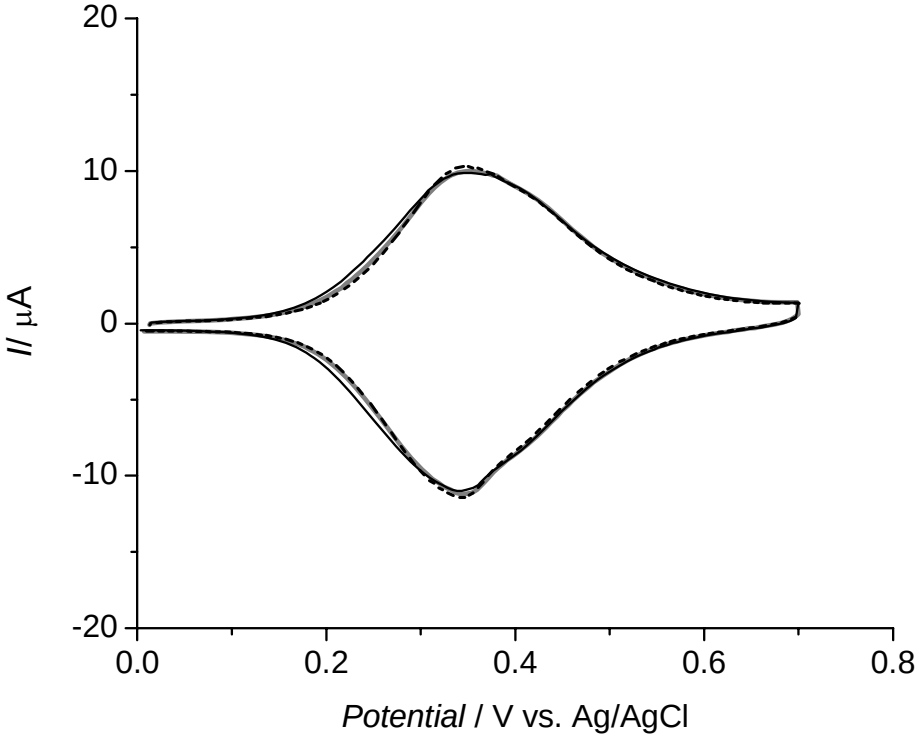

Figure 2-3. Investigation of the long term stability of the Fc-thiol layer. The Au nanotube membrane sample (nanotube inside diameter = 10 nm) was mounted in the U-tube cell with 0.1 M $KClO_4$ in both half-cells, and voltammograms were obtained after 2 days (solid black curve), 4 days (solid gray curve), and 6 days (dashed black curve) of storage unpotentiostated in the reduced (Fc) state. The half-cell solutions were not degassed and the U-tube cell was not protected from light.

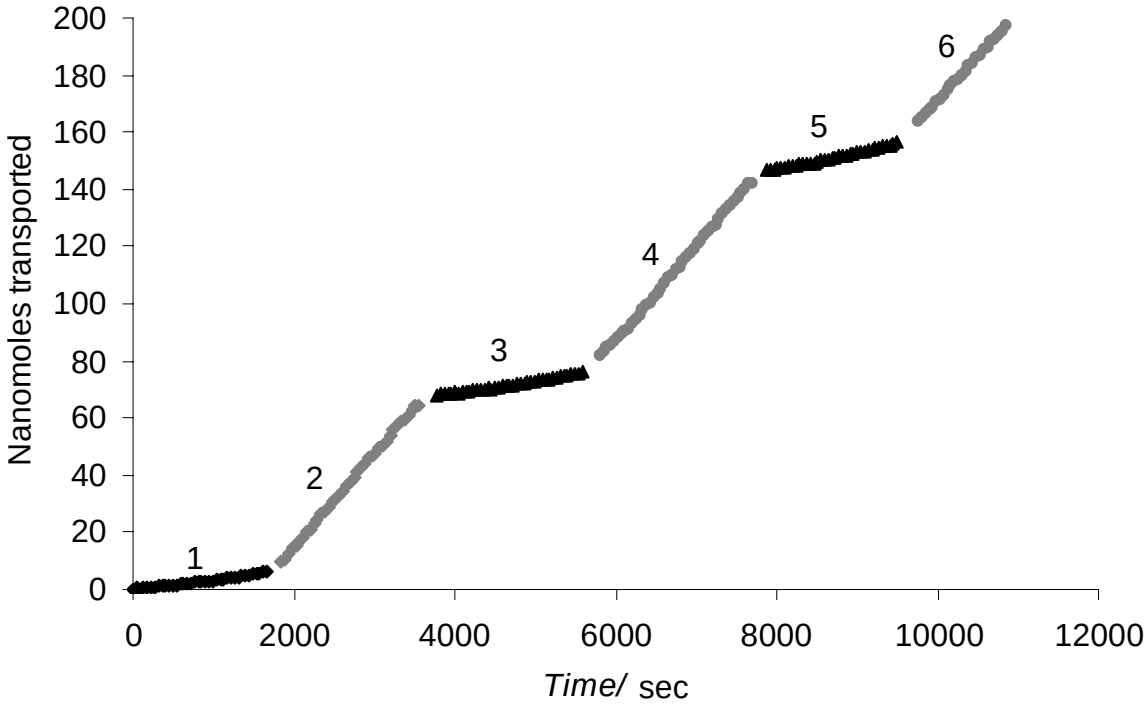

Figure 2-4. Plot of nanomoles of MV^{2+} transported across a nanotube membrane (nanotube inside diameter = 10 nm) vs. time. Data points for lines 1, 3 and 5 were obtained with a potential of 0.7 V vs. Ag/AgCl applied to the membrane. Data points for lines 2, 4 and 6 were obtained with a potential of 0 V vs. Ag/AgCl applied to the membrane. The slopes of these straight lines are used calculate to the flux of MV^{2+}. The feed solution was 20 mM in MV^{2+}.

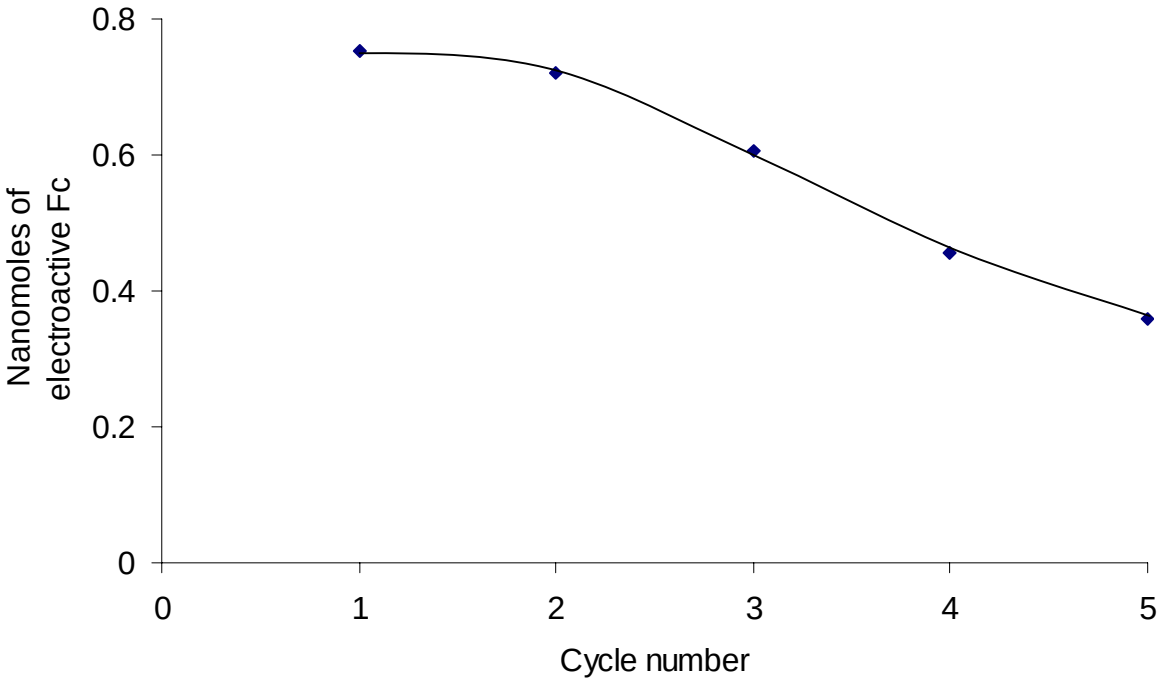

Figure 2-5. Moles of electroactive Fc vs. cycle number for a membrane containing 16 nm-diameter Au nanotubes.

CHAPTER 3
KINETICS OF FERRICINIUM DECOMPOSITION CONFINED WITHIN GOLD NANOTUBES- EFFECT OF THE NANOSCALE ENVIRONMENT ON KINETICS

Introduction

We have been investigating a general method for preparing nanomaterials called template synthesis.[3,4,6] This method entails synthesis of the desired material within the cylindrical and monodisperse pores of a nanopore membrane or other solid. Using this method, a new class of synthetic membrane was developed that contain monodisperse Au nanotubes with inside diameters that can be of molecular dimensions (<1 nm).[34,36-39,41] The Au nanotubes span the complete thickness of the membrane and can act as conduits for molecule and ion transport between solutions placed on either side of the membrane. We have been using these gold nanotube membranes to investigate how pore size, charge and chemistry affect transport selectivity in membranes. Of particular relevance to the work reported here, ion and chemical transport selectivity can be successfully introduced and modulated by chemisorbing thiols to the Au nanotube walls.[36,38,41]

We have recently reported an alternative method for electromodulating ion transport in Au nanotube membranes. This method entails chemisorbing to the Au nanotubes an alkyl thiol that contains a redox-active ferrocene (Fc) substituent. With this membrane system the charge density on the nanotube walls can be electromodulated Faradaically by using the potential applied to the Au nanotube membrane to control the position of equilibrium for the following redox reaction:[42,143-145]

$$Fc \rightarrow Fc^{+} + e^{-} \qquad (3\text{-}1)$$

We have found that when the nanotube-bound Fc is oxidized to Fc^{+}, the flux of a cationic permeate species is suppressed relative to when the Fc is in its reduced state. However, the flux difference between these states is lost with membrane use because when the Fc is present in the

Fc^+ state, it is susceptible to nucleophilic attack and decomposition.[153] The extent of Fc^+ decomposition is directly related to the strength of the nucleophile[155] and it is a first order decay in aqueous solutions.[159]

In this chapter, we report the results of nanotube pore size affect on Fc^+ decomposition. For this purpose, it was necessary to remove the Fc-thiol on Au surface films leaving only the Fc-thiol lining the Au nanotube walls. This was accomplished by briefly (30 sec) exposing both faces of the membrane to an argon plasma (mild conditions). The behavior of four membranes with different pore sizes were investigated and compared to the decay in commercial gold button electrode. The results suggest that the decay rate increases with increasing pore size and in all cases it is found to obey first order decay kinetics. Furthermore, the decay pattern resembles a surface-like decay as the pore size of the membrane increases.

Experimental

Materials

Polycarbonate filtration membranes (30 nm-, 50 nm-, 200 nm- and 600 nm- diameter pores) were obtained from Osmonics Inc. Commercial gold-plating solution (Oromerse SO Part B) was obtained from Technic Inc. Na_2SO_3, $NaHCO_3$, NH_4OH, HNO_3, methanol and formaldehyde were obtained from Fisher and used as received. $SnCl_2$ was used as received from Aldrich, as were $KClO_4$, $AgNO_3$ and triflouoroacetic acid from Acros Organics, ethanol (absolute) from Aaper, and 11-ferrocenyl-1-undecanethiol from Dojindo Chemicals. Purified water was obtained by passing house-distilled water through a Millipore, Milli-Q system.

Electroless Gold Deposition

The electroless deposition or plating method described previously was used to deposit gold nanotubes within the pores of the nanopore polycarbonate membranes.[59] In general terms, this entails depositing gold along the pore walls so that each pore becomes lined with a gold

nanotube. Briefly, the template membrane was first immersed into methanol for five minutes and then immersed for 45 min into a solution that was 0.025 M in $SnCl_2$ and 0.07 M in trifluoroacetic acid. This yields the Sn-sensitized form of the membrane.[17] The membrane was then immersed into an aqueous ammoniacal $AgNO_3$ solution (0.029 M Ag^+) for 7.5 minutes and then immersed in methanol for 5 minutes. The gold plating bath was prepared by mixing 0.5 ml of the commercial gold-plating solution with 20 mL of an aqueous solution that was 0.127 M in Na_2SO_3, 0.625 M in formaldehyde, and 0.025 M in $NaHCO_3$.

The bath pH was lowered to 10 by drop wise addition of 1 M H_2SO_4 prior to immersion of the membrane. During electroless deposition, the temperature of the bath was maintained at 4 °C. Membranes were placed in the gold-plating bath for different periods of time to obtain nanotubes of different inside diameters.[36,149] The inside diameter of the nanotube was determined using the gas-flux measurement described previously[36] where the pore diameter was < 50 nm. For bigger pores, electron micrographs of the pores obtained via Hitachi S4000 FE-SEM were used to calculate the pore diameter. Gold nanotube membranes with pore diameters 10 ± 2.0, 28 ± 2.6, 65 ± 7.5, and 284 ± 20 nm were used in this work.

Membrane Sample Preparation and Thiol Modification

The electroless-plating method yields the Au nanotubes lining the pore walls as well as thin Au films covering both faces of the membrane.[17] The Au films do not block the mouths of the nanotubes at the membrane faces and can be used to make electrical contact to all of the nanotubes in parallel.[39] This was accomplished by applying a copper tape with a conductive adhesive (3M, #1181) to the outer edge of one Au surface film.[17]

The membrane sample was prepared by sandwiching the nanotube membrane between two pieces of electrically insulating plastic tape (3M Scotch brand no. 375). Each piece of tape had a 0.2 cm^2-area hole punched through it, and the holes were aligned on either side of the membrane.

This insulating tape also covered the conductive tape used to make electrical contact to the membrane. The end of the copper tape protruding from the membrane sample was used as the electrode lead for electrochemical experiments in which the membrane sample was the working electrode. Details of this electrode fabrication method are described elsewhere in the literature.[17] The Au surface films and Au nanotube walls were modified with the thiol 11-ferrocenyl-1-undecanethiol, here after called Fc-thiol. This was accomplished by mounting the assembled membrane sample between the two halves of a U-tube permeation cell[34,36,39] and filling both half-cells with a 2 mM solution of Fc-thiol dissolved in ethanol. The membrane sample was exposed to this solution for 20 h, followed by thorough washing with ethanol. A commercial gold button electrode (Bioanalytical Systems, Inc. IN) was modified under the same conditions after being polished with alumina nanoparticles.

Surface Thiol Removal

The Fc-thiol modified gold nanotube membrane sample was placed into the vacuum chamber of a reactive-ion etching system (Samco model RIE-1C). The plasma conditions were - 13.56 MHz, 50 W, 10 Pa Ar pressure, Ar flow rate =12 sccm. In order to confirm the removal of Fc monolayer from the membrane surface, we have used a Kratos Analytical Surface Analyzer XSAM 800 with a Mg source that is normal to the sample surface. This instrument was used to detect the surface Fe $2p_{3/2}$ peak for membranes before and after Ar plasma etching for different etching times.

Electrochemical Experiments

After the plasma etching, the membrane was washed with ethanol and water and then subjected to electrochemical experiments. Electrochemical experiments were done with the membrane sample mounted in the U-tube cell. 0.1 M $KClO_4$ electrolyte solution was added to both half-cells, equilibrated for 1-2 days and bubbled with Argon for 30 minutes before the

experiment. Argon was also purged into the system throughout the experiment. The Au nanotube membrane was made the working electrode in a conventional three-electrode experiment where the counter electrode was a Pt wire and the reference was an Ag/AgCl electrode with 3 M NaCl. A Solartron SI 1287 electrochemical interface module (Solartron Analytical, Hampshire, England) connected to a PC running CorrView and CorrWare software (Scribner Asc. Inc., NC) was used.

In order to observe and calculate the decay in the Fc^+, the membrane sample was held at 0.7 Volts for ~ 6 hours during which cyclic voltammograms (CVs) were taken periodically. The cathodic half cycles of these CVs were then used to calculate the amount of redox-active Fc for each CV. The same conditions were also applied to Fc-thiol modified gold button electrode which was not exposed to any plasma treatment.

Results and Discussion

Surface Fc-Thiol Removal

In order to study the effect of pore size on Fc^+ decay, we needed a technique to remove all Au surface Fc but do not destroy the Fc-thiol lining the Au nanotube walls. We have first used O_2 plasma conditions, but it removed nonspecifically all Fc-thiol from the gold membrane even at short times under mild conditions. Ar plasma etching, however, proved to be useful to selectively remove the surface Fc-thiol monolayer. Figure 3-1 shows the cyclic voltammograms of freshly modified membranes before and after the Ar plasma treatment with different etching times. In order to find the minimum etching time that is necessary to remove Au-surface Fc-thiols, we have used membranes that have pores filled with Au. Since these membranes can not have any Fc-thiol inside the pores, a successful plasma removal should show no sign of Fc in the voltammogram. This is achieved at 30 seconds (Figure 3-1B) and further proved by XPS studies (Figure 3-2, Curve C). The Fe $2p_{3/2}$ peak at 711 ev disappears even after 5 seconds (Figure 3-2,

Curve B) although the voltammogram (Figure 3-1A) still shows some trace which indicates the greater sensitivity of the CV method.

When these conditions were applied to a membrane with open pores, the plasma removes surface Fc monolayer and leaves the Fc monolayer inside the Au nanotube walls. Figure 3-3 shows the voltammograms of a membrane before and after plasma treatment. This membrane has pores with 20 nm inside pore diameter. In this case the amount of redox-active Fc is decreased by 40 %, which is equivalent to the relative amounts of Au surface-film vs. Au nanotube-wall surface area (assuming cylindrical pores of 10 nm radius). Voltammograms like Figure 3-3 (solid line) were also used to calculate the surface coverage of ferrocene. The coverage for all membrane systems were ~ 2 times the predicted packing limitation of 4.5×10^{-10} mol/cm^2,[145,160] which is due to the rough surface structures of electroless plated gold membranes.[161]

Electrochemical Decay Studies

Figure 3-4 shows cyclic voltammograms of four membranes with different inside pore diameters that are subjected to 0.7 Volts for ~ 6 hours. The same conditions were also applied to a Fc-thiol modified commercial gold button electrode to compare the Fc decomposition for a flat surface with no pores (Figure 3-5). The spiky peaks observed in Figure 3-5 suggest that there are strong attractive interactions in this environment.[162] Examination of CVs in Figures 3-4 and 3-5 indicates that the bigger the pore size the faster the decay and the more it resembles a flat-surface-like behavior. For pore sizes ≤ 65 nm, there is clearly a negative shift with increasing time which is most pronounced for R = 10 nm (Figure 3-4A). We suspect that the mild hydrophobicity of Fc-thiol is responsible for this observation. We and others[163] have obtained contact angles (θ) < 80° for Fc terminated alkane thiol monolayers on gold surfaces where as SAMs formed by long-chain alkane thiols have θ values of ~ 115°.[164]

This shift in the CVs to more negative potentials as it decays indicates that the environment around the Fc groups becomes more hydrophilic with increasing scan number. This has been observed before, and indicates that with prolonged scanning the Fc/Fc^+ groups in the monolayer film become more accessible to water and counterions.[165] The hydrophobicity is most pronounced with the smallest pore because the volume of the Fc-thiol that is filling the pore has the biggest ratio in the R =10 nm case. As the pore size gets bigger this ratio gets smaller. There is no clear shift where R = 284 nm (Figure 3-4D). In this case the hydrophobic contribution is minimal and the Fc groups are already accessible to water and counterions as there is no clear shift just similar to the flat surface gold electrode.

In order to compare the decay constants, semi logarithmic plots of normalized cathodic charge against time[166] were examined (Figure 3-6). Linear plots were obtained for each system, obeying the first order decay kinetics that is previously observed in aqueous solutions for ferricinium.[159,166] Studies in aqueous solution have shown that ferricinium cations (Fc^+) decompose through an exchange of cyclopentadienyl anions (Cp^-) with another nucleophile. (e.g., OH^-, Cl^-, NO_3^-)[153,155,156] The rate of exchange increases with the donor strength of the nucleophile. The decomposition of Fc^+ can be summarized as follows:[155]

$$FeCp_2^+ + n\ L \Leftrightarrow FeL_n^{3+} + 2\ Cp^- \qquad (3\text{-}2)$$

assuming that in a primary step ligand exchange around the Fe (III) ion occurs. In this reaction L can be a solvent molecule, a neutral nucleophilic agent or a monovalent anion. The Cp^- can then reduce undissociated $FeCp_2^+$ to $FeCp_2$ in a follow-up reaction and Cp radicals form.

Fc^+ decomposition is observed in electrolytes containing perchlorate anion.[153,163] It is found that increasing the pH increases the extent of decomposition substantially which is due to the increased concentration of hydroxide ion.[153] In the current system, both ClO_4^- and OH^- can

initiate the Fc^+ decomposition although the latter has a much smaller concentration ($[ClO_4^-]$ = 0.1 M and $[OH^-] = 2.0 \times 10^{-6}$ M). Table 3-1 shows the increase in decay constants with increasing pore size. This constant approaches to that of a flat gold surface for R = 285 nm. As mentioned above, the increasing accessibility of water and counterions to Fc groups with increasing pore size should be a factor in such an observation.

More importantly, the tendencies of ClO_4^- vs. OH^- towards an alkane-like environment are different. Extraction of ion-pairing complexes of perchlorate into organic phases is a well defined technique to detect trace amounts of perchlorate in aqueous samples.[167-169] In this case, perchlorate being a weak lipophilic nucleophile is the dominant anion inside the alkane-like environment of the small pores which results in slower decay rates. As the pore gets larger and more hydrophilic, OH^- (strong nucleophile) partitioning into that pore increases and thus the rate constant gets bigger. Other potential nucleophile in this system is water, but its donor strength is insufficient for Fc^+ decomposition.[155,170] It is also interesting to note that the decay constants of ferrocene and 1,1–dimethyl ferrocene molecules in bulk aqueous phosphate buffer has similar values[166] as the Fc monolayers studied in this work (Table 3-1).

Conclusion

Recently, we have shown the affect of Fc^+ decomposition on electromodulating ion transport through gold nanotube membranes.[43] In this paper, we have elucidated the nanotube pore size affect on Fc^+ decomposition. Fc-thiol monolayers on Au surface film were successfully removed by briefly exposing both surfaces of the membrane to argon plasma. The decomposition of Fc^+ inside the Au nanotube walls were then studied for four membranes with different pore sizes and compared with a flat surface electrode. The results suggest that the decay rate increases with increasing pore size and in all cases it is found to obey first order decay

kinetics. Furthermore, the decay pattern resembles a surface-like decay as the pore size of the membrane increases.

We suspect that limited accessibility of the counterions inside the small pores and their different tendencies towards a lipophilic environment are responsible for the slower decay rate. This is due to the constrained geometry of these small pores and the more pronounced hydrophobic character of Fc- thiol monolayers. As the pore size gets bigger, both of these affects are lost and the membrane behaves just like a flat-surface electrode. The negative shift in the voltammograms was also more pronounced for smaller and more hydrophobic pores. This shift in the CVs to more negative potentials as it decays indicates that the environment around the Fc groups becomes more hydrophilic with increasing scan number.

Table 3-1. Fc^+ decay constants for different membrane systems and for bulk aqueous solutions of Fc compounds in phosphate solutions at neutral pH.[166]

Case Studied	Decay Constant (sec^{-1})
R = 10 nm	0.7×10^{-5}
R = 28 nm	0.9×10^{-5}
R = 65 nm	1.4×10^{-5}
R = 284 nm	1.9×10^{-5}
Gold Button Electrode	2.1×10^{-5}
Ferrocene	1.4×10^{-5}
1,1'-dimethyl ferrocene	0.6×10^{-5}

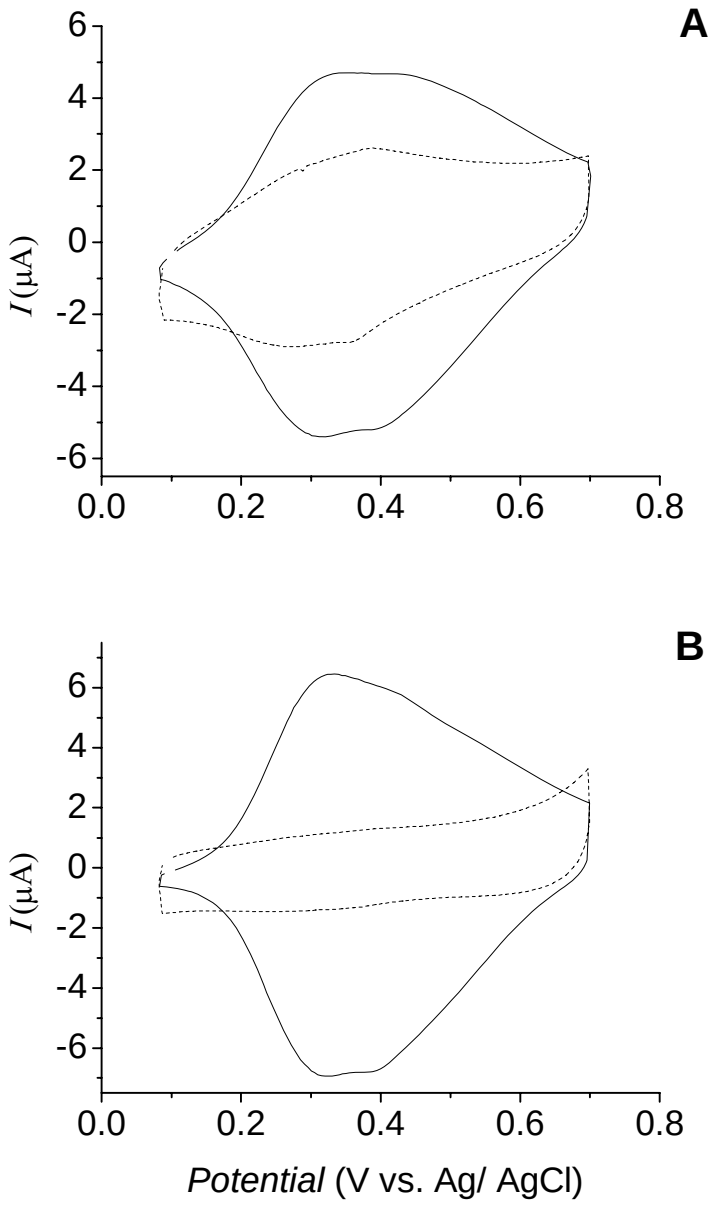

Figure 3-1. Finding the optimum etching time for surface Fc-thiol removal. Cyclic voltammograms of Fc –thiol modified gold nanotube membranes before (solid curves) and after (dashed curves) Argon plasma etching. The electrolyte is 0.1 M $KClO_4$ and the membranes have pores filled with gold. Increasing the Argon etching time from A) 5 sec to B) 30 sec removes all Surface-Fc.

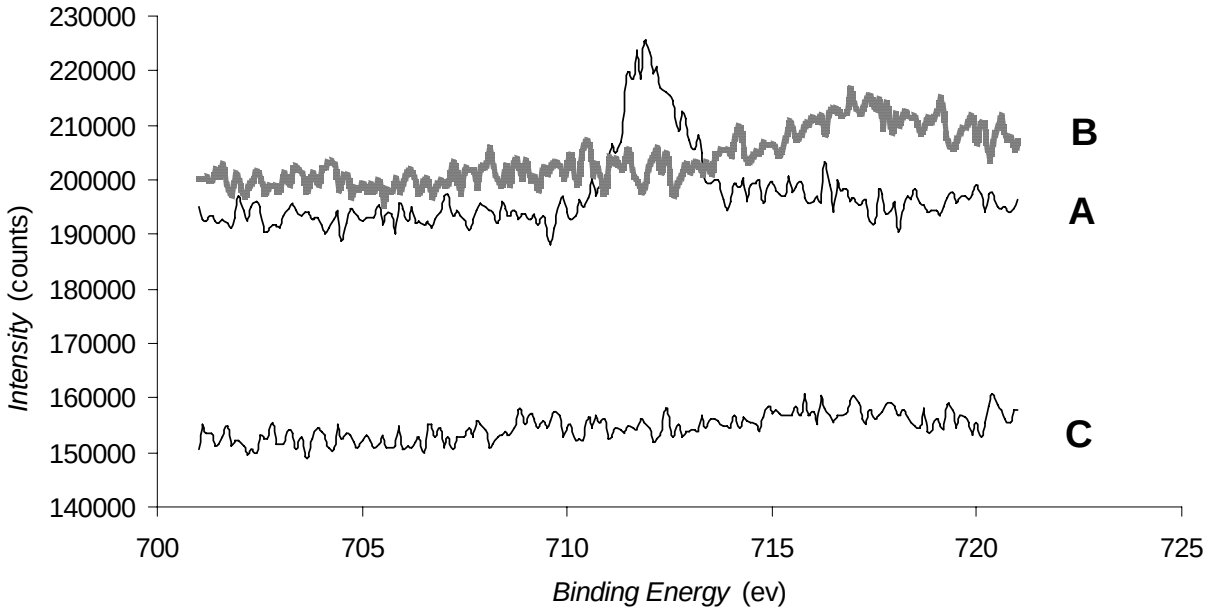

Figure 3-2. XPS spectra of the Fc-thiol modified gold membrane after A) 0 sec, B) 5 sec and C) 30 sec of Argon plasma etching. The Fe $2p_{3/2}$ peak is detected at 711 eV and it disappears even after 5 second etching. A Kratos XSAM surface analyzer with a Mg source normal to the membrane surface has been used. The gold membrane is plated overnight to fill the pores with gold completely.

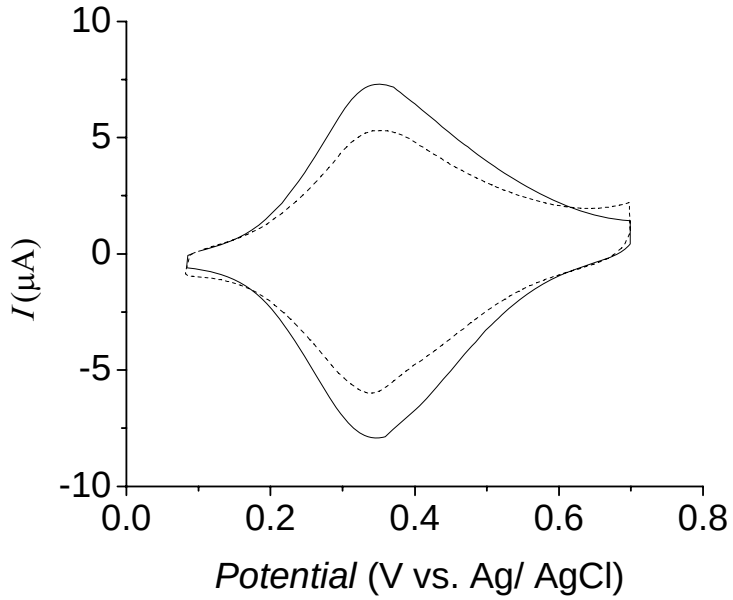

Figure 3-3. Cyclic voltammograms of a Fc-thiol modified membrane before (solid curve) and after (dashed curve) 30 sec of Argon plasma etching. The membrane has pores with 20 nm inside pore diameter. The dashed curve corresponds to Fc-thiol monolayer lining only inside the nanotube walls.

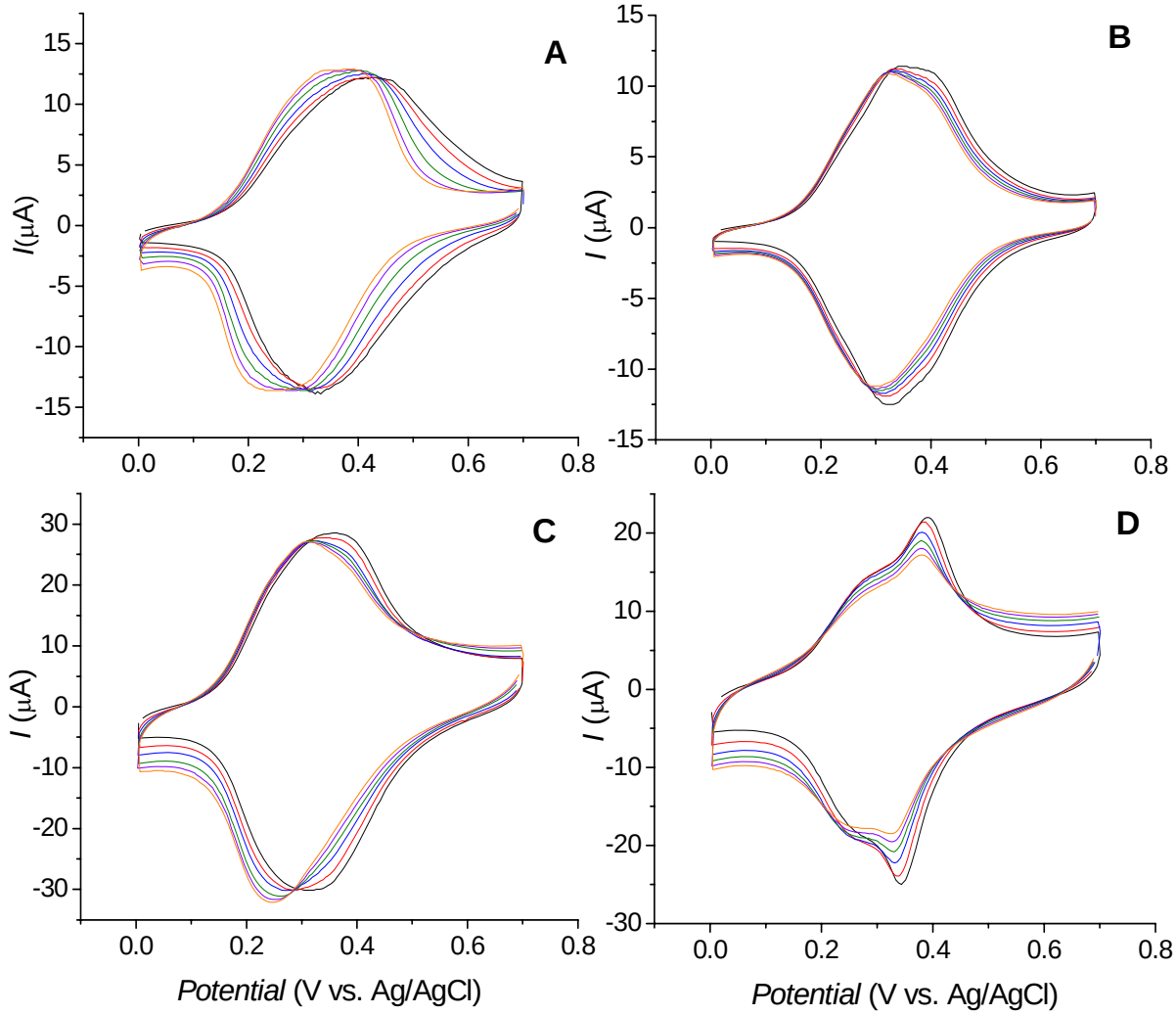

Figure 3-4. Cyclic voltammograms of four different gold nanotube membranes with pore diameters A) R = 10 nm, B) R = 28 nm, C) R = 65 nm, and D) R = 284 nm. Scans were recorded sequentially after holding E_{app} at 0.7 V for 0 min (black), 35 min (red), 105 min (blue), 175 min (green), 245 min (violet) and 315 min (orange). Scan rate is 20 mV/sec.

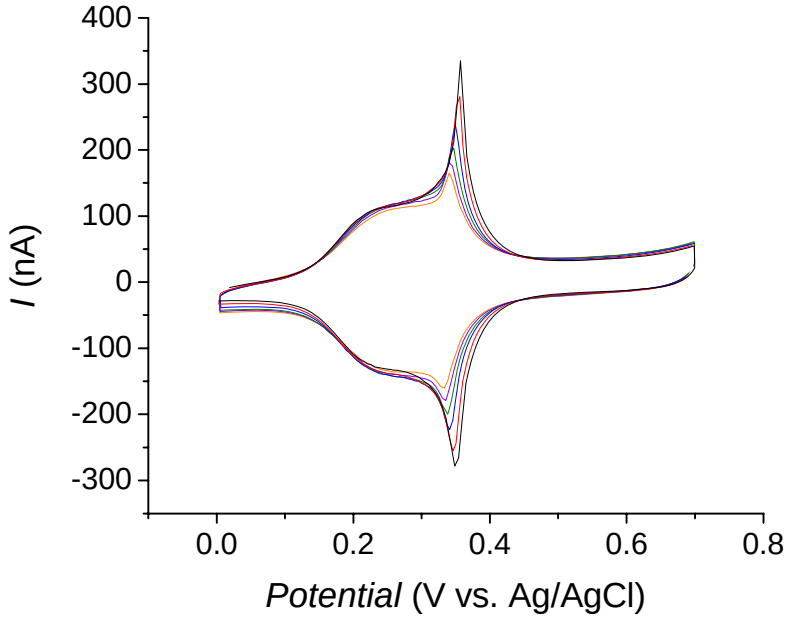

Figure 3-5. Cyclic voltammograms of modified gold button electrode. Scans were recorded sequentially after holding E_{app} at 0.7 V for 0 min (black), 35 min (red), 105 min (blue), 175 min (green), 245 min (violet) and 315 min (orange). Scan rate is 20 mV/sec.

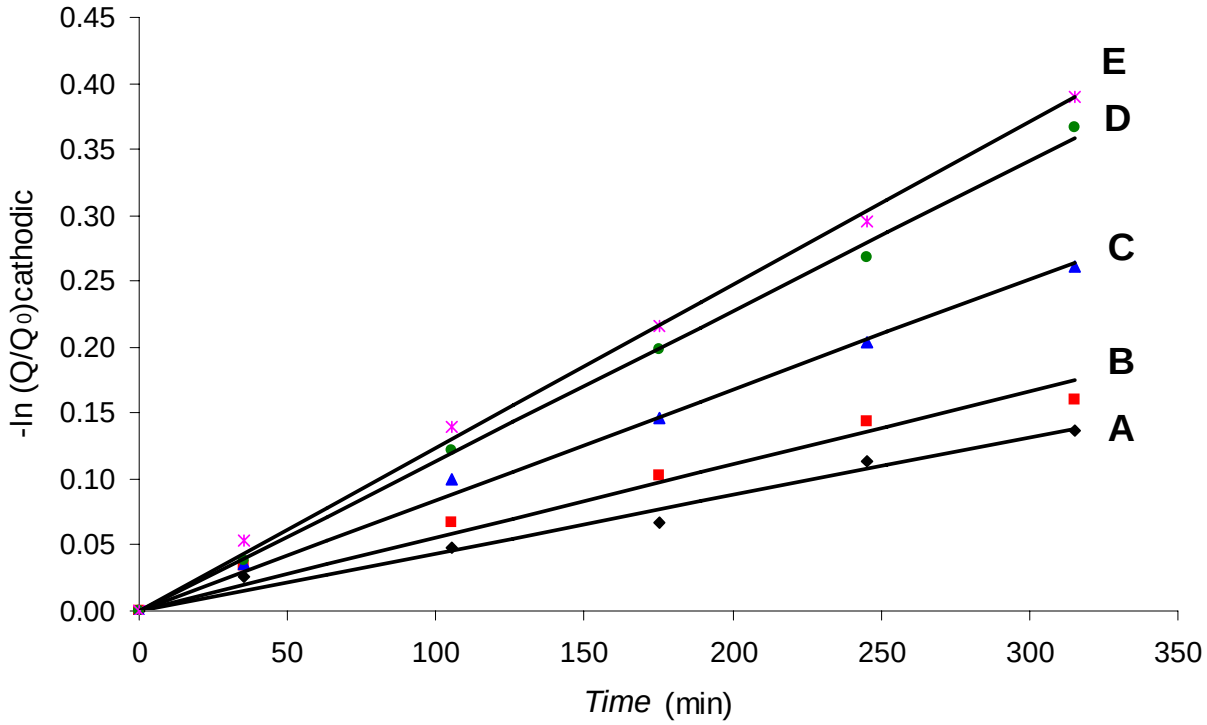

Figure 3-6. First order kinetic plots for the loss of the Fc^+ for A) R = 10 nm, B) R = 28 nm, C) R = 65 nm, D) R = 284 nm and E) gold button electrode.

CHAPTER 4
PLASMA-ETCHED NANOPORE POLYMER FILMS AND THEIR USE AS TEMPLATES TO PREPARE NANO TEST TUBES

Introduction

We recently introduced a new class of tubular nanostructures called nano test tubes.[47,48] Unlike conventional nanotubes, which are open at both ends, nano test tubes are open on one end and closed on the other. They are made by the template-synthesis method, in which the pores in a nanopore material are used as templates to prepare nanotubes.[3,4,6] The key to obtaining nano test tubes is using a template in which the pores are closed on one end (Figure 4-1A). When the tube-forming material is deposited within such pores, both the pore walls and the closed pore end get coated with this material, and closed-end test tubes are obtained. The outside diameter of these nano test tubes is determined by the pore diameter of the template, and the length of the tubes is determined by the template thickness.[47]

Nanopore alumina films, prepared by electrochemical oxidation of Al metal,[76,171] have pores that are closed on one end, provided the alumina is not removed from the underlying Al surface.[18] In our prior work, we used such alumina films as templates to prepare silica nano test tubes.[47] There is, however, a limitation with regard to the dimensions of the nano test tubes that can be obtained with these nanopore alumina templates. Specifically, it is difficult to obtain short (<500 nm long) test tubes. This is because such short nano test tubes require ultra-thin alumina templates, which means that very brief anodization times must be used. However at very short times, anodization of aluminum shows irregular growth patterns and the resulting alumina film does not have a regular pore structure.[71]

Our motivation for making smaller nano test tubes comes from our interest in investigating uptake of such tubes by living cells, with the ultimate goal of using these tubes as drug- or DNA-delivery vehicles. We believe that for such applications it would be advantageous to have tubes

that are small in length relative to the dimensions of the cell. Because of this limitation with the alumina templates, we have been investigating methods for preparing thinner nanopore templates so that shorter nano test tubes might be obtained. One such method builds on Masuda's concept of using a nanopore alumina membrane as a plasma etch mask.[172,173] This technology entails removing a nanopore alumina film from the underlying Al surface so that the pores are open at both faces of the resulting alumina membrane. The free-standing alumina membrane is then placed on a substrate, and a plasma is used to etch a replica of the alumina pore structure into the surface of the substrate (Figure 4-1B). We have used this method to prepare nanopore carbon anodes for battery applications[18] and nanowell glass surfaces for applications in analytical chemistry.[70,174]

We have recently modified this mask/etch technology so that it can be used to produce pores in an underlying polymer (photoresist) film, as opposed to the harder materials (glass,[70,174] diamond,[172,173] graphite[18]) etched previously. Furthermore, we have shown that with this modified mask/etch method the distance that the pores propagate into the photoresist film can be controlled by varying the etch time. Hence, by controlling the etch time, we effectively control the thickness of the nanopore layer etched into the surface of the photoresist. We have used such plasma-etched nanopore photoresist films as templates to prepare silica nano test tubes. As expected the length of the test tubes is determined by the thickness of the porous photoresist layer, and test tubes with lengths of 380 nm were obtained, shorter than any test tubes obtained using an alumina template.[47] We report preliminary results of these investigations here.

Experimental

Materials

Aluminum foil (99.99%) was obtained from Alfa Aesar, and microscope premium finest glass slides from Fisher. PMGI SF 15, a polydimethylglutarimide-based positive photoresist,

was purchased from MicroChem Corp. Ethanol (absolute, Aaper), tetraethyl orthosilicate (Aldrich), HCl (Fisher), and 1165 Microposit Remover (a 1-methyl-2-pyrolidinone-based system for dissolving the PMGI photoresist, Shipley) were used as received. Purified water was obtained by passing house-distilled water through a Millipore, Milli-Q system.

Preparation of the Nanopore Alumina-Membrane Masks

The nanopore alumina membranes were prepared in house using the well-known two-step electrochemical anodization method.[18] Briefly, after annealing and polishing the aluminum foil, a nanopore alumina film was formed across the Al surface by anodization. This film was then dissolved in acidic CrO_3, and a second anodized alumina film was formed. This film was removed from the underlying Al surface using the voltage-reduction method.[175] The resulting free-standing nanopore alumina membrane has two faces - the one that was exposed to the solution, and the one that was adjacent to the Al substrate, during anodization. These faces are not identical,[18] and we delineate them, here, as the solution-side and the Al-side faces. The pore diameter, as determined from scanning electron microscopic (SEM) images of the solution-side face (Figure 4-2A), was 79±7 nm. The alumina membrane thickness was ~1.5 μm (Figure 4-2B). SEMs were obtained using a Hitachi S4000 FE-SEM. Prior to imaging, the surface of the SEM sample was sputtered with a thin Au/Pd film using a Desk II Cold Sputter instrument (Denton Vacuum, LLC).

Preparation of the Nanopore Polymer-Replica Films

Glass microscope slides (2 cm x 2 cm) were washed with copious amounts of ethanol and blown dry with nitrogen. A Model 6700 spincoater (Speedline Technologies, IN) was used to coat one surface of the slide with the PMGI SF 15 photoresist; ~2 ml of the photoresist were dispensed, the terminal spin speed was 10,000 rpm, and the spin time was 45 sec. The resulting polymer film (~4 μ thick) was cured in air at 190 °C for 15 minutes.

As per our prior work,[18,70] the general strategy was to place the nanopore alumina-membrane mask onto the surface of the polymer film, and use a plasma-etch method to "burn" a replica of the alumina pore structure into the polymer surface (Figure 4-1B). However, we discovered that when the alumina mask was placed directly on top of the polymer film, a replica of the alumina pore structure could not be obtained; instead, large diameter (~500 nm) pits were burned into the surface of the polymer film. In order to obtain a faithful replica, it proved necessary to sputter-coat the polymer film with a thin metal film, and then place the nanopore alumina-membrane mask on this metal film (Figure 4-3). Three different metals - Au, Ag, and Au/Pd - were investigated, with the best results obtained with Au/Pd. The Au/Pd films were sputtered using the Desk II Cold Sputter instrument, with 45 mA sputtering current, 75 mTorr Ar pressure, and 60 sec sputtering time. The film thickness was ~30 nm.

The alumina-membrane mask was placed on top of the Au/Pd-coated polymer film with the solution-side face of the membrane facing down. The masked substrate was placed into the vacuum chamber of a reactive-ion etching system (Samco model RIE-1C) and subjected to two plasma-etch treatments. The first was a 2-minute Ar-plasma etch (physical etch,[111]). The plasma conditions were - 13.56 MHz, 140 W, 10 Pa Ar pressure, Ar flow rate =12 sccm. The second etch was a chemical etch[111,176]using an O_2/Ar- plasma. The plasma conditions were - 13.56 MHz, 140 W, 10 Pa O_2 pressure, O_2 flow rate = 10 sccm, 10 Pa Ar pressure, Ar flow rate = 12 sccm.

Preparation of the Silica Nano Test Tubes

A key objective of this work was to show that the pores in these nanopore polymer-replica films could be used as templates to prepare nano test tubes. To demonstrate this, a sol-gel method described previously[47] was used to deposit silica nano test tubes within the pores of the polymer-replica films. Briefly, a 50/5/1 (by volume) mixture of ethanol, tetraethyl orthosilicate

and 1M HCl was prepared and allowed to hydrolyze for 30 min. The nanopore polymer-replica film was immersed into this sol (PMGI SF 15 is insoluble in ethanol) with sonication for 30 sec and then kept under vacuum in a desiccator for 5 more minutes. The sol-impregnated film was dried in air, and then oven cured for ~5 h at 100 °C, to yield silica nano test tubes[47] within the pores of the polymer-replica film.

To liberate the nano test tubes, the nanopore polymer-replica film was dissolved by overnight immersion in the 1165 Microposit Remover solution. The liberated test tubes were collected by filtration and rinsed with copious amounts of the remover and ethanol. Transmission electron microscopy (TEM) samples were prepared by re-suspending the liberated nano test tubes in ethanol and immersing a TEM grid into this suspension. TEM images were obtained with a Hitachi H-7000 microscope.

Results and Discussion

As noted above, it proved necessary to coat the surface of the polymer film with a thin Au/Pd layer prior to applying the alumina etch mask and plasma etching. The alumina-mask:Au/Pd:polymer-film assembly (Figure 4-3) was then first etched with an Ar plasma (physical etch).[111] This brief Ar-plasma etch removes the portions of the Au/Pd film beneath the pores in the nanopore alumina mask. Put another way, the Ar plasma creates a replica of the alumina pore structure in the Au/Pd film, and thus exposes the portions of the polymer film in the regions beneath the alumina pores. The assembly (Figure 4-3) was then subjected to an O_2/Ar plasma (chemical etch)[111] to remove the exposed portions of the polymer film beneath the alumina pores; *i.e.,* the O_2/Ar plasma is responsible for replicating the pore structure of the mask in the polymer film.

Figure 4-4 shows surface and cross-sectional images of the polymer film after four minutes of etching with the O_2/Ar-plasma. Some reproduction of the pore structure of the alumina-mask

can be seen in the surface image (Figure 4-4A), but the pores propagate only a very small distance into the polymer film (Figure 4-4B). Analogous images after 8 minutes of etching with the O_2/Ar-plasma show that the pore structure has been faithfully reproduced in the surface of the polymer film (Figure 4-5A), and that the pores obtained propagate, with uniform diameter, ~380 nm into the upper surface of the film (Figure 4-5B). The pore diameter is 81±7 nm identical to the diameter of the pores in the alumina mask. When the pores in this polymer film were used as templates to prepare silica nano test tubes, tubes with diameters of 83±8 nm and lengths of 380±24 nm were obtained (Figure 4-5C). As would be expected,[47] not only are the diameters equivalent to the pore diameter, but the length is equivalent to the thickness of the porous part of the polymer film.

By controlling the O_2/Ar-plasma etch time; the distance that the pores propagate into the upper surface of the polymer film can be varied. For example, a film that was etched for 10 min had 85±8 nm diameter pores (Figure 4-6A) that propagated ~1 μm into the polymer film (Figure 4-6B). Correspondingly, the nano test tubes synthesized within the pores of this film were ~100 nm in diameter and 1000±105 nm in length (Figure 4-6C and D). In this case obtaining an accurate value for the tube diameter is problematic, because as can be seen in Figure 4-6B, the pore is wider at the mouth than at the bottom. As a result the outside diameter of the tubes is likewise larger at the mouth (Figures 4-6C and D). Note that the metal film is still present on top of the polymer film (Figure 4-6B).

When longer etch times (*e.g.,* 12 min) were used, much larger scale damage is produced in the polymer film, and faithful reproduction of the pores in the alumina mask is no longer achieved (Figure 4-7). This is because for such long etch times the metal film on the surface of polymer film is damaged and partly removed and, as a result, the pores merge at the polymer

film surface (Figure 4-7A). This damage could be detected with the naked eye, as the faint black color of the Au/Pd coating could no longer be observed. Hence, again, we see the essential role played by the metal film in producing a faithful replica of the alumina mask in the underlying polymer.

Conclusions

We have extended the alumina-mask, plasma-etch concept to a new substrate material - a photoresist polymer film. In so doing we created a new type of nanopore polymer template for use in template synthesis of nanomaterials. An appealing feature of this new template is that the distance that the pores propagate into the surface of the polymer film can be controlled by varying the plasma etch time. This allows for corresponding control over the lengths of the nano test tubes prepared by template synthesis within the pores. Via this route, we have successfully prepared silica nano test tubes that were over 100 nm shorter than the shortest tubes prepared in an alumina-film template.[47] It is also of interest to note that this general procedure can be thought of as a relatively high throughput nanotube synthesis technology. This is because there are ~10^{10} pores per cm^2 of template area; so for example, with 10 cm^2 of template, we can make 10^{11} nano test tubes.

Another appealing feature of these new polymer-film templates is that they can be used for both aqueous-based (including both acidic and basic solution) and organic-based (including most aliphatic alcohols, ketones and ethers) template synthesis. Nevertheless, these films can be dissolved, when needed, in the photoresist remover solution to liberate the nano test tubes synthesized within the pores. We are currently further exploring the plasma-etch process in attempts to make even thinner nanopore polymer replica films.

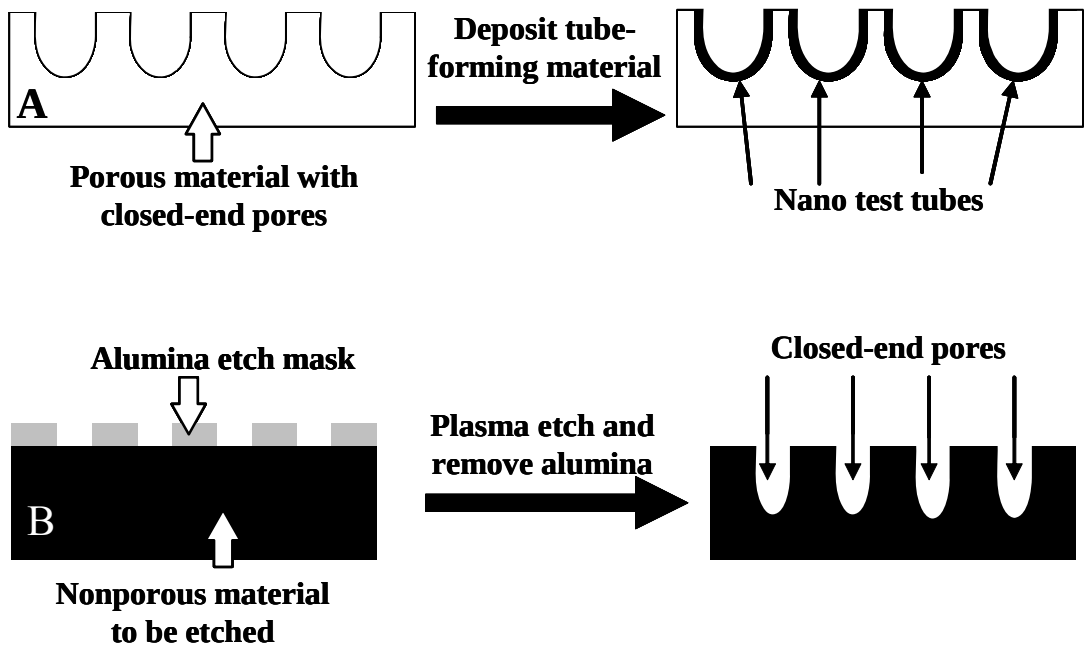

Figure 4-1. Schematic diagrams of A) the concept of using a template with closed-end pores to prepare correspondingly closed-end nano test tubes, and B) the alumina-mask plasma-etch method to prepare closed-end pores in an underlying substrate material.

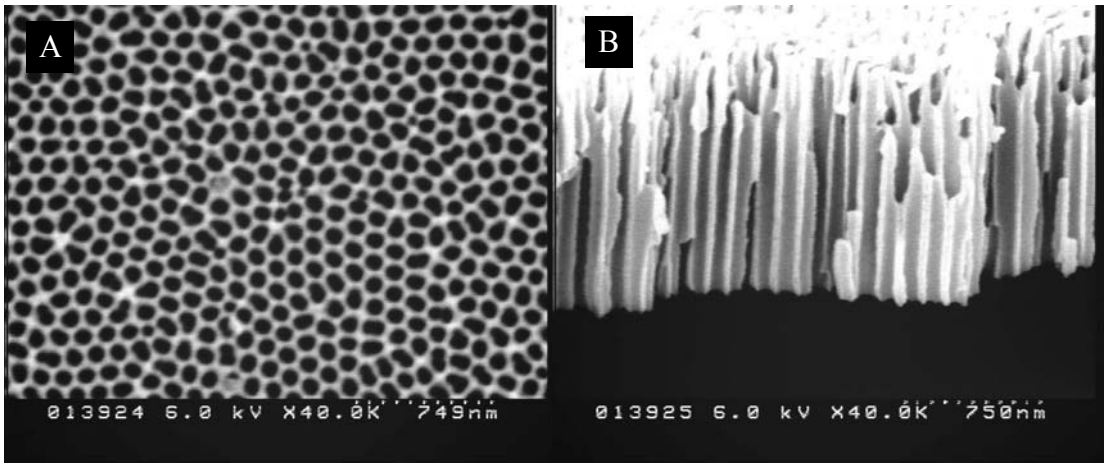

Figure 4-2. SEM images of the nanopore alumina-membrane mask; A) Top view; B) cross-sectional view.

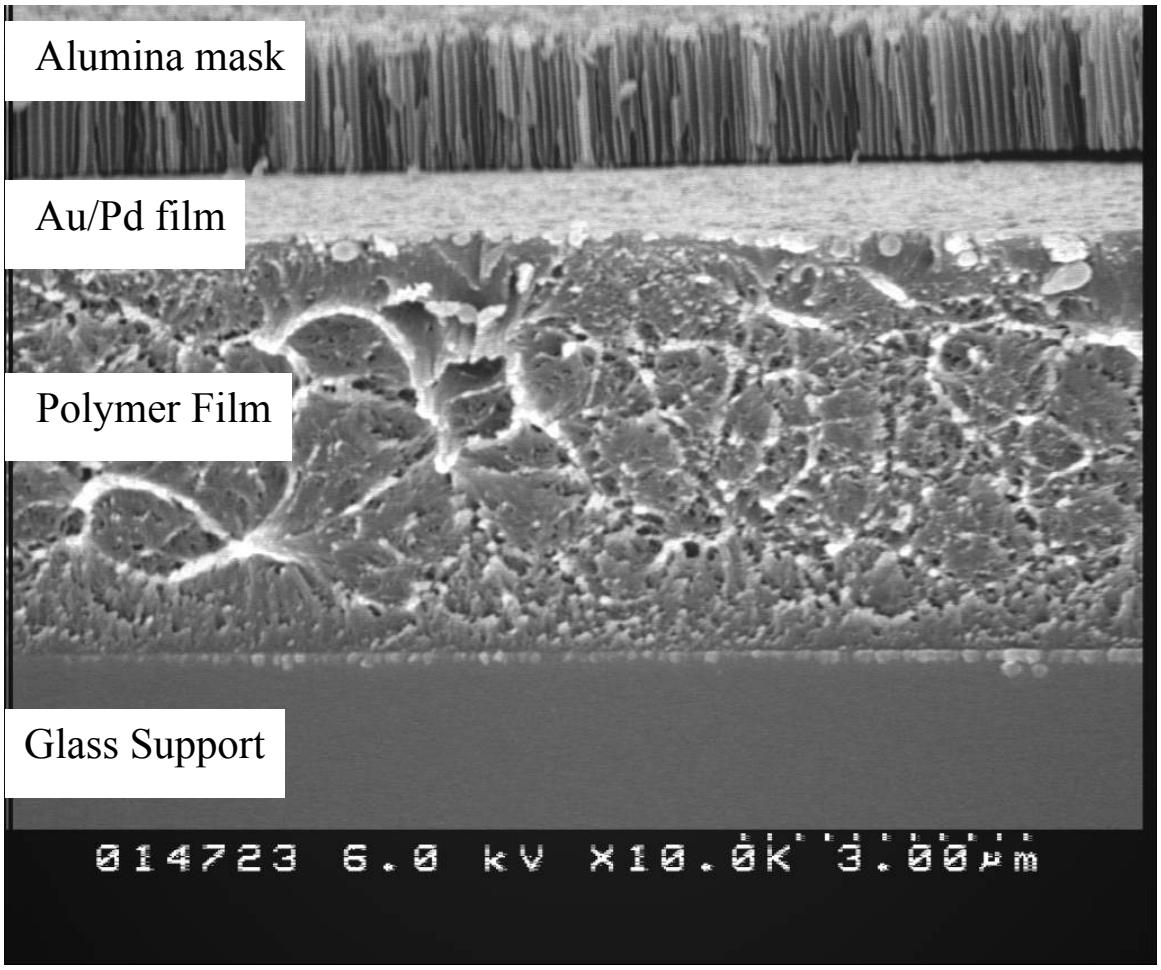

Figure 4-3. Cross sectional SEM of the Al-mask:Au/Pd-film:polymer-film assembly.

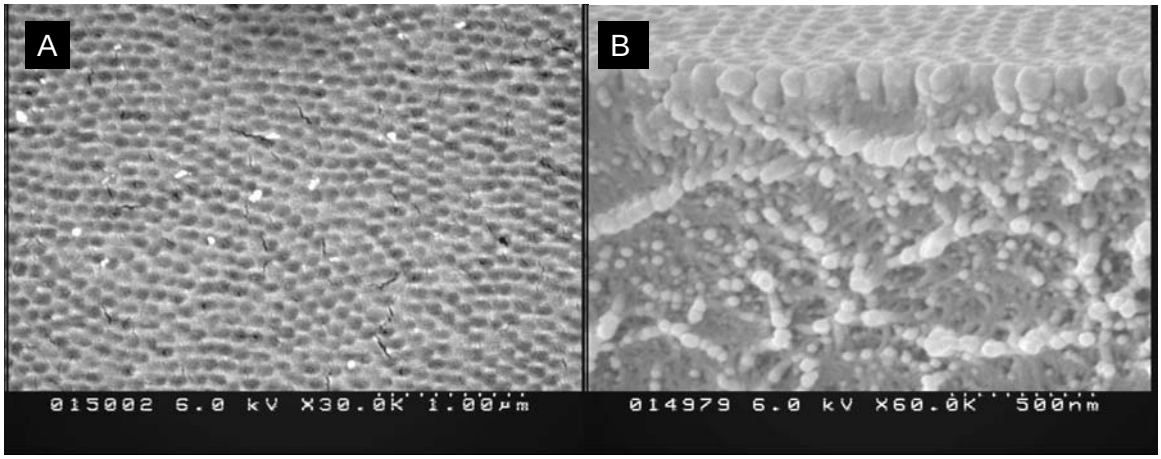

Figure 4-4. SEM images of A) the polymer-film surface and B) the cross-section of the film after 4 min of O_2/Ar plasma etching.

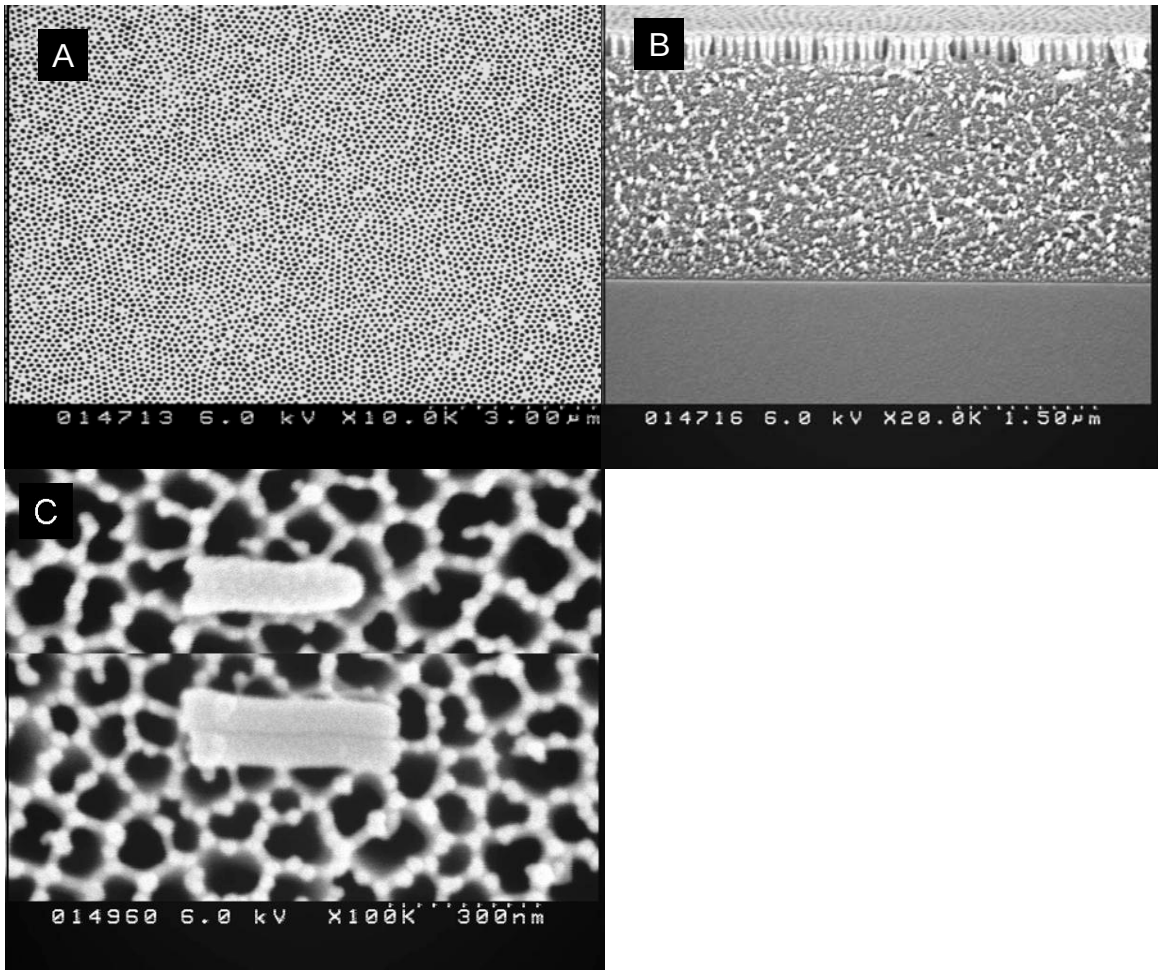

Figure 4-5. SEM images of A) the polymer-film surface and B) the cross-section of the film after 8 min of O_2/Ar plasma etching. C) SEM images of silica nano test tubes synthesized in the pores of this polymer film.

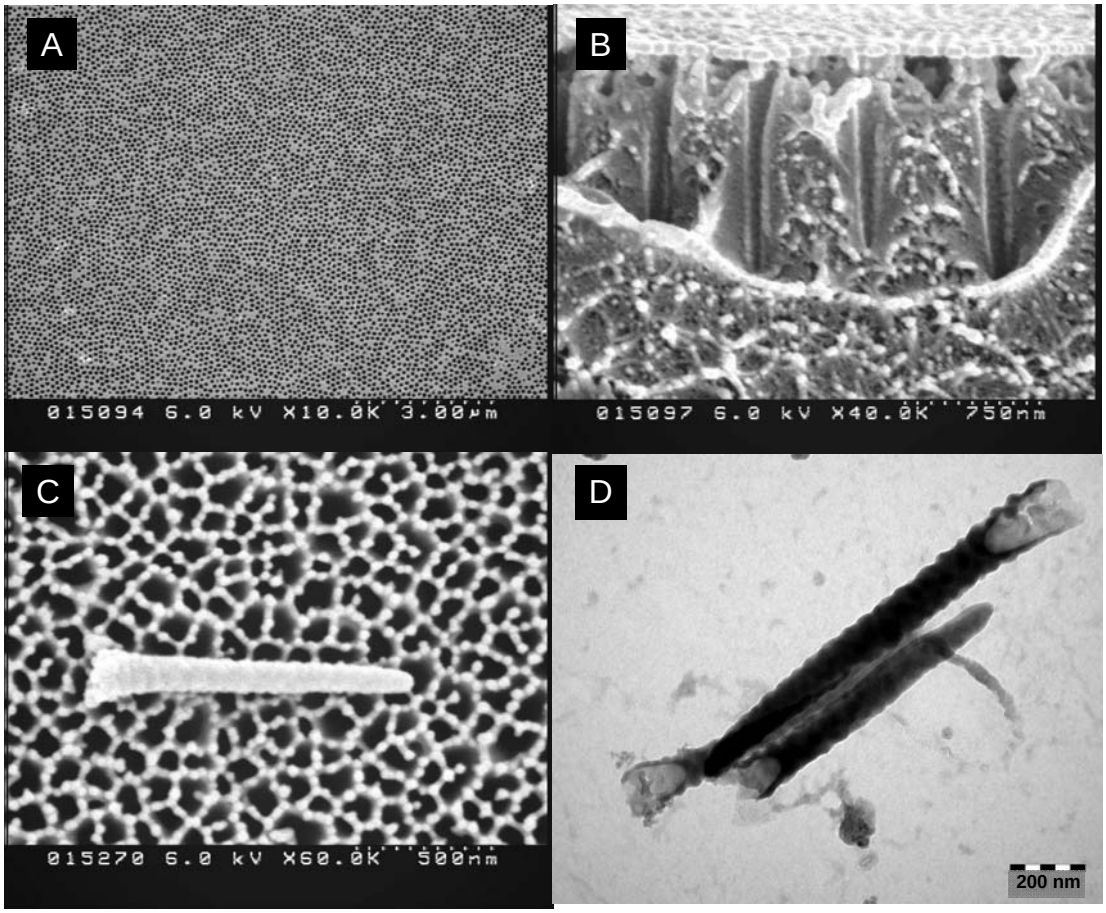

Figure 4-6. SEM images of A) the polymer-film surface and B) the cross-section of the film after 10 min of O_2/Ar plasma etching. C) SEM and D) TEM images of silica nano test tubes synthesized in the pores of this polymer film.

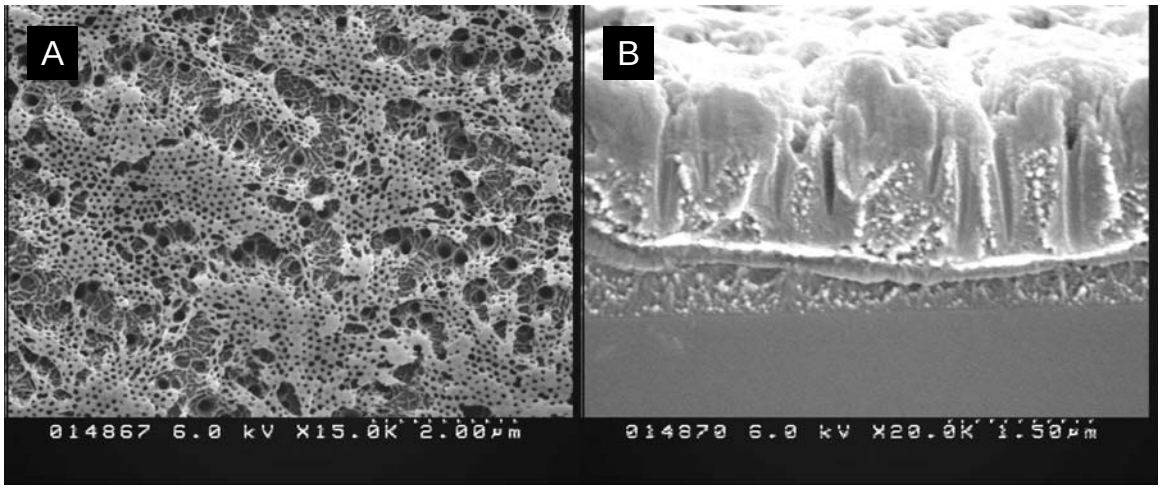

Figure 4-7. SEM images of A) the polymer-film surface and B) the cross-section of the film after 12 min of O_2/Ar plasma etching.

CHAPTER 5
SILICA NANO TEST TUBES AS DELIVERY DEVICES; PREPARATION AND BIOCHEMICAL MODIFICATION

Introduction

The application of nanomaterials such as nanoparticles, nanotubes, nanorods, and nanowires in biological systems has attracted great interest in the fields of materials science and biochemistry.[2,177] Because of their dimensions, which make them suitable for application in biological systems, the potential of nanomaterials for biodetection,[178-181] bioseperation,[45] and biomolecule delivery[118,120,121,125,126,142] has been explored.[116] In particular, the use of nanomaterials in biomolecule delivery has been shown to present various advantages such as increased efficacy,[113] protection of drugs[114] or genetic material[115,116] from potential environmental damage and reduced drug toxicity.[117] Spherical nanoparticles are almost always used because these shapes are easier to make and can be synthesized from a diverse range of materials, such as liposomes,[118,119] polymers,[120,121] dendrimers[122] and various inorganic compounds.[46,115,123] Unlike nanospheres, nanotubes have unique hollow structures however their use as biomolecule carriers are still very rare.[116,142,182]

We have pioneered a technology, called template synthesis, for preparing monodisperse nanotubes of nearly any size and composed of nearly any material.[3,183,184] These nanotubes have a number of attributes that make them potential candidates for biomolecule delivery applications. First, nanotubes have larger inner diameters than nanoparticles which allow nanotubes to carry a correspondingly larger payload. In addition, the template method allows independent modification of the distinct inner and outer surfaces of the tubes. Multifunctional delivery vehicles can be obtained by this differential modification scheme. Such delivery tools attracted great interest in biomedical applications, for example, multifunctional nanomaterials are

considered to be ideal units for the cancer-specific therapeutic and imaging agents.[125] Finally, the tubes can be synthesized from various materials and their dimensions are easily controlled.[45]

We have shown the application of differentially modified silica nanotubes as smart nanophase extractors for enantiomeric drug molecules.[45] Chen and colleagues demonstrated the preparation of fluorescent silica tubes for gene delivery.[116] After the attachment of quantum dots, the tubes were loaded with green fluorescent protein (GFP) plasmid and incubated with monkey kidney COS-7 cells. The loaded tubes are shown to be non-toxic to the cells, they initiate approximately 10-20 % of the cells to express GFP and they also act as physical shields to protect the genetic material form enzymatic degradation. The tubes, however, lack differential modification and capping as they are necessary for targeted delivery[46,47] and the tube size is controlled by physical polishing which is inappropriate for obtaining tubes with lengths < 1 μm.

Novel nanostructures called nano test tubes have been recently introduced by the Martin group.[47,48] Silica nano test tubes are prepared by sol-gel synthesis of silica in the pores of alumina template that remains attached to underlying aluminum metal. Unlike the previously mentioned nanotubes that are open on both ends, nano test tubes are closed on one end and open on the other. The use of test tubes as potential universal drug delivery vehicles was exploited where these nano test tubes could be filled with a payload and then the open end corked with a chemically labile cap.[48] We have developed a capping strategy that involves the Schiff's base reaction to form imine linkages between the test tubes and the aldehyde-modified polystyrene corks.[48] Lee and coworkers have described a selective partial functionalization method using controlled gold nanoparticle diffusion in nanotubes and prepared Au-capped silica nano test tubes by seed-mediated gold-growth.[185] The same group has also introduced magnetic nano test tubes that has a layer of Fe_3O_4 prepared by dip-coating.[186]

In our earlier work, we have used the conventional sol-gel method to obtain silica nano test tubes in the pores of alumina template.[46,47] Although the procedure is easy, it can be challenging to control the thickness and morphology.[101] This chapter compares the preparation techniques for silica nano test tube fabrication using the conventional and surface sol-gel methods and illustrates the subsequent differential tube modification strategy for their use in cell incubation studies. Defective test tubes were obtained with the conventional sol-gel method and it was attributed to the small changes in the viscosity of the gel. Layer-by-layer addition of silica with the surface sol-gel method allowed the preparation of defect-free uniform silica nano test tubes. We have differentially modified these test tubes using silane and Schiff-base chemistry to impart biochemical functionality for the cell studies. Before the template was removed, the inner tube surface was labeled with a fluorophore. The liberated fluorescent-tubes were then modified with a target or a control antibody and then incubated with breast carcinoma cells. The preliminary results suggest that the tubes modified with the target antibody attaches much more readily to the cell membrane surfaces than the tubes modified with the control antibody.

Experimental

Materials

Aluminum foil (99.99%) was obtained from Alfa Aesar. Microscope premium finest glass slides, methanol, chromium trioxide, oxalic acid, NaOH, H_3PO_4, H_2SO_4 and HCl were obtained from Fischer and used as received. Tetraethylorthosilicate(TEOS), silicon tetrachloride, carbon tetrachloride, 3-(amino-propyl)triethoxysilane(APTS), Rhodamine B Isothiocyanate, sodium cyanoborohydride, IgG from Rabbit serum, and Albumin Bovine Serum were used as received from Sigma-Aldrich as were ethanol (absolute) from Aaper, N,N- Dimethylformamide from Acros, Alexa 488 carboxylic acid-succinimidyl ester and Alexa Flour 488 labeled goat anti-rabbit IgG from Invitrogen, and 3-(trimethoxysilyl)propyl aldehyde from UCT Chemicals. IGF-

IRα and IGF-IRβ rabbit polyclonal antibodies were obtained from Santa Cruz Biotechnology, Inc. Purified water was obtained by passing house-distilled water through a Millipore, Milli-Q system.

Preparation of the Nanopore Alumina-Membrane Templates

The nanopore alumina membranes were prepared in house using the well-known two-step electrochemical anodization method.[18,171] Briefly, after annealing and polishing the aluminum foil, a nanopore alumina film was formed across the Al surface by anodization. This film was then dissolved in acidic CrO_3, and a second anodized alumina film was formed using oxalic acid electrolyte. This yields the desired ordered nanopore alumina film on both surfaces of the aluminum film. Unlike the work described in the previous chapter, the alumina film is not detached from the aluminum so the template remains attached to the underlying Al metal. It is also important to note that in the first work we reported the preparation of silica nano test tubes; we have attached a glass substrate to one surface of Al with epoxy for stability reasons, which yielded alumina growth only on one side of Al metal.[47]

Preparation of the Silica Nano Test Tubes

Two different sol-gel methods were used to deposit silica nano test tubes within the pores of the nanopore alumina template (Figure 5-1). In the conventional sol-gel method:[47,48] a 50/5/1 (by volume) mixture of ethanol, tetraethyl orthosilicate and 1M HCl was prepared and allowed to hydrolyze for 30 min. The alumina template was immersed into this sol with sonication for 30 sec and then kept under vacuum in a desiccator for 5 more minutes. The sol-impregnated template was dried in air, and then oven cured for ~5 h at 100 °C, to yield silica nano test tubes[47,48] within the pores of the nanopore alumina template. The surface film was removed by wiping the membrane surface with a laboratory tissue soaked in EtOH.

In the surface sol-gel method;[101] two-step deposition cycles, in which the adsorption of a molecular precursor ($SiCl_4$) and the hydrolysis steps are separated by a post-adsorption wash. An alumina template was immersed in $SiCl_4$ solution in CCl_4 (85 mol-%) for 2 min and quickly soaked in a CCl_4 beaker. The template was then washed with CCl_4 and immersed in a second CCl_4 beaker for 15 min to remove unbound $SiCl_4$ from the pores. These steps were done in a polyacrylic box under 30 psi nitrogen flow to limit $SiCl_4$ polymerization by atmospheric water which occurs at ambient conditions and results in silica deposition with uncontrollable thickness. Finally, the template was soaked in CCl_4/MeOH 1:1 (2 min) and EtOH (5 min) to displace CCl_4, and dried in a N_2 stream. Then the template was immersed in deionized water for 5 min, washed in a beaker with MeOH (2 min). After 10 deposition cycles the silica deposited template was cured at 100 °C for 1 h. The surface film was removed by briefly (1 min) exposing both sides of the nanopore template to a reactive-ion plasma etching system (Samco model RIE-1C). The plasma conditions were - 13.56 MHz, 140 W, 20 Pa Ar pressure, Ar flow rate = 20 sccm.

To liberate the nano test tubes, the nanopore alumina template was dissolved in 0.1 M NaOH for 3-6 h. The liberated test tubes were collected either by centrifugation (14,000 rpm for 14 min in all experiments involving centrifugation) or filtration and washed several times with water and ethanol. Transmission electron microscopy (TEM) samples were prepared by re-suspending the liberated nano test tubes in ethanol and immersing a TEM grid into this suspension. TEM images were obtained with a Hitachi H-7000 microscope. Scanning electron microscopy (SEM) was also used to characterize the alumina template and the filtered free silica nano test tubes. SEM images were obtained using a Hitachi S4000 FE-SEM. Prior to imaging, the surface of the SEM sample was sputtered with a thin Au/Pd film using a Desk II Cold Sputter instrument (Denton Vacuum, LLC).

Silica Nano Test Tube Modification with Fluorophore

The labeling of silica nano test tubes with fluorophores were done while the tubes were still embedded in the alumina template. This means only the inner walls of the tubes are accessible for chemical modifications. The surface modifications were done using silanization chemistry and the structures of all silanes are shown in Figure 5-2. In each case the inner tubule walls were modified with amine functional groups which are then covalently coupled to Rhodamine or Alexa Flour-488 (Figure 5-3).[70,187] Briefly a solution that was 5 % APTS, 90% ethanol, and 5 % acetate buffer (50mM, pH 5.2) was hydrolyzed for 20 min and the template is immersed into this solution for 1 h. The template was then thoroughly washed with ethanol and cured in an oven at 100 °C for 3h. Rhodamine attachment was done by immersing the amine functionalized template into a 5 mM Rhodamine B Isothiocyanate solution in dry DMF for 12 h in a desiccator. This was followed by extensive washing with DMF and EtOH. To modify the inner tube surfaces with Alexa-488, a 0.1 mg/ml solution of Alexa 488 carboxylic acid-succinimidyl ester in 10 mM phosphate-buffered saline (PBS) buffer (pH is adjusted to 8.1 by 0.1 M NaOH) was prepared. The amine modified template was then immersed into this solution in a desiccator for 12 h and then washed with buffer and ethanol before the tubes were liberated from the template.

A fluorescence microscopy system described previously[188] was used to obtain fluorescence images of the labeled test tubes and to measure the fluorescence intensity from glass slides that are used to confirm the antibody attachment. (See antibody modification.) This system combines an Axioplan 2 imaging microscope (Zeiss) with a J&M-PMT photometry system detector (SpectrAlliance), for measuring fluorescence intensity. In addition, the system is equipped with a digital CCD camera (Zeiss) to obtain both fluorescence and optical images. The excitation source for all fluorescence measurements was a mercury lamp. A beam splitter was used to send the

reflected fluorescent light from the sample to the detector and the CCD camera. The Rhodamine B was excited at 570 nm, and the emission was collected through a 590-nm band-pass filter and The Alexa 488 was excited at 495 nm, and the emission was detected through a 515-nm band-pass filter.

Antibody Modification

The fluorescently labeled tubes were liberated and then washed by centrifugation at 14,000 rpm three times with H_20 and then three times with ethanol. The outer tube walls were functionalized with aldehyde groups by an aldehyde terminated siloxane linker.[189] The aldehyde groups were then reacted by well-known Schiff-base chemistry to amine sites on the protein to be immobilized.[190-192] Briefly a solution that was 5 % 3-(trimethoxysilyl)propyl aldehyde, 90% ethanol, and 5 % acetate buffer (50mM, pH 5.2) was hydrolyzed for 15 min and the tubes were dispersed in this solution and reacted for 30 min with frequent vortexing. The aldehyde modified tubes were centrifuged and vortexed three times with ethanol and then three times with 10 mM PBS, at pH 7.4. The antibodies were coupled to the aldehyde-terminated outer tube surfaces by dispersing these tubes in the same PBS buffer that contains 0.2 mg/ml antibody and 4 mM $NaBH_3CN$ for 12 h at 4 °C with occasional vortexing. The tubes were either modified with Rabbit polyclonal IGF-IRα (target) or IGF-IRβ (control) antibodies and the tube concentration was ~10^{10} tubes/ml. After the antibody modification, the tubes were washed three times with PBS buffer by centrifugation and dispersed in 10 mM PBS, at pH 7.4 that contains 0.2 mg/ml bovine serum albumin (BSA) and 4 mM $NaBH_3CN$. This step is required to quench the remaining aldeyhde sites on the outer tube walls and was done by allowing the tubes in this solution for 2 h at room temperature with vortexing. Finally, the tubes were washed three times

with 10 mM PBS (pH=7.4) by centrifugation and dispersed in the same buffer for cell incubation studies.

Covalent attachment of antibody by Schiff-base chemistry was confirmed on glass slides. Two glass slides were coated with a single layer of silica by surface sol-gel method and both slides were functionalized with aldehyde silane as mentioned above and dried in a vacuum desiccator for 5 h. First slide was then modified with Rabbit IgG and the second with BSA where both proteins were 1 mg/ml in a pH 7.4, 10 mM PBS containing ~ 4 mM $NaBH_3CN$. The slides were washed with PBS and treated with 1/5 diluted sea block buffer (Pierce, # 37527) for 2h. Both slides were then exposed to Alexa Flour 488 labeled goat anti-rabbit IgG (20 μg/ml in PBS, pH 7.4) for ~ 10 h at 4°C. After rinsing with PBS and water the slides were dried under N_2 stream and their fluorescence was compared by J&M-PMT photometry system detector.

Cell Incubation Studies

MDA-MB-231 breast carcinoma cells (American Type Culture Collection, Manassas, VA) were maintained in Dulbecco's modification of Eagle's medium (Fisher Scientific) with 10% fetal bovine serum (Invitrogen, Carlesbad, CA) and 0.5 mg/mL Gentamycin (Sigma, St. Louis, MO) at 37 °C in 5% CO_2/air. Cells were plated in Corning 24 well cell culture clusters and grown for 48-60 h prior to incubation.[193]

The cells were incubated with 10 mM PBS (pH=7.4) containing 0.2 mg/ml BSA solution for 30 min to prevent nonspecific binding of the tubes to the cell surface. These cells were washed with cell media buffer and then incubated with the antibody-modified fluorescent silica nano test tubes (tube concentration was ~ 10^9 tubes/ml) for 1 h and then washed five times with cell media buffer prior to imaging. Note that two separate wells were used for the incubation of cells with the tubes; one for the target antibody-modified tubes and the other for the control antibody-modified tubes (non-competitive).

Fluorescence imaging was conducted with a confocal microscope setup consisting of an Olympus IX-81 inverted microscope with an Olympus Fluoview 500 confocal scanning system and a tunable argon ion laser (488 nm). The images were taken with a 20x objective and the fluorescence was detected by a 505-525 nm band-pass filter. Microplate reader experiment was conducted with a Tecan Safire microplate reader with 24 well Corning cell culture plates and the excess cell media buffer was removed from the plates prior to measurements. The excitation wavelength was 488 nm and the emission was collected at 520 nm.

Results and Discussions

Defect-Free Silica Nano Test Tube Preparation

We have previously reported silica nano test tube preparation using nanopore alumina templates.[47] Nanopore alumina was grown only on one side of the Al foil as the other side was attached to a glass support with epoxy for stability reasons. However, when the template is dissolved, the epoxy leaches out into the solution and contaminates the tube samples (Figure 5-4). Using thicker aluminum foils eliminates the need for such supports and yields alumina film on both surfaces of the Al metal (Figure 5-5, only one side is shown for simplicity.). When the conventional sol-gel method is applied to obtain silica test tubes from these templates, clean test tubes are obtained in larger quantities (Figure 5-6). Note that the tube diameter reflects the template pore diameter (~ 80 nm) and the tube length reflects the template thickness (~ 1 μm).

Silica nano test tubes can be prepared with conventional sol-gel quite easily (< 5 min), however, the resulting tubes do not have reproducible structures (Figure 5-6C). Tubes with holes were often observed and changing the Al foil purity, hydrolysis time, TEOS concentration or dissolving conditions as well as the use of glass supported alumina templates yielded similar defective structures. These "bamboo-like nanofibers" were first reported by Zhang[194] where they have shown that the viscosity of the gel determines whether the silica nanostructure will be a

wire, a tube or a bamboo-like nanofiber. The defective nanostructures in our case are observed since small variations during the sol-gel preparation (e.g. temperature or humidity) can change the viscosity of the gel.

A surface sol-gel method was used to have a better control over the resulting silica nano test tubes. This method involves repeats of two-step deposition cycles, in which the adsorption of a molecular precursor ($SiCl_4$) and the hydrolysis steps are separated by a post-adsorption wash (Figure 5-1). Ideally the technique can limit each adsorption to a single monolayer, however thicker layers have been found for planar oxide films.[104,106,195] Nevertheless, it allows very fine control over film thickness because a nanometer or sub-nanometer thick layer is grown on each cycle.[101] Control over the atmospheric water is necessary as it rapidly polymerizes $SiCl_4$ precursor and a silica layer deposits on the alumina template surface with uncontrollable thickness (Figure 5- 7). This control is achieved by purging nitrogen stream throughout the adsorption steps.

A thin layer of silica (~15 nm) is deposited on the inner pore walls of the nanopore alumina template and on the top template surface from a $SiCl_4$ solution (85 mol-% in CCl_4) after 10 deposition cycles (Figure 5-8). The silica film on the template surface, which normally binds the nanotubes together, is removed by exposing both faces of the template to argon plasma. Figure 5-9A shows one such template after 1 min Ar-plasma treatment. When it is immersed in acid briefly, the alumina partly dissolves and reveals the protruding silica nanotube mouths that are not inter-connected (Figure 5-9B). Free silica nano test tubes with very smooth surface structures are obtained as the template is completely dissolved (Figure 5-10). Nano test tubes with different lengths can also be synthesized using alumina templates of various thicknesses. We have successfully varied the tube length from 100 nm to 6 μm (Figure 5-10C, D). The ability

to tailor the tube dimensions is an important factor since this can affect the payload capacity of such nanotubes for delivery applications.[46]

Differential Modification

In addition to the geometric control, the template method also allows to independently modify the inner and outer surfaces of the tubes. When the tubes are still embedded in the template, only the inner surfaces are exposed to modifications. Once this inner surfaces is modified and the template in removed, the outer tube surfaces of the free tubes are accessible, which can be further functionalized with a different chemistry (Figure 5-11). A variety of functional groups can be attached to the silica surfaces via silane chemistry[196] using commercially available reagents. Previously, such differentially functionalized silica tubes are shown to selectively extract enantiomeric drugs from a racemic solution.[45]

The motivation for making differentially functionalized silica nano test tubes stems for an interest in using these tubes as drug- or DNA- delivery vehicles. The test tube geometry is ideal for conveniently filling of the nanotube with the biomolecule of interest and by applying a cap to the open end, the biomolecule could be kept "bottled-up" inside until it is ready to be delivered. We have successfully shown the capping of the tubes with polystyrene balls using simple imine linkages.[48] Potential biomedical applications will require that the outer surfaces of the tubes should be modified with various moieties (protein, nucleic acids, organic functional groups) to target the nanostructures to their destinations. Template-based synthesis approach makes it possible to add these modifications after release from the alumina template.[45,46]

Proof-of-principle studies were done where the inner tube surfaces are labeled with fluorescent tags and the outer tube surfaces are modified with tumor specific antibodies. Rhodamine B or Alexa Flour-488 labeled test tubes were prepared by first reacting the inner tube surfaces with APTS while the tubes were still embedded in the template. The resultant primary

amine groups and then covalently coupled (Figure 5-3) to isothiocyanate or succinimidyl ester groups. Figure 5-12 shows such tubes after they have been released from a 6 μ-thick template (same template used for the tubes in Figure 5-10D). Since Alexa-488 is much more resistant to photobleaching than other organic dyes,[197] further studies only involved test tubes that are modified with this fluorophore.

In order to immobilize the protein, the outer tube walls of the free fluorescent tubes are functionalized with aldehyde moieties by an aldehyde terminated siloxane linker[189] (Figure 5-11). The aldehyde groups are then reacted by well-known Schiff-base chemistry to amine sites on the protein to be immobilized.[190-192] This covalent immobilization chemistry is first confirmed with a glass slide experiment where two glass slides are reacted with aldehyde silane. The first slide is then modified with rabbit IgG and the second slide is modified with BSA. When both slides were exposed to Alexa Flour 488 labeled goat anti rabbit IgG solution; the first slide emitted distinct fluorescence at 530 nm where as the second slide showed negligible emission (Figure 5-13). This showed the successful covalent attachment of bioactive rabbit IgG on silica surface with the Schiff-base chemistry.

Cell Incubation Results

The cell incubation experiments were done with Alexa 488-labeled silica nano test tubes that were modified with IGF-IRα or IGF-IRβ antibodies using Schiff-base chemistry for protein immobilization. IGF-IRα and IGF-IRβ are rabbit polyclonal antibodies raised against the α and β subunits of the insulin-like growth factor-I receptor (IGF-IR), respectively.[198] IGF-IR is a transmembrane protein that stimulates growth in many different cell types, blocks apoptosis, and may stimulate the growth of some types of cancer and over-expression of the IGF-IR gene has been reported in breast cancer cells.[199] A recent study with MDA-MB-231 breast carcinoma cells has shown that the extracellular α subunit of the IGF-IR protein showed specific activity for the

IGF-IRα antibody, and no activity was observed for the IGF-IRβ antibody.[200] Consequently, to observe specific cell reaction for the silica nano test tubes, two sets of nano test tubes were prepared. The first set was modified with IGF-IRα (target) and the second set with IGF-IRβ (control) antibody.

Figure 5-14 displays fluorescence images of two different breast carcinoma cell culture samples incubated with Alexa-488 labeled silica nano test tubes that are modified either with the target (Figure 5-14A) or with the control antibody (Figure 5-14B). Qualitative observation suggests that the tubes modified with target antibody attaches much more readily to the cell membrane surfaces than the tubes modified with control antibody. The tubes are generally attached to the membrane surfaces of live (elliptical) and dead (circular) cells and not on the well bottom. Extensive tube attachment to the well bottom was observed with tubes that are left unmodified on their outer surfaces. Further 3D sectioning studies of the confocal microscopy images are required to understand if any of the tubes are internalized by the carcinoma cells.

We have used the same cell samples in order to compare the whole-plate cell fluorescence intensities using a microplate reader. The result shows a fluorescence intensity ratio of more than an order of magnitude for the cells that are incubated with the target antibody-modified tubes (Fl. Int. = 5495 a.u.) compared to the cells incubated with the tubes modified with control antibody (Fl. Int. = 435 a.u.). More experiments need to be conducted to verify these results. It is also important to note that these incubation studies were carried out after the cells have been treated with BSA. When the cells were not treated with BSA prior to tube incubation, very similar fluorescence results were obtained from the target and control antibody-modified tubes which shows nonspecific binding of both tube types to the cell membrane surface.

As a future direction, aptamer-modified nano test tubes can be used for more selective results. It has been recently reported by Tan and coworkers that aptamer-conjugated magnetic silica nanoparticles can be used for the selective and sensitive detection and collection of acute leukemia cells.[178] Furthermore, clever strategies need to be developed for the efficient loading and release of biomolecules into and out of these test tubes in order to use them as successful delivery devices.

Conclusion

We have substantiated a technique for the fabrication of uniform defect-free silica nano test tubes using alumina membrane templates. First, the advantage of using alumina films grown on both sides of the Al metal for having cleaner samples was shown, and then the test tube fabrication methods were compared. We have obtained defective test tubes with the conventional sol-gel method and this was attributed to the small changes in the viscosity of the gel. Uniform defect-free silica nano test tubes were prepared by layer-by-layer addition of silica through the surface sol-gel method. We have shown that argon plasma etching can be used to remove the silica film on the template surface that normally binds the nanotubes together. Using silane and Schiff-base chemistry, we have independently modified the inner and outer surfaces of these test tubes to investigate selective cell response via cell incubation experiments. The inner tube surfaces were first labeled with Alexa-488 fluorophore and then the template was removed. The liberated fluorescent-tubes were modified with either a target (IGF-IRα) or a control antibody (IGF-IRβ) and then incubated with breast carcinoma cells. The fluorescence imaging and the microplate reader data suggest that the tubes modified with target antibody attaches much more readily to the cell membrane surfaces than the tubes modified with control antibody. More experiments need to be conducted to verify these results.

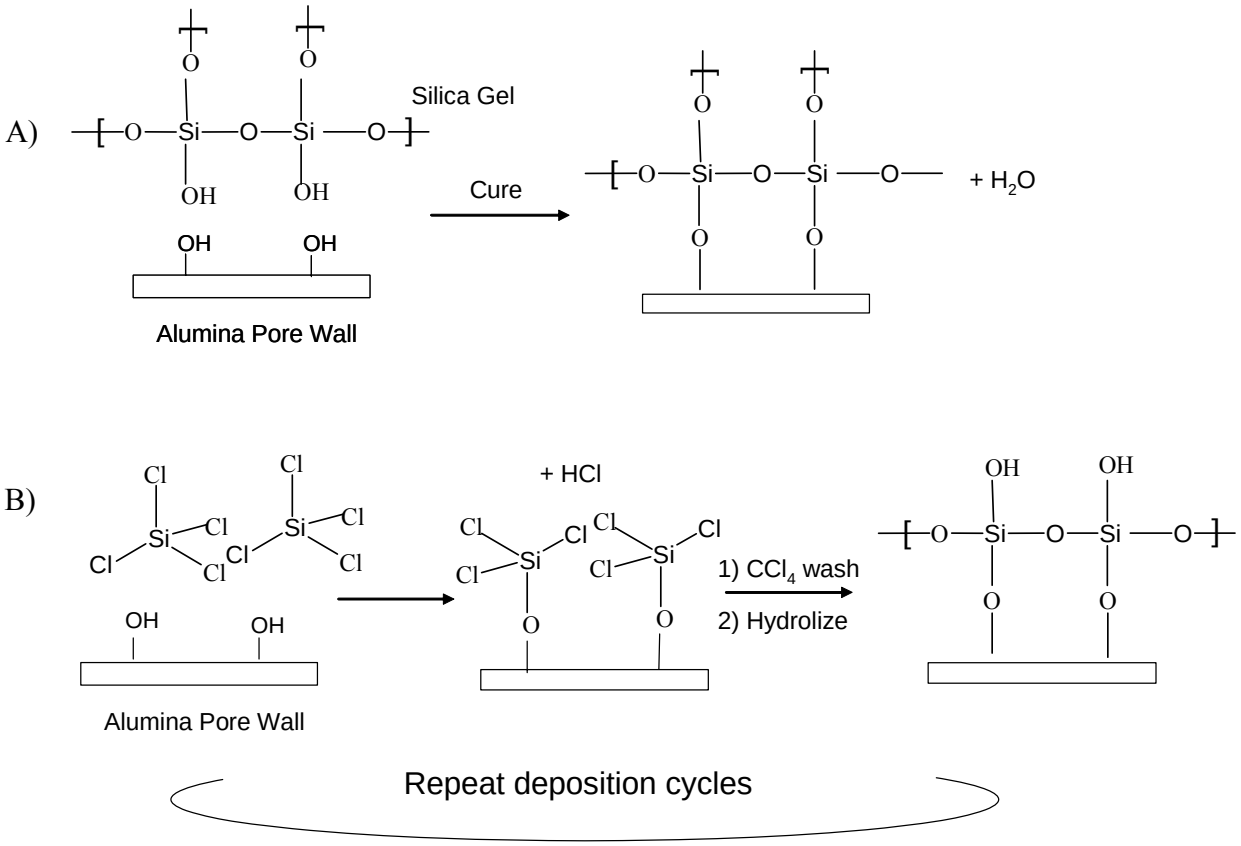

Figure 5-1. Schematic of silica deposition on alumina surface by A) conventional sol-gel and B) surface sol-gel method.

A) Tetraethylorthosilicate (TEOS)

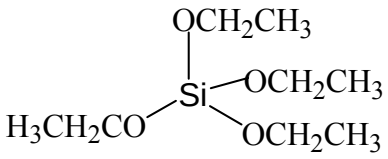

B) Silicon tetrachloride

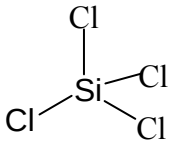

C) 3-(amino-propyl)triethoxysilane (APTS)

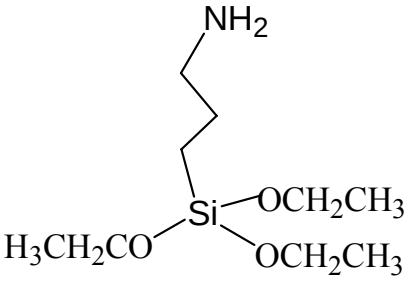

D) 3-(trimethoxysilyl)propyl aldehyde

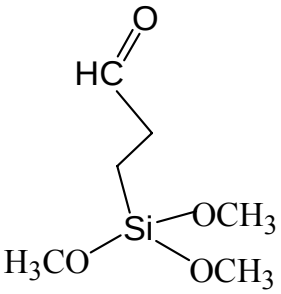

Figure 5-2. The structures of the silanes used for surface modifications.

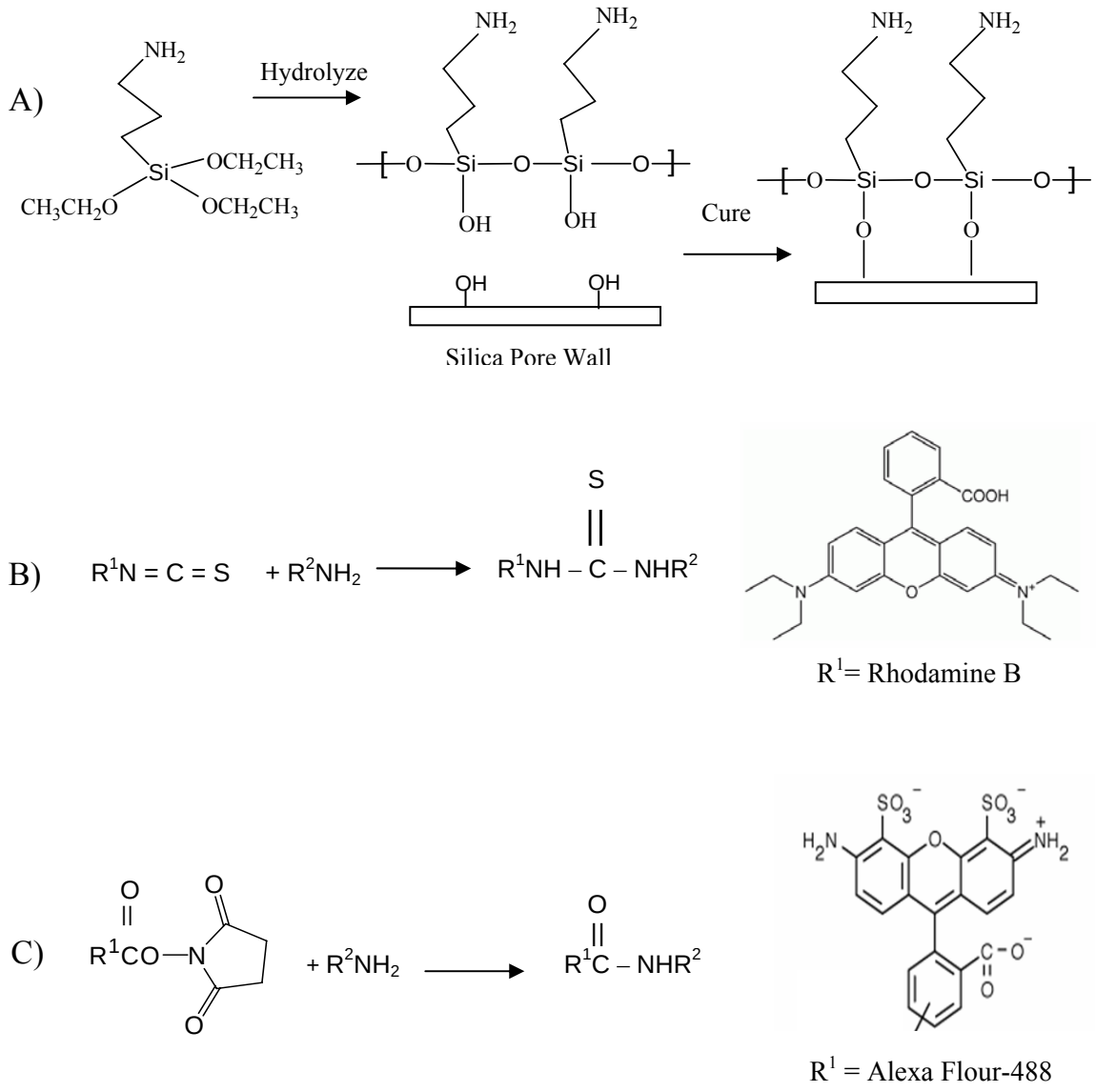

Figure 5-3. Modification of the tube walls with fluorophore. A) The silica inner tube walls are functionalized with amino silane. The primary amine groups are then covalently coupled to B) Rhodamine B or C) Alexa Flour-488 dyes.

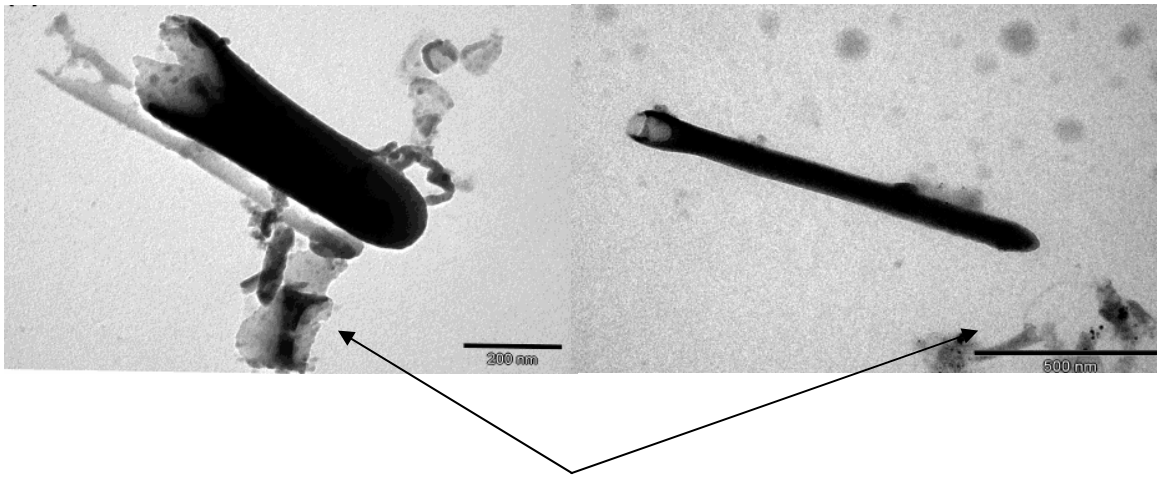

Figure 5-4. TEM images of test tube samples obtained from a glass supported alumina template.

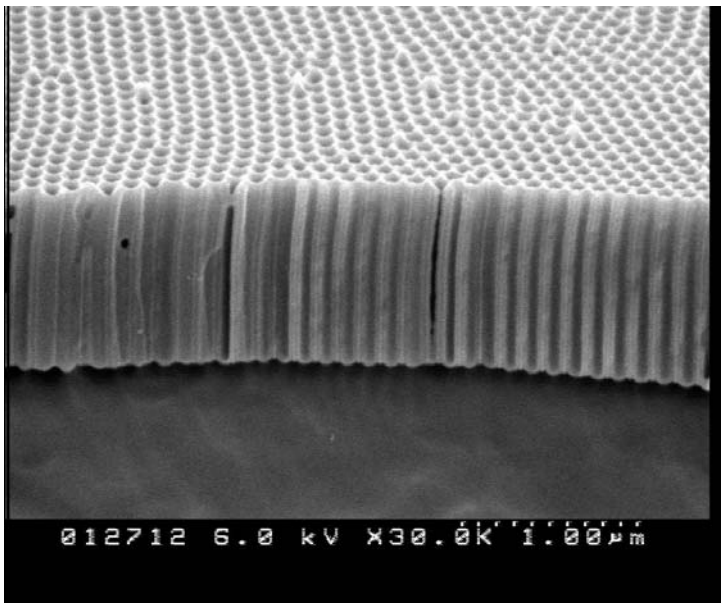

Figure 5-5. SEM image of the cross-section of the alumina template.

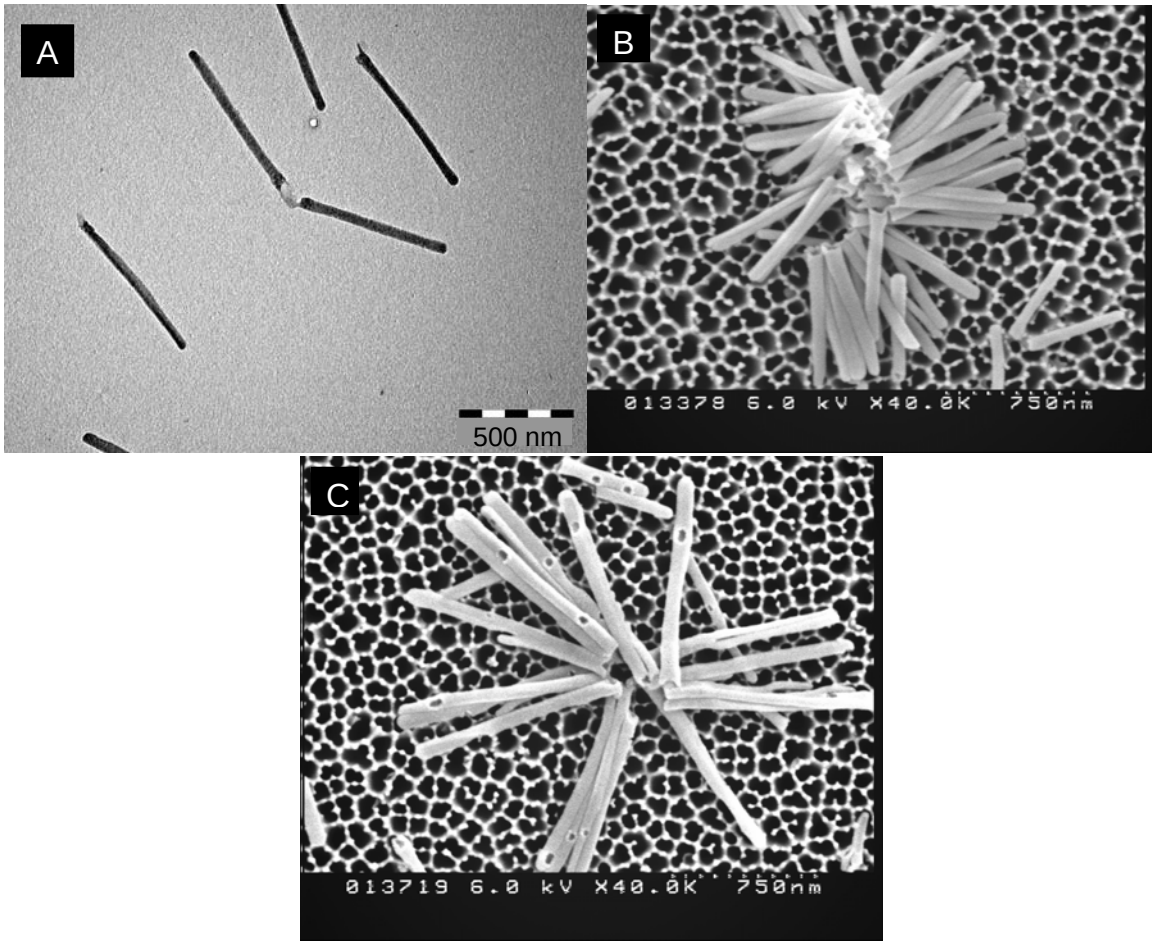

Figure 5-6. A) TEM and B,C) SEM images of the tubes obtained by conventional sol-gel method.

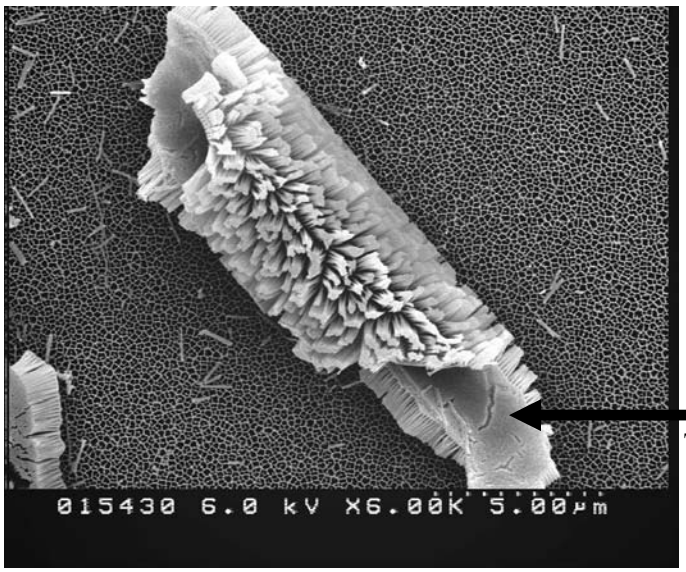

Figure 5-7. Silica deposition with surface sol-gel method without humidity control.

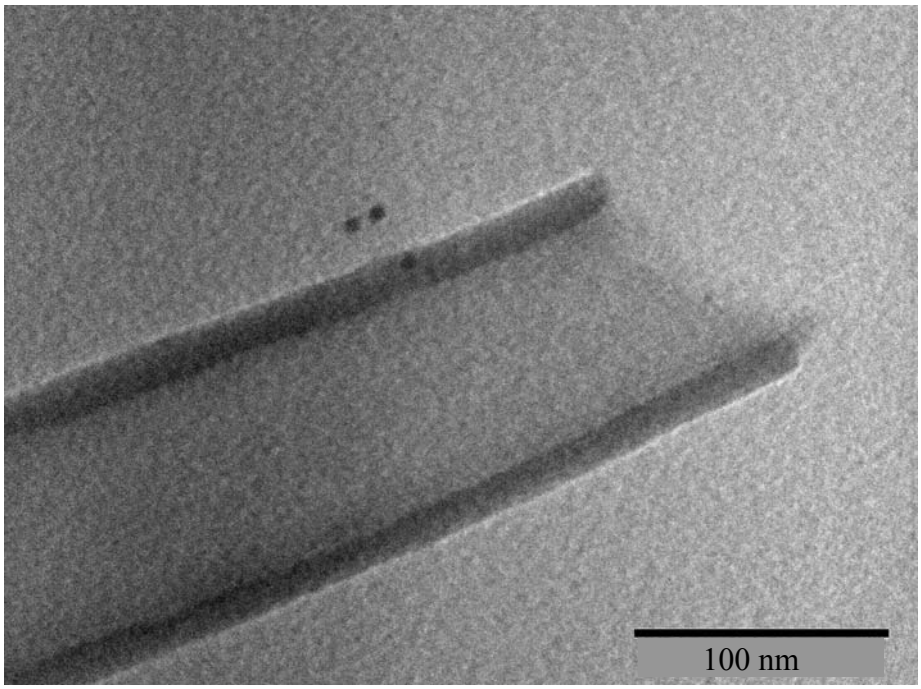

Figure 5-8. High resolution TEM image of the silica nano test tube with ~15 nm tube wall thickness.

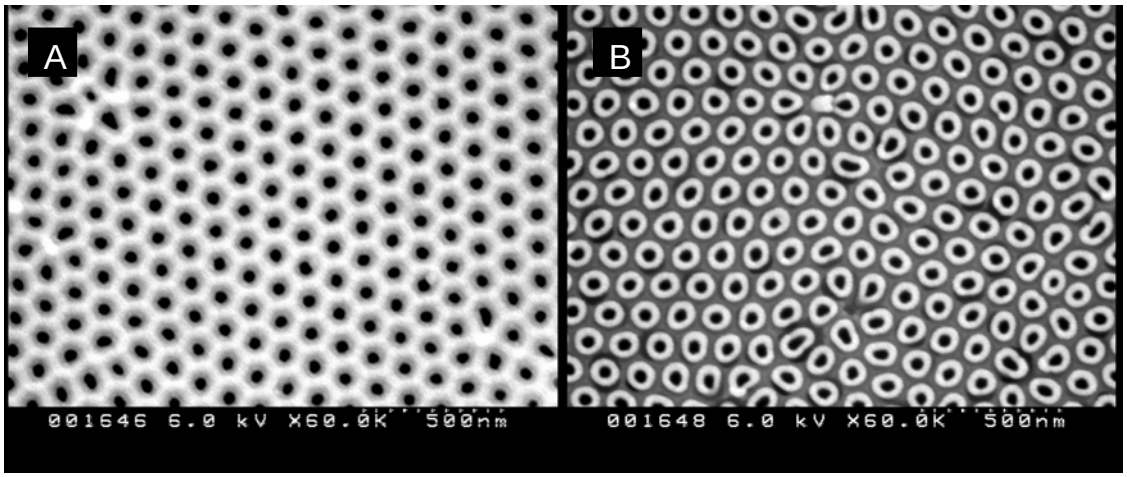

Figure 5-9. SEM image of the surface of silica deposited template A) after 1 min Ar plasma and B) after briefly dissolving the alumina template.

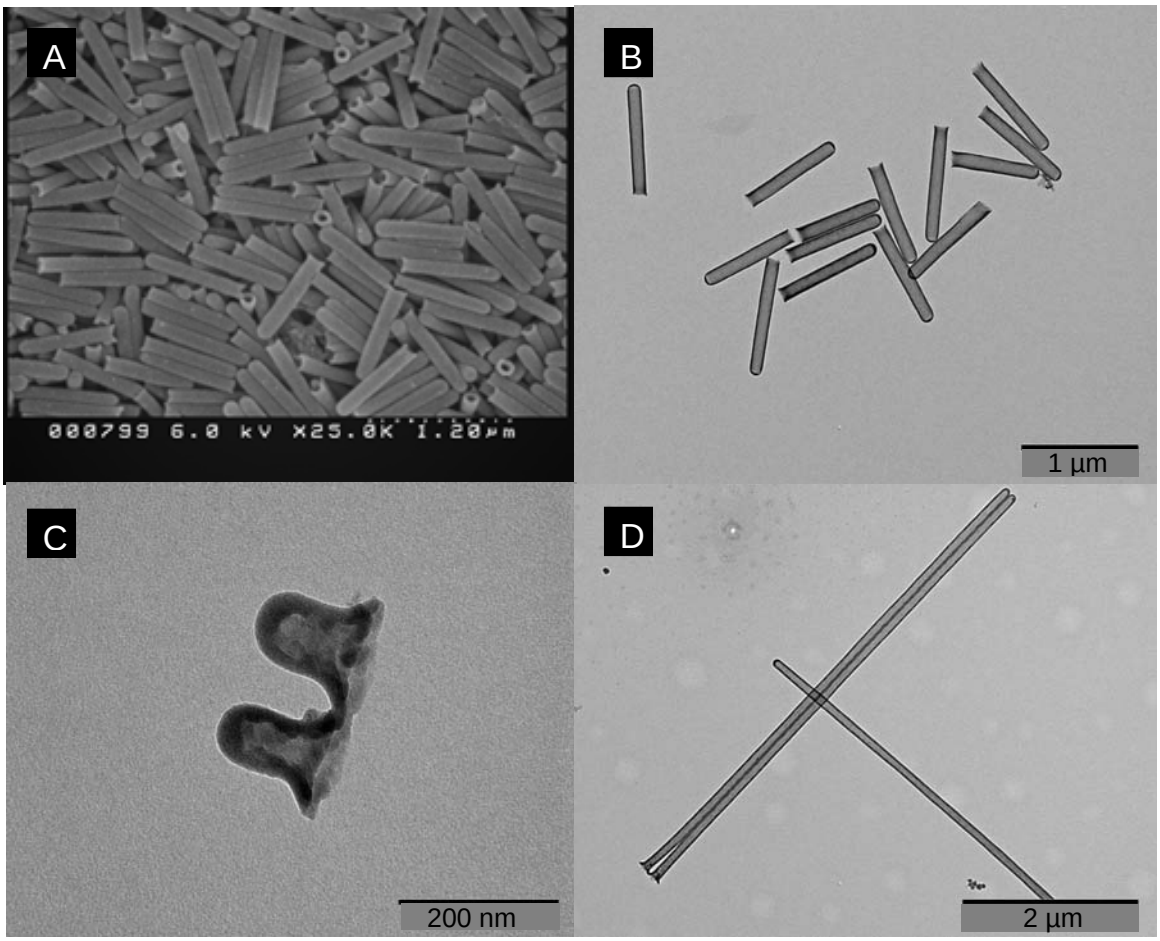

Figure 5-10. SEM (A) and TEM (B,C, and D) images of silica nano test tubes with different lengths. The templates in which these tubes are synthesized were anodized for A,B) 12 min, C) 1.5 min and D) 1 h.

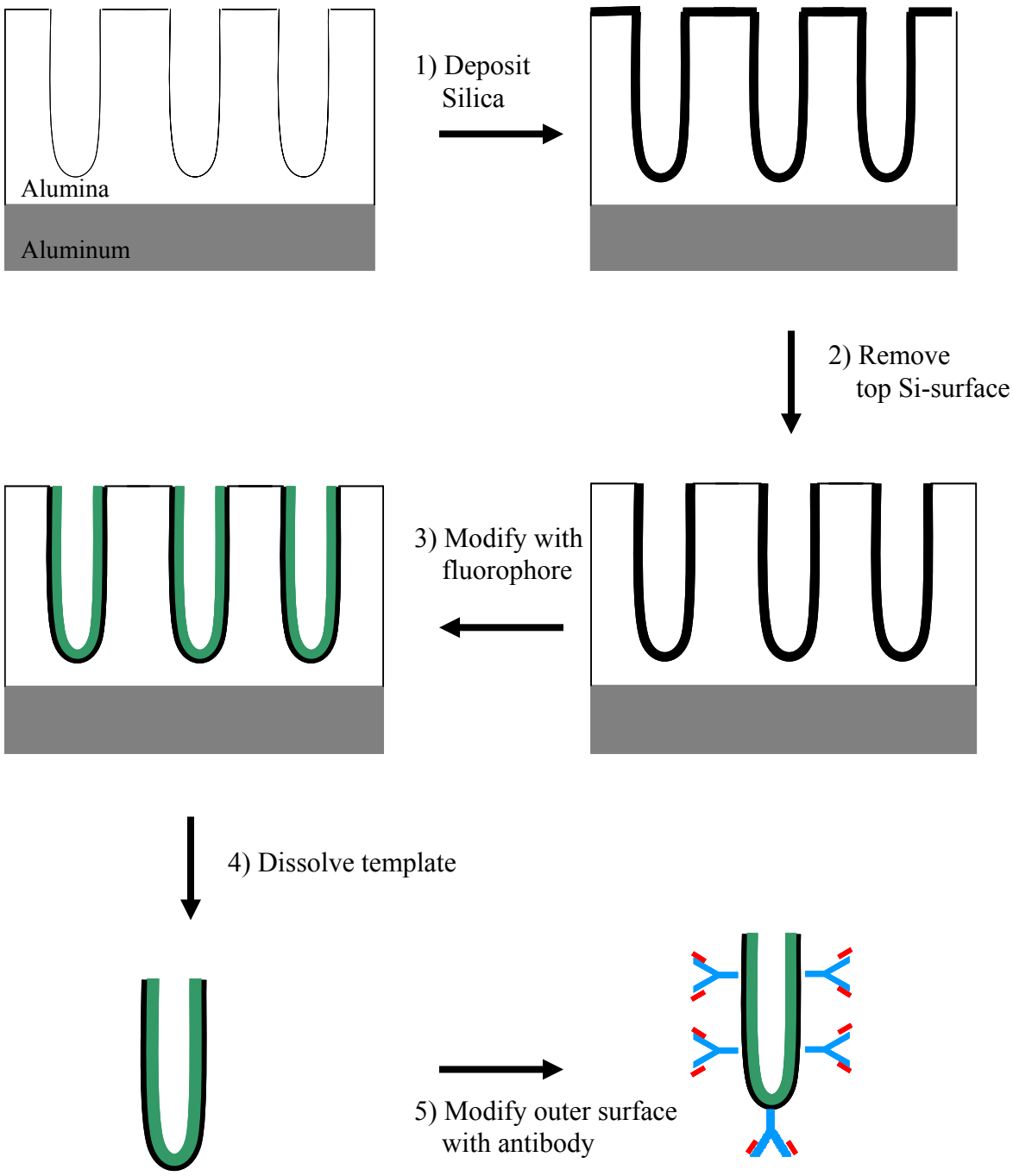

Figure 5-11. Preparation and differential modification of the silica nano test tubes.

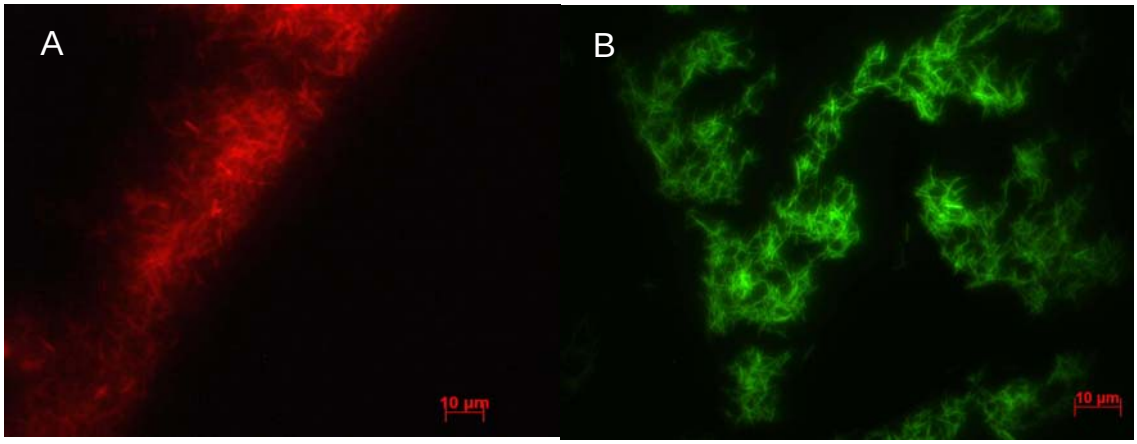

Figure 5-12. Fluorescence microscopy images of A) Rhodamine B and B) Alexa Flour-488 labeled silica nano test tubes. Scale bars are 10 µm and acquisition time is 1.8 sec.

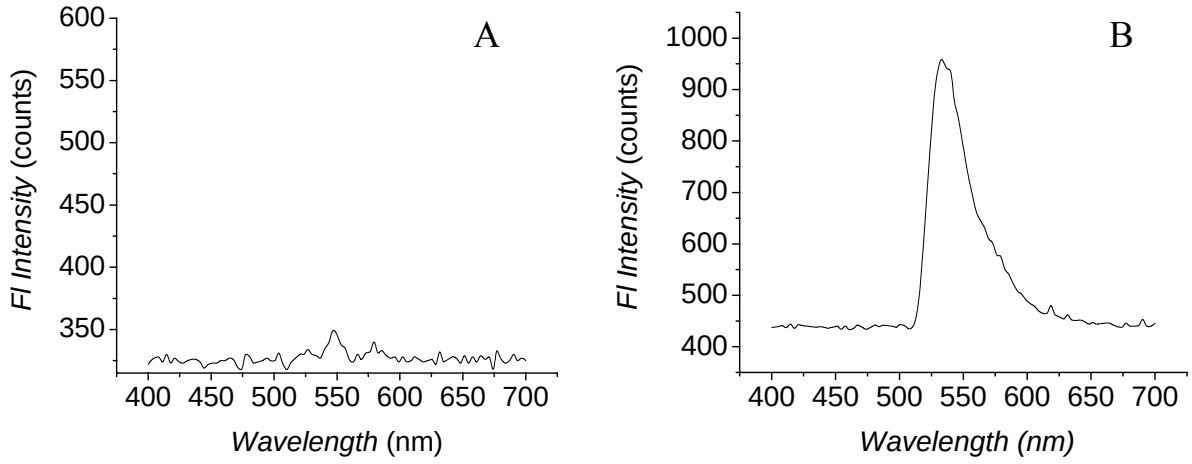

Figure 5-13. Fluorescence spectra of A) Rabbit IgG and B) BSA modified glass slides after exposure to a solution containing Alexa 488- tagged anti-rabbit IgG.

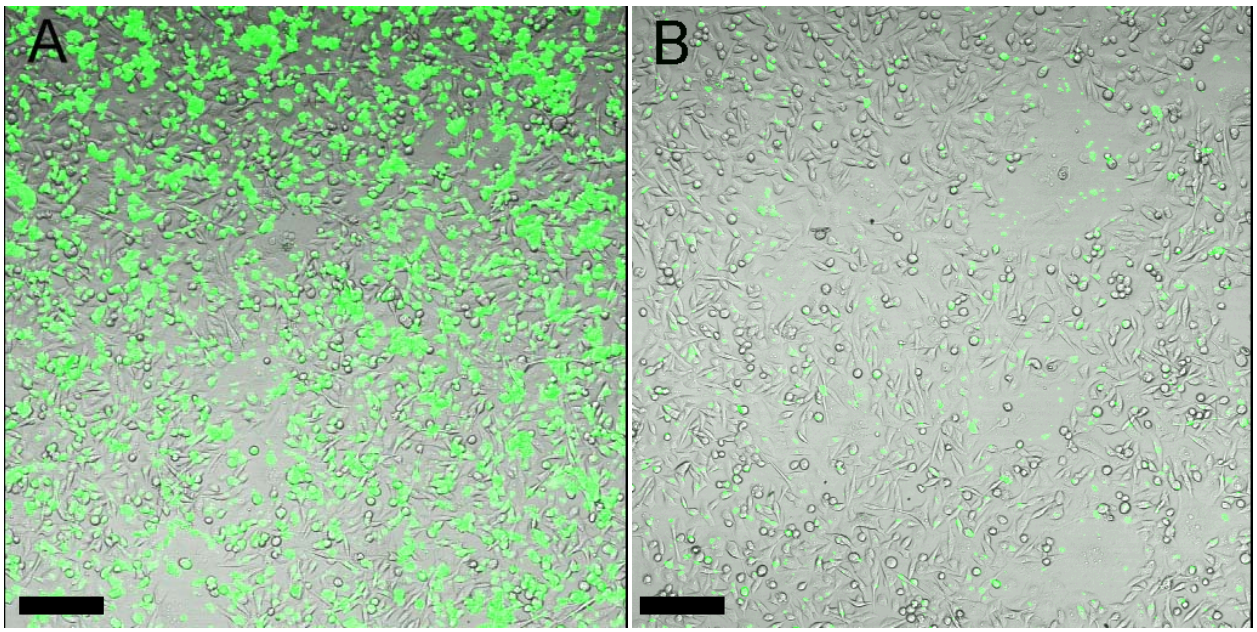

Figure 5-14. Fluorescence images of two different breast carcinoma cell culture samples incubated with Alexa-488 labeled silica nano test tubes. A) test tubes are modified with target antibody B) test tubes are modified with control antibody. Scale bars represent 200 μm.

CHAPTER 6
CONCLUSIONS

The aim of this dissertation is to develop membrane platforms for applications in ion transport modulation and biomolecule carrier fabrication. The use of template synthesized gold nanotube membranes and silica nano test tubes have been the common themes in this research. Chapter 1 provides background information about the template synthesis approach and its applications that are related to this work. The preparation of the track-etched polycarbonate and anodized aluminum oxide template membranes is presented in detail. Reviews of electroless gold deposition, sol-gel technology, silane chemistry and plasma etching that are frequently used in later chapters are then given. A brief overview of the delivery vehicles used in biomolecule transport is also provided.

We have been interested in developing strategies for controlling the rates of ion transport through gold nanotube membranes. Chapter 2 introduces a new method for electromodulated ion transport across such membranes. We have shown that cation transport through Au nanotube membranes can be electromodulated by controlling the extent of oxidation of a Fc-thiol attached to the Au surfaces. Electrochemical characterization of the Fc-thiol modified Au nanotube membranes is first examined. Surface confined cyclic voltammograms were obtained and the stability of these voltammograms was found to depend on the redox state of Fc and the type electrolyte.

We have found that when the nanotube-bound Fc is oxidized to Fc^+, the flux of a cationic permeate species is suppressed relative to when the Fc is in its reduced state. We have defined an electromodulation selectivity coefficient for cation transport, α. As would be expected, higher α values are obtained for membranes containing smaller inside-diameter nanotubes. For the 10 nm-diameter nanotubes a maximum value of $\alpha = 9.4$ was obtained. A decrease in α values has

been observed which is due in part to decomposition of Fc^+. Membranes modified with decamethyl-ferrocene with smaller diameters are suggested for more stable systems with higher α values.

The unstable nature of Fc^+ has been further investigated in Chapter 3 with special interest to its decay properties in constrained geometries. Previous studies have shown that the Fc^+ decomposition is a first order decay in bulk aqueous solutions. The Fc^+ decay properties of four membranes with different pore sizes were investigated in an aqueous electrolyte and compared to the decay for commercial gold button electrode. After the membrane samples were modified with Fc-thiol monolayer, they were exposed to argon plasma that removes Fc-thiol on Au surface films leaving only the Fc-thiol lining the Au nanotube walls. The results suggest that the decay rate increases with increasing pore size and in all cases it is found to obey first order decay kinetics. Furthermore, the decay pattern resembles a surface-like decay as the pore size of the membrane increases. These results were attributed to the mildly hydrophobic character of Fc-thiol monolayer and the varying availability of counterions inside the pores as the pore dimensions change.

The use of silica nano test tubes, that are introduced by the Martin group, as potential universal drug delivery vehicles was exploited where these nano test tubes could be filled with payload and then the open end corked with a chemically labile cap.[48] Our long range objective with these test tubes is to impart multifunctionality through differential modification for developing a technology for cell specific biomolecule delivery. Generally the synthesis involves deposition of silica within the pores of a nanopore alumina template via sol-gel chemistry.

Chapter 4 describes the fabrication of a unique nanopore polymer template and its use for silica nano test tube production. A plasma etch method, using a nanopore alumina film as the

mask, was used to etch a replica of the alumina pore structure into the surface of a polymer (photoresist) film. In doing so, we created a new type of nanopore polymer template for use in template synthesis of nanomaterials. An appealing feature of this new template is that the distance that the pores propagate into the surface of the polymer film can be controlled by varying the plasma etch time. This allows for corresponding control over the lengths of the nano test tubes prepared by template synthesis within the pores. Via this route, we have successfully prepared silica nano test tubes that were over 100 nm shorter than the shortest tubes prepared in an alumina-film template.[47]

In Chapter 5, we have substantiated the fabrication method for the preparation of uniform silica nano test tubes using alumina templates and then illustrated the response of breast carcinoma cells to test tubes that have been biochemically modified. When conventional sol-gel method was used, defective test tubes were obtained. This was attributed to the small changes in the viscosity of the gel. Uniform defect-free silica nano test tubes were prepared by the layer-by-layer addition of silica through the surface sol-gel method. We have used argon plasma etching to remove the silica film on the template surface, which normally binds the nanotubes together. Using silane and Schiff-base chemistry, we have independently modified the inner and outer surfaces of these tubes for the cell incubation studies. The inner tube surfaces were first labeled with a fluorophore and then the template was removed. The liberated fluorescent-tubes were modified with either a target or a control antibody and then incubated with breast carcinoma cells. The fluorescence data suggest that the tubes modified with target antibody attaches much more readily to the cell membrane surfaces than the tubes modified with control antibody.

LIST OF REFERENCES

(1) Klabunde, K. J. *Nanoscale Materials in Chemistry*; Wiley-Interscience: New York, 2001.

(2) Martin, C. R.; Kohli, P. *Nature Rev. Drug Discov.* **2003**, *2*, 29-37.

(3) Martin, C. R. *Science* **1994**, *266*, 1961-1966.

(4) Martin, C. R.; Mitchell, D. T. *Anal. Chem.* **1998**, *70*, 322A-327A.

(5) Ozin, G. A. *Adv. Mater.* **1992**, *4*, 612-649.

(6) Hulteen, J. C.; Martin, C. R. *J. Mater. Chem.* **1997**, *7*, 1075-1087.

(7) Martin, C. R.; Mitchell, D. T. *Electroanal. Chem.* **1999**, *21*, 1-74.

(8) Choi, Y.; Baker, L. A.; Hillebrenner, H.; Martin, C. R. *Phys. Chem. Chem. Phys.* **2006**, *8*, 4976-4988.

(9) Fleischer, R. L.; Price, P. B.; Walker, R. M. *Nuclear Tracks in Solids. Principles and Applications*; University of California Press: Berkeley, 1975.

(10) Hornyak, G. L.; Patrissi, C. J.; Martin, C. R. *J. Phys. Chem. B* **1997**, *101*, 1548-1555.

(11) Tonucci, R. J.; Justus, B. L.; Campillo, A. J.; Ford, C. E. *Science* **1992**, *258*, 783-785.

(12) Beck, J. S.; Vartuli, J. C.; Roth, W. J.; Leonowicz, M. E.; Kresge, C. T.; Schmitt, K. D.; Chu, C. T. W.; Olson, D. H.; Sheppard, E. W.; et al. *J. Am. Chem. Soc.* **1992**, *114*, 10834-10843.

(13) Clark, T. D.; Ghadiri, M. R. *J. Am. Chem. Soc.* **1995**, *117*, 12364-12365.

(14) Hou, S.; Wang, J.; Martin, C. R. *J. Am. Chem. Soc.* **2005**, *127*, 8586-8587.

(15) Hou, S.; Wang, J.; Martin, C. R. *Nano Lett.* **2005**, *5*, 231-234.

(16) Wirtz, M.; Martin, C. R. *Adv. Mater.* **2003**, *15*, 455-458.

(17) Menon, V. P.; Martin, C. R. *Anal. Chem.* **1995**, *67*, 1920-1928.

(18) Li, N.; Mitchell, D. T.; Lee, K.-P.; Martin, C. R. *J. Electrochem. Soc.* **2003**, *150*, A979-A984.

(19) Che, G.; Jirage, K. B.; Fisher, E. R.; Martin, C. R. *J. Electrochem. Soc.* **1997**, *144*, 4296-4302.

(20) Che, G.; Lakshmi, B. B.; Fisher, E. R.; Martin, C. R. *Nature* **1998**, *393*, 346-349.

(21) Patrissi, C. J.; Martin, C. R. *J. Electrochem. Soc.* **2001**, *148*, A1247-A1253.

(22) Sides, C. R.; Martin, C. R. *Adv. Mater.* **2005**, *17*, 125-128.

(23) Cai, Z.; Lei, J.; Liang, W.; Menon, V.; Martin, C. R. *Chem. Mater.* **1991**, *3*, 960-967.

(24) Menon, V. P.; Lei, J.; Martin, C. R. *Chem. Mater.* **1996**, *8*, 2382-2390.

(25) Martin, C. R. *Acc. Chem. Res.* **1995**, *28*, 61-68.

(26) Cho, S. I.; Kwon, W. J.; Choi, S.-J.; Kim, P.; Park, S.-A.; Kim, J.; Son, S. J.; Xiao, R.; Kim, S.-H.; Lee, S. B. *Adv. Mater.* **2005**, *17*, 171-175.

(27) Scopece, P.; Baker, L. A.; Ugo, P.; Martin, C. R. *Nanotechnology* **2006**, *17*, 3951-3956.

(28) Heins, E. A.; Siwy, Z. S.; Baker, L. A.; Martin, C. R. *Nano Lett.* **2005**, *5*, 1824-1829.

(29) Harrell, C. C.; Choi, Y.; Horne, L. P.; Baker, L. A.; Siwy, Z. S.; Martin, C. R. *Langmuir* **2006**, *22*, 10837-10843.

(30) Mara, A.; Siwy, Z.; Trautmann, C.; Wan, J.; Kamme, F. *Nano Lett.* **2004**, *4*, 497-501.

(31) Siwy, Z.; Trofin, L.; Kohli, P.; Baker, L. A.; Trautmann, C.; Martin, C. R. *J. Am. Chem. Soc.* **2005**, *127*, 5000-5001.

(32) Lee, S.; Zhang, Y.; White, H. S.; Harrell, C. C.; Martin, C. R. *Anal. Chem.* **2004**, *76*, 6108-6115.

(33) Siwy, Z. S. *Adv. Funct. Mater.* **2006**, *16*, 735-746.

(34) Jirage, K. B.; Hulteen, J. C.; Martin, C. R. *Science* **1997**, *278*, 655-658.

(35) Yu, S.; Lee, S. B.; Kang, M.; Martin, C. R. *Nano lett.* **2001**, *1*, 495-498.

(36) Jirage, K. B.; Hulteen, J. C.; Martin, C. R. *Anal. Chem.* **1999**, *71*, 4913-4918.

(37) Steinle, E. D.; Mitchell, D. T.; Wirtz, M.; Lee, S. B.; Young, V.; Martin, C. R. *Anal. Chem.* **2002**, *74*, 2416-2422.

(38) Lee, S. B.; Martin, C. R. *Chem. Mater.* **2001**, *13*, 3236-3244.

(39) Nishizawa, M.; Menon, V. P.; Martin, C. R. *Science* **1995**, *268*, 700-702.

(40) Kang, M.; Martin, C. R. *Langmuir* **2001**, *17*, 2753-2759.

(41) Lee, S. B.; Martin, C. R. *J. Am. Chem. Soc.* **2002**, *124*, 11850-11851.

(42) Miller, S. A.; Martin, C. R. *J. Am. Chem. Soc.* **2004**, *126*, 6226-6227.

(43) Buyukserin, F.; Kohli, P.; Wirtz, M. O.; Martin, C. R. *Small* **2007**, *3*, 266-270.

(44) Lee, S. B.; Mitchell, D. T.; Trofin, L.; Nevanen, T. K.; Soederlund, H.; Martin, C. R. *Science* **2002**, *296*, 2198-2200.

(45) Mitchell, D. T.; Lee, S. B.; Trofin, L.; Li, N.; Nevanen, T. K.; Soederlund, H.; Martin, C. R. *J. Am. Chem. Soc.* **2002**, *124*, 11864-11865.

(46) Hillebrenner, H.; Buyukserin, F.; Stewart, J. D.; Martin, C. R. *Nanomedicine* **2006**, *1*, 39-50.

(47) Gasparac, R.; Kohli, P.; Mota, M. O.; Trofin, L.; Martin, C. R. *Nano Lett.* **2004**, *4*, 513-516.

(48) Hillebrenner, H.; Buyukserin, F.; Kang, M.; Mota, M. O.; Stewart, J. D.; Martin, C. R. *J. Am. Chem. Soc.* **2006**, *128*, 4236-4237.

(49) Buyukserin, F.; Kang, M.; Martin, C. R. *Small* **2007**, *3*, 106-110.

(50) Fleischer, R. L.; Price, P. B.; Symes, E. M. *Science* **1964**, *143*, 249-250.

(51) Apel, P. *Radiat. Meas.* **2001**, *34*, 559-566.

(52) Fischer, B. E.; Spohr, R. *Rev. Mod. Phys.* **1983**, *55*, 907-948.

(53) Vater, P. *Nucl. Tracks Radiat. Meas.* **1988**, *15*, 743-749.

(54) Lueck, H. B.; Matthes, H.; Gemende, B.; Heinrich, B.; Pfestorf, W.; Seidel, W.; Turuc, S. *Nucl. Instrum. Methods Phys. Res., Sect. B* **1990**, *B50*, 395-400.

(55) Kravetz, L. I.; Dmitriev, S. N.; Apel, P.; Yu, P. *Russ. High Energy Chem.* **1997**, *31*, 25-28.

(56) Trautmann, C.; Bruechle, W.; Spohr, R.; Vetter, J.; Angert, N. *Nucl. Instrum. Methods Phys. Res., Sect. B* **1996**, *111*, 70-74.

(57) Mallory, G. O.; Hadju, J. B. *Electroless Plating: Fundamentals and Applications*; American Electroplaters and Surface Finishers Society: Orlando, FL, 1990.

(58) Brumlik, C. J.; Menon, V. P.; Martin, C. R. *J. Mater. Res.* **1994**, *9*, 1174-1183.

(59) Martin, C. R.; Nishizawa, M.; Jirage, K. B.; Kang, M. *J. Phys. Chem. B* **2001**, *105*, 1925-1934.

(60) McDermott, J. *Plating of Plactics with Metals*; Noyes Data Corp.: Park Ridge, NJ, 1974.

(61) Jeans, J. H. *An Introduction to the Kinetic Theory of Gases*; Cambridge Univ. Press: Cambridge, 1939.

(62) Petzny, W. J.; Quinn, J. A. *Science* **1969**, *166*, 751-753.

(63) Datta, R.; Dechapanichkul, S.; Kim, J. S.; Fang, L. Y.; Uehara, H. *J. Membr. Sci.* **1992**, *75*, 245-263.

(64) Keller, F.; Hunter, M. S.; Robinson, D. L. *J. Electrochem. Soc.* **1953**, *100*, 411-419.

(65) Wood, G. C.; Osulliva, J. P. *Electrochim. Acta* **1970**, *15*, 1865-1876.

(66) Thompson, G. E.; Wood, G. C. *Nature* **1981**, *290*, 230-232.

(67) Lee, W.; Scholz, R.; Niesch, K.; Gosele, U. *Angew. Chem. Int. Edn* **2005**, *44*, 6050-6054.

(68) Zhi, L. J.; Wu, J. S.; Li, J. X.; Kolb, U.; Mullen, K. *Angew. Chem. Int. Edn* **2005**, *44*, 2120-2123.

(69) Lee, W.; Ji, R.; Gosele, U.; Nielsch, K. *Nat. Mater.* **2006**, *5*, 741-747.

(70) Kang, M.; Yu, S.; Li, N.; Martin, C. R. *Langmuir* **2005**, *21*, 8429-8438.

(71) Ding, G. Q.; Zheng, M. J.; Xu, W. L.; Shen, W. Z. *Nanotechnology* **2005**, *16*, 1285-1289.

(72) Chik, H.; Xu, J. M. *Mat. Sci. Eng., R* **2004**, *43*, 103-138.

(73) Furneaux, R. C.; Rigby, W. R.; Davidson, A. P. *Nature* **1989**, *337*, 147-149.

(74) Almawlawi, D.; Coombs, N.; Moskovits, M. *J. Appl. Phys.* **1991**, *70*, 4421-4425.

(75) Jessensky, O.; Muller, F.; Gosele, U. *J. Electrochem. Soc.* **1998**, *145*, 3735-3740.

(76) Masuda, H.; Fukuda, K. *Science* **1995**, *268*, 1466-1468.

(77) Li, A. P.; Muller, F.; Birner, A.; Nielsch, K.; Gosele, U. *J. Vac. Sci. Technol., A* **1999**, *17*, 1428-1431.

(78) Masuda, H.; Yamada, H.; Satoh, M.; Asoh, H.; Nakao, M.; Tamamura, T. *Appl. Phys. Lett.* **1997**, *71*, 2770-2772.

(79) Li, A. P.; Muller, F.; Gosele, U. *Electrochem. Solid State Lett.* **2000**, *3*, 131-134.

(80) Liu, C. Y.; Datta, A.; Wang, Y. L. *Appl. Phys. Lett.* **2001**, *78*, 120-122.

(81) Toh, C.-S.; Kayes, B. M.; Nemanick, E. J.; Lewis, N. S. *Nano Lett.* **2004**, *4*, 767-770.

(82) Masuda, H.; Hasegwa, F.; Ono, S. *J. Electrochem. Soc.* **1997**, *144*, L127-L130.

(83) Jessensky, O.; Muller, F.; Gosele, U. *Appl. Phys. Lett.* **1998**, *72*, 1173-1175.

(84) Li, A. P.; Muller, F.; Birner, A.; Nielsch, K.; Gosele, U. *J. Appl. Phys.* **1998**, *84*, 6023-6026.

(85) Diggle, J. W.; Downie, T. C.; Goulding, C. W. *Chem. Rev.* **1969**, *69*, 365-405.

(86) Xu, T. T.; Piner, R. D.; Ruoff, R. S. *Langmuir* **2003**, *19*, 1443-1445.

(87) Ebelman, M. *Ann. Chimie. Phys.* **1846**, *16*, 129.

(88) Graham, T. *J. Chem. Soc.* **1864**, *17*, 318.

(89) Hench, L. L.; West, J. K. *Chem. Rev.* **1990**, *90*, 33-72.

(90) Aergerter, M. A.; Mehrota, R. C.; Oehme, I.; Reisfeld, R.; Sakka, S.; Wolfbets, O.; Jorgensen, C. K. *Optical and Electrical Phenomena in Sol-Gel Glasses and Modern Applications*; Springer-Verlag: Berlin, 1996.

(91) Lakshmi, B. B.; Patrissi, C. J.; Martin, C. R. *Chem. Mater.* **1997**, *9*, 2544-2550.

(92) Livage, J.; Henry, M.; Sanchez, C. *Prog. Solid State Chem.* **1988**, *18*, 259-341.

(93) Pope, E. J. A.; Sakka, S.; Klein, E. D. *Sol-Gel Science and Technology*; American Ceramic Society: Columbus, Ohio, 1995.

(94) Prassas, M.; Phalippou, J.; Zarzycki, J. *J. Mater. Sci.* **1984**, *19*, 1656-1665.

(95) Hench, L. L. *Sol-Gel Silica: Processing, Properties and Technology Transfer*; Noyes Publications: New York, 1998.

(96) Piccaluga, G.; Corrias, A.; Ennas, G.; Musinu, A. *Sol-Gel Preparation and Characterization of Metal-Silica an Metal Oxide-Silica Nanocomposites*; Trans Tech Publications Ltd: Switzerland, 2000.

(97) Artaki, I.; Zerda, T. W.; Jonas, J. *Mater. Lett.* **1985**, *3*, 493-496.

(98) Schmidt, H.; Kaiser, A. *Glastechn Ber* **1981**, *54*, 338-342.

(99) Lakshmi, B. B.; Dorhout, P. K.; Martin, C. R. *Chem. Mater.* **1997**, *9*, 857-862.

(100) Zhang, M.; Bando, Y.; Wada, K. *J. Mater. Res.* **2000**, *15*, 387-392.

(101) Kovtyukhova, N. I.; Mallouk, T. E.; Mayer, T. S. *Adv. Mater.* **2003**, *15*, 780-785.

(102) Colvin, V. L.; Goldstein, A. N.; Alivisatos, A. P. *J. Am. Chem. Soc.* **1992**, *114*, 5221-5230.

(103) Iler, R. K. *J. Colloid Interface Sci.* **1966**, *21*, 569-&.

(104) Ichinose, I.; Senzu, H.; Kunitake, T. *Chem. Mater.* **1997**, *9*, 1296-1298.

(105) Nicolau, Y. F.; Menard, J. C. *J. Cryst. Growth* **1988**, *92*, 128-142.

(106) Kovtyukhova, N. I.; Buzaneva, E. V.; Waraksa, C. C.; Martin, B. R.; Mallouk, T. E. *Chem. Mater.* **2000**, *12*, 383-389.

(107) Kovtyukhova, N. I.; Martin, B. R.; Mbindyo, J. K. N.; Mallouk, T. E.; Cabassi, M.; Mayer, T. S. *Mater. Sci. Eng., C* **2002**, *19*, 255-262.

(108) Arkles, B. *Chemtech* **1977**, *7*, 766-778.

(109) Anon *Plastics Additives & Compounding* **2003**, *5*, 40-45.

(110) Plueddeman, F. P. *Silane Coupling Agents*; Plenum Press: New York, USA, 1982.

(111) Madou, M. J. *Fundamentals of Microfabrication*; CRC Press: Boca Raton, 2002.

(112) Furuya, A.; Shimokawa, F.; Matsuura, T.; Sawada, R. *Proc. Int. Conf. Intell. Mater., 1st* **1993**, 57-60.

(113) Paul, M.; Laatiris, A.; Fessi, H.; Dufeu, B.; Durand, R.; Deniau, M.; Astier, A. *Drug Dev. Res.* **1998**, *43*, 98-104.

(114) Carino, G. P.; Jacob, J. S.; Mathiowitz, E. *J. Controlled Release* **2000**, *65*, 261-269.

(115) Roy, I.; Ohulchanskyy, T. Y.; Bharali, D. J.; Pudavar, H. E.; Mistretta, R. A.; Kaur, N.; Prasad, P. N. *Proc. Natl. Acad. Sci. U. S. A.* **2005**, *102*, 279-284.

(116) Chen, C.-C.; Liu, Y.-C.; Wu, C.-H.; Yeh, C.-C.; Su, M.-T.; Wu, Y.-C. *Adv. Mater.* **2005**, *17*, 404-407.

(117) Perkins, W. R.; Ahmad, I.; Li, X.; Hirsh, D. J.; Masters, G. R.; Fecko, C. J.; Lee, J.; Ali, S.; Nguyen, J.; Schupsky, J.; Herbert, C.; Janoff, A. S.; Mayhew, E. *Int. J. Pharm.* **2000**, *200*, 27-39.

(118) Lasic, D. D. *J. Controlled Release* **1997**, *48*, 203-222.

(119) Torchilin, V. P. *Nature Rev. Drug Discov.* **2005**, *4*, 145-160.

(120) Langer, R. *Nature* **1998**, *392*, 5-10.

(121) Duncan, R. *Nature Rev. Drug Discov.* **2003**, *2*, 347-360.

(122) Svenson, S.; Tomalia, D. A. *Advan. Drug Delivery Rev.* **2005**, *57*, 2106-2129.

(123) Gemeinhart, R. A.; Luo, D.; Saltzman, W. M. *Biotechnol. Prog.* **2005**, *21*, 532-537.

(124) Gomez-Hens, A.; Manuel Fernandez-Romero, J. *TrAC, Trends in Analytical Chemistry* **2005**, *24*, 9-19.

(125) Ferrari, M. *Nat. Rev. Cancer* **2005**, *5*, 161-171.

(126) Luo, D.; Saltzman, W. M. *Nat. Biotechnol.* **2000**, *18*, 33-37.

(127) Park, J. W.; Hong, K.; Kirpotin, D. B.; Papahadjopoulos, D.; Benz, C. C. *Adv. Pharmacol.* **1997**, *40*, 399-435.

(128) Allen, C.; Maysinger, D.; Eisenberg, A. *Colloid Surface B* **1999**, *16*, 3-27.

(129) La, S. B.; Okano, T.; Kataoka, K. *J. Pharm. Sci.* **1996**, *85*, 85-90.

(130) Thurmond, K. B., II; Huang, H.; Clark, C. G., Jr.; Kowalewski, T.; Wooley, K. L. *Colloid Surface B* **1999**, *16*, 45-54.

(131) Kwon, G. S.; Kataoka, K. *Advan. Drug Delivery Rev.* **1995**, *16*, 295-309.

(132) Kabanov, A. V.; Kabanov, V. A. *Advan. Drug Delivery Rev.* **1998**, *30*, 49-60.

(133) Tomalia, D. A.; Baker, H.; Dewald, J.; Hall, M.; Kallos, G.; Martin, S.; Roeck, J.; Ryder, J.; Smith, P. *Polymer J.* **1985**, *17*, 117-132.

(134) Liu, M.; Kono, K.; Frechet, J. M. J. *J. Controlled Release* **2000**, *65*, 121-131.

(135) Kobayashi, H.; Kawamoto, S.; Sakai, Y.; Choyke, P. L.; Star, R. A.; Brechbiel, M. W.; Sato, N.; Tagaya, Y.; Morris, J. C.; Waldmann, T. A. *J. Natl Cancer Inst.* **2004**, *96*, 703-708.

(136) Haensler, J.; Szoka, F. C., Jr. *Bioconjug. Chem.* **1993**, *4*, 372-379.

(137) Kukowska-Latallo, J. F.; Bielinska, A. U.; Johnson, J.; Spindler, R.; Tomalia, D. A.; Baker, J. R., Jr. *Proc. Natl. Acad. Sci. U. S. A.* **1996**, *93*, 4897-4902.

(138) Anderson, W. F. *Nature* **1998**, *392*, 25-30.

(139) Crystal, R. G. *Science* **1995**, *270*, 404-410.

(140) Tripathy, S. K.; Black, H. B.; Goldwasser, E.; Leiden, J. M. *Nat. Med.* **1996**, *2*, 545-550.

(141) Thomas, M.; Klibanov, A. M. *Proc. Natl. Acad. Sci. U. S. A.* **2003**, *100*, 9138-9143.

(142) Kam, N. W. S.; Jessop, T. C.; Wender, P. A.; Dai, H. *J. Am. Chem. Soc.* **2004**, *126*, 6850-6851.

(143) Page, J. A.; Wilkinson, G. *J. Am. Chem. Soc* **1952**, *74*, 6149-6151.

(144) Boltz, J. M.; Wrighton, M. S. *J. Am. Chem. Soc* **1978**, *100*, 5257-5262.

(145) Chidsey, C. E. D.; Bertozzi, C. R.; Putvinski, T. M.; Mujsce, A. M. *J. Am. Chem. Soc* **1990**, *112*, 4301.

(146) Burgmayer, P.; Murray, R. W. *J. Am. Chem. Soc.* **1982**, *104*, 6140.

(147) Zinger, B.; Miller, L. L. *J. Am. Chem. Soc.* **1984**, *106*, 6841.

(148) Pile, D. L.; Hillier, A. C. *J. Memb. Sci.* **2002**, *208*, 119-131.

(149) Wirtz, M.; Miller, S. A.; Martin, C. R. *Int. J. Nanosci.* **2002**, *1*, 255-268.

(150) Lakshmi, B. B.; Martin, C. R. *Nature* **1997**, *388*, 758-760.

(151) Rowe, G. K.; Creager, S. E. *Langmuir* **1991**, *7*, 2307-2312.

(152) Uosaki, K.; Sato, Y.; Kita, H. *Langmuir* **1991**, *7*, 1510-1514.

(153) Popenoe, D. D.; Deinhammer, R. S.; Porter, M. D. *Langmuir* **1992**, *8*, 2521-2530.

(154) Bard, A. J.; Faulkner, L. R. *Electrochemical Methods*, 1st ed.; John Wiley&Sons: New York, 1980.

(155) Prins, R.; Korswagen, A. R.; Kortbeek, A. G. T. G. *J. Organomet. Chem.* **1972**, *39*, 335-344.

(156) Holecek, J.; Handlir, K.; Klikorka, J.; Nguyen Dinh, B. *Collect. Czech. Chem. Commun.* **1979**, *44*, 1379-1387.

(157) Noviandri, I.; Brown, K. N.; Fleming, D. S.; Gulyas, P. T.; Lay, P. A.; Masters, A. F.; Phillips, L. *J. Phys. Chem. B* **1999**, *103*, 6713-6722.

(158) Zahl, A.; Van Eldik, R.; Matsumoto, M.; Swaddle, T. W. *Inorg. Chem.* **2003**, *42*, 3718-3722.

(159) Lenhard, J. R.; Murray, R. W. *J. Am. Chem. Soc.* **1978**, *100*, 7870-7875.

(160) Seiler, P.; Dunitz, J. D. *Acta Crystallographica, Section B: Structural Crystallography and Crystal Chemistry* **1979**, *B35*, 1068-1074.

(161) Wharnton, J. E.; Park, D.; Martin, C. R. Unpublished results.

(162) Walczak, M. M.; Popenoe, D. D.; Deinhammer, R. S.; Lamp, B. D.; Chung, C.; Porter, M. D. *Langmuir* **1991**, *7*, 2687-2693.

(163) Abbott, N. L.; Whitesides, G. M. *Langmuir* **1994**, *10*, 1493-1497.

(164) Sondag-Huethorst, J. A. M.; Fokkink, L. G. J. *Langmuir* **1992**, *8*, 2560-2566.

(165) Espenscheid, M. W.; Martin, C. R. *J. Electroanal. Chem.* **1985**, *188*, 73-84.

(166) Szentrimay, R.; Yeh, P.; Kuwana, T. *Electrochemical Studies of Biological Systems*; American Chemical Society: Washington, DC, 1977.

(167) Burns, D. T.; Tungkananuruk, N. *Anal. Chim. Acta* **1987**, *199*, 237-240.

(168) Ensafi, A. A.; Rezaei, B. *Anal. Lett.* **1998**, *31*, 167-177.

(169) Magnuson, M. L.; Urbansky, E. T.; Kelty, C. A. *Anal. Chem.* **2000**, *72*, 25-29.

(170) Pendin, A. A.; Zakhar'evskii, M. S.; Leont'ev'skaya, P. K. *Kinet. Katal.* **1966**, *7*, 1074-1077.

(171) Masuda, H.; Satoh, M. *Jpn. J. Appl. Phys., Part: 2 Lett.* **1996**, *35*, L126-L129.

(172) Honda, K.; Rao, T. N.; Tryk, D. A.; Fujishima, A.; Watanabe, M.; Yasui, K.; Masuda, H. *J. Electrochem. Soc.* **2000**, *147*, 659-664.

(173) Honda, K.; Rao, T. N.; Tryk, D. A.; Fujishima, A.; Watanabe, M.; Yasui, K.; Masuda, H. *J. Electrochem. Soc.* **2001**, *148*, A668-A679.

(174) Kang, M.; Yu, S.; Li, N.; Martin, C. R. *Small* **2005**, *1*, 69-72.

(175) Furneaux, R. C.; Rigby, W. R.; Davidson, A. P. *Nature* **1989**, *337*, 147-149.

(176) Li, N.; Yu, S.; Harrell, C. C.; Martin, C. R. *Anal. Chem.* **2004**, *76*, 2025-2030.

(177) Niemeyer, C. M. *Angew. Chem. Int. Ed.* **2001**, *40*, 4128-4158.

(178) Herr, J. K.; Smith, J. E.; Medley, C. D.; Shangguan, D.; Tan, W. *Anal. Chem.* **2006**, *78*, 2918-2924.

(179) Chan, W. C.; Nie, S. *Science* **1998**, *281*, 2016-2018.

(180) Cui, Y.; Wei, Q.; Park, H.; Lieber, C. M. *Science* **2001**, *293*, 1289-1292.

(181) Rosi, N. L.; Mirkin, C. A. *Chem. Rev.* **2005**, *105*, 1547-1562.

(182) Jang, J.; Ko, S.; Kim, Y. *Adv. Funct. Mater.* **2006**, *16*, 754-759.

(183) Cepak, V. M.; Martin, C. R. *Chem. Mater.* **1999**, *11*, 1363-1367.

(184) Miller, S. A.; Young, V. Y.; Martin, C. R. *J. Am. Chem. Soc.* **2001**, *123*, 12335-12342.

(185) Son, S. J.; Lee, S. B. *J. Am. Chem. Soc.* **2006**, *128*, 15974-15975.

(186) Son, S. J.; Reichel, J.; He, B.; Schuchman, M.; Lee, S. B. *J. Am. Chem. Soc.* **2005**, *127*, 7316-7317.

(187) Archibald, D. D.; Qadri, S. B.; Gaber, B. P. *Langmuir* **1996**, *12*, 538-546.

(188) Kang, M.; Trofin, L.; Mota, M. O.; Martin, C. R. *Anal. Chem.* **2005**, *77*, 6243-6249.

(189) Bruening, C.; Grobe, J. *J. Chem. Soc., Chem. Commun.* **1995**, 2323-2324.

(190) Yoshioka, M.; Mukai, Y.; Matsui, T.; Udagawa, A.; Funakubo, H. *J. Chromatogr.* **1991**, *566*, 361-368.

(191) Stubbings, D.; Bubb, M. O.; Conradie, J. D. *Anal. Biochem.* **1993**, *210*, 159-162.

(192) Franzelius, C.; Ackermann, I.; Deinl, I.; Angermaier, L.; Machbert, G. *Journal of Analytical Toxicology* **1998**, *22*, 359-362.

(193) Medley, C. D.; Drake, T. J.; Tomasini, J. M.; Rogers, R. J.; Tan, W. *Anal. Chem.* **2005**, *77*, 4713-4718.

(194) Zhang, M.; Bando, Y.; Wada, K.; Kurashima, K. *J. Mater. Sci. Lett.* **1999**, *18*, 1911-1913.

(195) Fang, M.; Kim, C. H.; Martin, B. R.; Mallouk, T. E. *Journal of Nanoparticle Research* **1999**, *1*, 43-49.

(196) Steinle, E. D.; Mitchell, D. T.; Wirtz, M.; Lee, S. B.; Young, V. Y.; Martin, C. R. *Anal. Chem.* **2002**, *74*, 2416-2422.

(197) Panchuk-Voloshina, N.; Haugland, R. P.; Bishop-Stewart, J.; Bhalgat, M. K.; Millard, P. J.; Mao, F.; Leung, W.-Y.; Haugland, R. P. *J. Histochem. Cytochem.* **1999**, *47*, 1179-1188.

(198) Sepp-Lorenzino, L. *Breast Cancer Res. Treat.* **1998**, *47*, 235-253.

(199) Zhang, H.; Yee, D. *Clin. Cancer Res.* **2006**, *12*, 6323-6325.

(200) Rogers, R. J. Unpublished results.

BIOGRAPHICAL SKETCH

Fatih Buyukserin, the last of three children in the family of Husniye and Hasan Fehmi Buyukserin, was born in Konya, Turkey, on February 15th, 1980. He graduated from Bilkent University in 2001 with a Bachelor of Science degree in chemistry. His interest in nanotechnology started here while he was studying the physical properties of silver nanoparticles under the guidance of Dr. Serdar Ozcelik. He took this to the next step by joining the research group of Dr. Charles R. Martin at the University of Florida in August 2001. He completed his research on template synthesis of nanomaterials in May 2007, obtaining a Doctor of Philosophy degree. He pursued a postdoctoral associate position at the University of Texas at Dallas working on multifunctional nanotubes for cancer diagnosis.